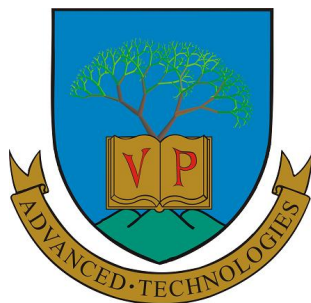


Universiy of Pannonia
Department of Electrical Engineering and Information Systems
Doctoral School of Information Science



OPTIMAL CURRENT CONTROL FOR DOMESTIC POWER CONVERTERS

DOI:.....

Doctoral (PhD) Thesis
Author: László Richárd Neukirchner

Supervisor: dr. Attila Magyar

Made at:
Universiy of Pannonia
Doctoral School of Information Science

Veszprém
2020

OPTIMAL CURRENT CONTROL FOR DOMESTIC POWER CONVERTERS

Értekezés doktori (PhD) fokozat elnyerése érdekében

Írta:
László Richárd Neukirchner

Készült a Universiy of PannoniaDoctoral School of Information
Sciencekeretében

Témavezető: dr. Attila Magyar
Elfogadásra javaslom: igen / nem

.....
aláírás

A jelölt a doktori szigorlaton %-ot ért el.

Az értekezést bírálóként elfogadásra javaslom:

Bíráló neve: : igen / nem

.....
aláírás

Bíráló neve: : igen / nem

.....
aláírás

A jelölt az értekezés nyilvános vitáján %-ot ért el.

Veszprém,

.....
a Bíráló Bizottság elnöke

A doktori (PhD) oklevél minősítése:

.....
az EDHT elnöke

Acknowledgement

I would like to express my special thanks of gratitude to my supervisor and teacher Dr. Attila Magyar as well as our principal of the doctoral school Prof. Katalin Hangos who gave me the wonderful opportunity to pursue this excellent project on optimal current control, which also helped me to develop and better myself on the field of scientific work, where I could really see myself grow and develop. I really feel gratitude to them. I would like to also thank Dr. Nimiród Kutasi, and his restless support and encouragement in the field of predictive control, as well as Dr. András Kelemen in the field of power electronics. Without they unquestionable and deep technical knowledge on the field, and they helpfulness, kindness and hospitality this doctoral thesis would not have happened. I would also recognise Dr. Peter Görbe who helped me to put the subject of voltage quality in context and accelerated my progress at the start of my PhD. studies, and Dr. Attila Fodor, who helped me on the field of current control, and system modeling, and also helped me organise my work and guide me in the forest of research. All of they contribution were invaluable to reach this stage of completion.

Any attempt at any level can't be satisfactorily completed without the support and guidance of my spouse Klaudia, my parents Anikó and László, my sister Elisabeth, and my friends. They helped me a lot with they spiritual and financial support in making this project, despite of their busy schedules. They always could find enough time and energy to give me enough attention and assistance.

I could not thank you enough!

Abstract

Starting the third decade after the millennium, in the European Union, the approach of the energy-, and with it the automotive industries has changed significantly since. The increasing governmental interventions on the industry, started with the bad reputation of diesel in passenger cars, and increasingly tighter restrictions on lead battery technologies, also Germany's renewable policies, dismantling nuclear plants encourage manufacturers and researchers for innovation in the direction of power efficiency. Solutions, which seemed to occupy the second place on the podium, have been re-assessed and re-thought in the light of this approach in terms of power topologies and algorithms alike. As the tide of renewable sources has taken the western Europe with a storm, with the high anticipation of getting rid of fossil fuels (or at least reduce their consumption), it brought down a myriad of problems to solve. The first of these is the high stochastic nature of these source, with the ever increasing demand on storage, to smoothen out the arms of the scale of supply and demand. The second comes with the incentive (policy maker, and civic alike in pursuit of "cheap" and non polluting energy) of installing these sources in residual areas, parking lots, schools, household roofs, just to name a few. On top of that, these actors have higher consumers in their disposal, using them on their whim, making the situation even worse.

This introduces two interesting, yet completely understandable phenomena, which act as the "symptoms" on the quality of our well accessible electric power for our consumers, due to the reason of these trends. The first is the harmonic distortion of the network's voltage phases, tackled with load regulations, and a wide range of active and passive filter designs. The second is the voltage phase asymmetry alias the voltage unbalance, appearing when uneven production, consumption, or distribution on the network.

This is a major yet often overlooked power quality problem in low voltage residential feeders due to the random location and rating of single-phase renewable sources and uneven distribution of household loads. Here a new indicator of voltage deviation is proposed that may serve as a basis of analysis and compensation methods in this dimension of power quality. The first half of this dissertation is about indicating such voltage asymmetry and mitigating it with a complex controller and electric power conversion structure, which is integrated with an optimization based control algorithm that uses asynchronous parallel pattern search as its engine. This structure uses current control on each phase to achieve the results, on the voltage quality. Additionally, the calculations showed, that the implementation could achieve noteworthy reductions in CO_2 .

emissions for an average household.

The second half is zooming down on the current control aspect itself, where a model of a power converter device is used for an optimal, predictive controller structure, to achieve the demanded efficiency, also with the calculation capacity in check. Starting with the design of a constrained optimal control of a current source rectifier, based on a mathematical model developed in Clarke and Park frame. Despite the clean establishment of the model's differential equations, the underlying bilinearity would make further controller design complicated. To comply with the system constraints an explicit model-based predictive controller was established. To simplify the control design, and eliminate the bilinearity from the equation system, a disjointed model was utilised due to the significant time constant differences between the AC and DC side dynamics. As a result, active damping was used on the AC side, and explicit model based predictive control on the DC side. The results are compared by simulation with the performance of a state feedback control.

Tartalmi Kivonat

Az ezredév forduló utáni harmadik évtized kezdetén az Európai unió hozzállása az autó- és energiaiparhoz nagyban megváltozott. A tagállamok rendletekkel és megszorításokkal való beavatkozása az ipari szférába rossz színben kezdte feltüntetni a dízelautókat, illetve erős szabályozásnak tette ki az ólom-savas akkumulátor alkalmazóit. Németország megújuló energia stratégiája, és atomerőműveinek lebontása új kihívások elé állította a kutatókat az energiáhatékonyság innovációja terén. Azon technológiai és algoritmikus megoldások, melyek eddig másodlagos helyen tűntek fel, most újra napvilágra kerültek át-gondoltabb formában az új körülményekhez igazodva. Eközben a megújuló energia vihara meghódította nyugat Európát. Ennek mellékterméke és hogy közben hogy a fosszilis üzemanyagoktól megszabaduljanak (vagy legalábbis csökkentsék használatukat), egy sor új megoldandó problémára vetett napvilágot. Az elsődleges ezek között az energiaforrások megerősödött sztochasztikus termelési és fogyasztási hajlama. Mindemellett a megnövekedett energia tárolási igény, hogy a kereslet és kínálatot szimbolizáló mérleg serpenyői egyensúlyba kerüljenek. A másodlagos az energiatakarékosság szándéka (mely törvényhozói és civil oldalon egyaránt az alsó, alacsony káros anyag kibocsátással járó energiát célozza meg), melynek során ezeket a megújuló forrásokat megnövekedett számban szerelik fel parkolókba, iskolákba, családi házak tetejére, hogy csak egy párat említsünk. Ezenfelül ezek a szereplők azóta megnövekedett energia igényével is rendelkeznek, tovább súlyosbítva a helyzetet. Ez két figyelemre méltó de ugyanakkor teljesen érthető jelenséget enged mutatni, melyek a fogyasztók által oly könnyen hozzáférhető energiaforrásaink a "szimptomáit" reprezentálják. Az első a hálózati fázis feszültségek felharmonikus torzítása, melyek fogyasztói szabályozással, és széles körű aktív és passzív szűréssel igyekeznek orvosolni. A második a fázis feszültség vektorok aszimmetriája, vagy más szóval feszültség aszimmetria, mely a fogyasztók és termelők kiegyszűlyozatlan hálózati eloszlásán alapulnak.

Ez a fontos, ugyanakkor sokszor elhanyagolt energiaminőségi probléma főként annak tudható be, hogy az alacsony feszültségű hálózatok háztartási termelőinek és fogyasztóinak időbeli és topológiai eloszlása véletlenszerű. Ebben a disszertációban egy új indikátor kerül bemutatásra a feszültség aszimmetria detektálására, mely alapul szolgálhat annak kompenzálsára egyaránt, hozzájárulva az áram minőségi kérdés ezen dimenziójához. A dolgozat első fele ennek a jelenségeknek a detektálására, és kompenzálsára helyezi a hangsúlyt. Mindezt egy komplex teljesítményelektronikai struktúra segítségével, mely optimalizációt alapuló szabályozási algoritmussal lett ellátva, mely aszimmetrikus

párhuzamos mintakereső algoritmust (APPS) használ. Ez a struktúra fázisonkénti áram szabályozást alkalmaz, hogy elérje a kiszabott minőségjavulási határértéket. Ezen felül számításokkal alátámasztott, hogy az implementáció jelentékeny mértékben csökkentheti egy átlagos háztartás CO_2 kibocsátását.

A dolgozat második fele magára az áramszabályozási aspektusra fókuszál. Ennek során egy teljesítményelektronikai berendezés Kirchoff egyenlet rendszerét modell alapú prediktív szabályozás alanyaként használtam fel, a hatékonyúság és a számítási kapacitás kritériumának jegyében. Ez egy áramvezérelt szaggató, korlátos, optimális szabályozásának létrehozásával lett elkezdve, matematikai modellje Clarke és Park koordináta rendszerben került felírásra. Ezt a modellt alapul véve, emellett a rendszert érintő korlátozásnak eleget téve, egy explicit modell alapú prediktív szabályozó került megtervezésre. Itt modell differencia egyenleteinek letisztultsága ellenére, az alárendelt bilinearitás további szabályozótervezési komplikációkhöz vezetett volna. A tervezési nehézségek és ezáltal az egyenlet rendszer bilinearitásának feloldására, egy egyen és váltó áramú oldalt szétcsatoló alkalmazás lett megvalósítva, felhasználva az AC és DC oldal időállandó-beli különbözőségét. Ennek eredményeképp aktív szűrés került implementálásra az AC, míg explicit modell alapú prediktív szabályozás lett megvalósítva a DC oldalon. Az eredmények szimulációs környezetben kerültek összehasonlításra egy állapotvisszacsatoláson alapuló szabályozás teljesítményével.

Abstrakt

List of contents

1	Introduction	1
2	Voltage unbalance indication	4
2.1	Literature overview	4
2.2	Definitions of voltage unbalance	6
2.2.1	Phenomena of voltage unbalance	7
2.2.2	Types of voltage deviations and norms	8
2.2.3	Non standardized approximation formulas	8
2.2.4	LVUR	9
2.2.5	PVUR	9
2.2.6	VUF and CVUF	10
2.3	Proposed geometrical indicator	12
2.4	The method's novelty compared to VUF	12
2.5	Summary	15
3	Voltage unbalance compensation	18
3.1	Literature overview	18
3.2	Power electronic components for current control	19
3.2.1	Galvanic decoupled bi-directional DC-DC converters . .	19
3.2.2	Current source inverters	20
3.3	Asynchronous parallel pattern search	22
3.4	Unbalance compensation with asym. inverter	25
3.4.1	Network structure	25
3.4.2	Problem statement	25
3.4.3	Control problem	26
	Asymmetrical inverter structure	27
	Measurements from a real unbalanced network	29
3.4.4	Optimization based control algorithm	30
3.5	Discussion	32
3.5.1	Dynamical simulation based experiments	32
3.5.2	Performance analysis	32
	Robustness analysis	33
3.5.3	Environmental effect	33
	Power loss reduction on the network	33
	CO ₂ footprint	34
3.6	Conclusion	35

3.7 Notations used in the chapter	37
4 Explicit predictive current control	38
4.1 Literature overview	38
4.2 Three-phase buck-type rectifiers	39
4.2.1 Coordinate transformations	43
Clarke transformation	43
Park transformation	43
4.3 Model based predictive control	44
4.3.1 Quadratic optimization and predictive control	44
Receding horizon control	51
Stability of MPC	53
4.4 Predictive control of a CSR	55
4.4.1 Modeling	55
Mathematical modeling of the CSR	55
Model simplification	57
Control structure	58
4.4.2 Control	59
DC-side explicit model predictive control	59
Active AC-side damping	62
4.4.3 Modulation	64
4.4.4 Discussion	67
Lyapunov stability	67
Computational effort	67
Horizon performance	69
Simulation results	69
Comparison with a state feedback control	69
4.5 Conclusion	72
4.6 Notations used in the chapter	73
5 Thesis and Summary	75
5.1 Summary	75
5.2 New scientific results	76
5.3 Applications and future work	78
5.3.1 Geometrical voltage unbalance norm	78
5.3.2 Voltage unbalance reducing inverter structure	79
5.3.3 Explicit model predictive control for buck-type rectifier .	79
5.4 Geometric approach to multi parametric programming	80
5.4.1 Storage of critical regions	84
5.5 Notations used in the appendix	85
5.6 Abbreviations	86

Chapter 1

Introduction

Growth of distributed generation from renewable energy sources and the nature of the electrical power grid initiated a trend to alter from a passive network to an active one. So called smart grids have the ability to provide much more in depth observable measurement results of their customers, grid operators and energy traders alike. Through voltage and current measurements, the habits of each actor (household, station, or industrial-commercial facility) can be easily mapped and taken into account. Moreover, the potential failure could be indicated and preemptively acted upon, before irreversible malfunction, significant amount of wear, or generally, the efficiency of energy consuming actor's power electric consumer's diminishes. In most cases, only smart metering is present, whilst central control and measurement is not an option.

In this new environment, the importance and difficulty of maintenance and operational stability and cost effective control of the distribution system are increasing together. With this in mind local solutions are the most convenient solutions, and as opposed to this expectation most of a household's possible renewable sources and loads are unevenly distributed, without mindful control over single phase power converters. Some of these could represent an unevenly high power consumption, or worse a locally significant energy source in times where it's most unnecessary, especially outside peak zones of consumption. The situation is further exacerbated by the stochastic on/off switching of the different types of loads. This cause stochastic disturbing unbalance in the load currents which cases unbalanced load of the low voltage transformer, and amplitude- and phase unbalance in the voltage phasor trough the serial impedance of the low voltage transportation line wires and connecting devices cables.

If we observe the opposite side, ideal generators supply symmetrical three-phase sinusoidal positive sequence voltages, which are balanced in terms of their amplitudes phase differences at a single frequency. With this in mind voltage (as such consumption- and production-) unbalance occurs on the network. The terminology of unbalance can be divided into amplitude unbalance, phase difference unbalance, and unbalanced harmonic disturbance. The occurrence of at least one of these features is enough for a distribution network to

become unbalanced.

Many countries have changed their regulating laws about power supply to allow for grid-tie inverter systems to provide spare power from renewable sources to local low voltage grids. The unbalance of the grid is further increased by using single phase grid tie inverter systems in the size of typical small household power plants (1 - 50 kW) and the produced electrical power originating from renewable power source (wind and solar) also admits stochastic behavior. This unbalance yields to a suboptimal operation of low voltage three phase transformers and machines to generate undesirable additional yield loss and increase in the probability of malfunction of the low voltage energy transportation system's components, or the effective current unbalance could cause additional power loss of the transportation line resistances or in the end complete shutdown.

To mitigate or avoid such situations an approach is required, where the system where aforementioned phenomena occurs is an optimization problem. However to formulate an optimization problem, many things should be established to formulate it properly. Most importantly, a cost function should be established which can be served as a measure of goodness for solving the question. For instance, if voltage unbalance would be eliminated, than the correct indicator of unbalance should serve as basis, moreover the deviation from the optimum could be quadratic.

Such tasks can not be achieved without proper instrumentation. To be able to apply control, where the voltage levels are designated, and the end user has no direct control (only the plant or transformer level has such), deviations can be addressed, and current control can be used as actuation. This way a control structure can be imagined for a power electric converter, where every step should count towards the optimum state, with respect to the energy (or control reserves), wear of the device (sub components, namely gates have finite switching capabilities), and safety constraints (designated level of current and voltage should not trespass a given hard constraint for the sake of malfunction avoidance, and soft constraint for the sake of reducing wear). Additionally it should not be forgotten, that with all the above, the device should operate in the domains of kHz or above, and it should be run on a cheap device, like an embedded micro-controller chip or digital signal processor (DSP). With all this in mind a power electric structure can be designed to fulfill the high standards of today's requirements. The problem is, conventional controllers can not achieve all this requirements. The methodology based on optimal control, was originally designed for highly complex, and safety critical systems, with huge amount of inputs and outputs, power plants, and chemical- or refinery plants. These systems though, have an incomparably lower time constant, which renders conventional model based predictive controllers useless in the domain of power electronics.

To marry the two approaches together, a solution came up from the automotive industry. A car is also a highly safety critical multiple-input, multiple-output (MIMO) system with obvious constraints, in increasingly changing environment. The main point is, to map the state and input space of the environment,

significantly reducing calculation demands based on the system complexity. Where constraints are present, finite states can be defined, either by hand (e.g. state machines) or by advanced mapping algorithms, and then in every state of operation, a relatively simple (linear if possible) rule where one state of the system dynamics could be substituted, then to make sure stepping on to the next most applicable rule can be achieved very fast. This way, by choosing the resolution of the mapping correctly (too fine resolution gives too high processing requirements, too low gives suboptimal dynamics), the predictive control approach can be applied in both worlds.

In this thesis..

Chapter 2

Voltage unbalance indication

In this chapter the basic topics of the thesis are discussed, as components for further understanding. First the phenomena of voltage unbalance on small distribution networks are shown and the ambiguities though the development of the concept, and at the end the norm currently being in use in the industry. It would be shown how many definitions are currently in use, thus the introduced ambiguity of definition, further validating the proposal in section (2.3). After the introduction the proposed geometrical indicator and control cost-function candidate, shall be discussed and compared against the standardised method, the voltage unbalance factor, VUF via correlation investigation.

2.1 Literature overview

Single phase power injections to the grid are mainly generated by domestic photovoltaic-(PV) and wind power plants. For off-grid, sometimes more complex solutions integrating diesel generators, PV and wind generators. Such as proposed, in [1], and [2], where presented the economical aspects of a PV system. The economic results are strongly influenced by the annual average isolation value, which encourages the areas most exposed to the sun and the southern areas. The consumption of consumers is not critically important, but the design principle used has as significant effect on the maximization of the performance of PV plants. In the paper [3] it is worth noticing, that autonomous photovoltaic systems are strongly responsible of their reactive energy requirements. To support photovoltaic systems with sufficient battery banks one should be able to establish that their reactive energy requirement share fairly compensated by the corresponding energy yield. Additionally, in [4] the author emphasizes that PV systems are increasingly being deployed in all over the world, and this is the source of a wide range of power quality problems. With a view on consistently measuring and assessing the power quality characteristics of PV systems, they had presented an in-depth overview and discussion of this topic.

The study [5] explored implementation issues of electric vehicle battery packs. They suggest that high voltage battery packs with large format cells has advantages in assembly, thermal management, monitoring and control, services

and maintenance. On the other hand, quality, reliability and limited specific energy of large format cells are obstacles need to overcome. Solving these problems will further affect the cost, performance, reliability and safety of the electric vehicles. Smart energy systems in specially in urban areas are discussed in [6] where a design methodology has been suggested.

Many power systems, voltage parameters change over time. Variation of power quality leads to thermal transients in electrical machines. This problem can be especially important in the case of low-power machines, because they have shorter time constants than high-power ones. The rate of thermal responses of a machine also significantly depends on the type of power quality disturbances. Voltage unbalance can cause machine overheating within a mere few minutes. Furthermore, fluctuating unbalance could cause an extraordinary rise in windings temperature and additional thermo-mechanical stress. Consequently, voltage unbalance is found to be more harmful to induction motors than the results from previous work [7]. Additionally beside the heat factor, voltage unbalance can cause increased reactive power [8], various copper loss [9] torque pulsation in electric motors [10]. The authors of [11] were discussing the effects of unbalanced voltage on a three-phase induction motor, one has to consider not only negative-sequence voltage but also the positive-sequence voltage. With the same voltage unbalance factor, the status of voltage unbalance could be judged by the magnitude of positive sequence voltage. Also the effect of voltage unbalance has been studied on three-phase four-wire distribution networks for different control strategies for three-phase inverter-connected distributed generation units on voltage unbalance in distribution networks [12]. Here the negative-sequence component and the zero sequence component were studied where unbalance conditions could lower stability margin and increasing the power losses. On the other hand, the adaptive coordination of distribution systems included distributed generation is also an emerging problem as it was discussed by [13]. A small voltage unbalance might lead to a significant current unbalance because of low negative sequence impedance as highlighted in [14]. As such a previous work of [15] a complex control unit has been proposed that is capable of lowering extant harmonic distortion. In the work of [16] the effect of a small domestic (photovoltaic) power plant on the power quality, mainly the total harmonic distortion has been examined. The aim of this work is to examine and compensate three phase voltage asymmetry of the electrical network based on the extended simulation model proposed by [15]. Further control methods were applied for the solution for balancing of the most sensitive with regard to electric energy quality part of power system in [17], minimizing the active power losses, stabilization of three-phase voltages, enhancement of asynchronous machine performance stability and reduction of errors occurring in power consumption measuring circuits.

In many articles the authors presents a different viewpoint of calculating unbalance on the network. [18] showed to assess the harmonic distortion and the unbalance introduced by the different loads connected to the same point of common coupling have been applied to an experimental distribution network. By [19] the focus was to bring out the ambiguity that crops up when we refer

to a particular value of voltage unbalance that exists in the system. By making use of the complex nature of voltage unbalance, the voltage combinations that lead to the calculation of complex voltage unbalance factor could be narrowed down to a great extent. A fast and accurate algorithm for calculating unbalance has been presented by [20]. The magnitudes of zero, positive, and negative sequences are obtained through simple algebraic equations based on the geometric figure, which is also called as 4 and 8 geometric partitions. Also a three-phase optimal power flow calculation methodology has been presented by [21], that is suitable for unbalanced power systems. The optimal algorithm uses the primal-dual interior point method as an optimization tool in association with the three-phase current injection method in rectangular coordinates.

2.2 Definitions of voltage unbalance

In a symmetric three-phase power supply system, three conductors each carry an alternating current of the same frequency and voltage amplitude relative to a common reference but with a phase difference of one third of a cycle between each. The common reference is usually connected to ground and often to a current-carrying conductor called the neutral. Due to the phase difference, the voltage on any conductor reaches its peak at one third of a cycle after one of the other conductors and one third of a cycle before the remaining conductor. This phase delay gives constant power transfer to a balanced linear load.

In general symmetric three-phase systems described, are simply referred to as three-phase systems because, although it is possible to design and implement asymmetric three-phase power systems (i.e., with unequal voltages or phase shifts), they are not used in practice because they lack the most important advantages of symmetric systems. In a three-phase system feeding a balanced and linear load, the sum of the instantaneous currents of the three conductors is zero. In other words, the current in each conductor is equal in magnitude to the sum of the currents in the other two, but with the opposite sign. The return path for the current in any phase conductor is the other two phase conductors.

Constant power transfer and cancelling phase currents would in theory be possible with any number (greater than one) of phases, maintaining the capacity-to-conductor material ratio that is twice that of single-phase power. However, two-phase power results in a less smooth (pulsating) torque in a generator or motor (making smooth power transfer a challenge), and more than three phases complicates infrastructure unnecessarily.

Three-phase systems may also have a fourth wire, particularly in low-voltage distribution. This is the neutral wire. The neutral allows three separate single-phase supplies to be provided at a constant voltage and is commonly used for supplying groups of domestic properties which are each single-phase loads. The connections are arranged so that, as far as possible in each group, equal power is drawn from each phase. Further up the distribution system, the currents are

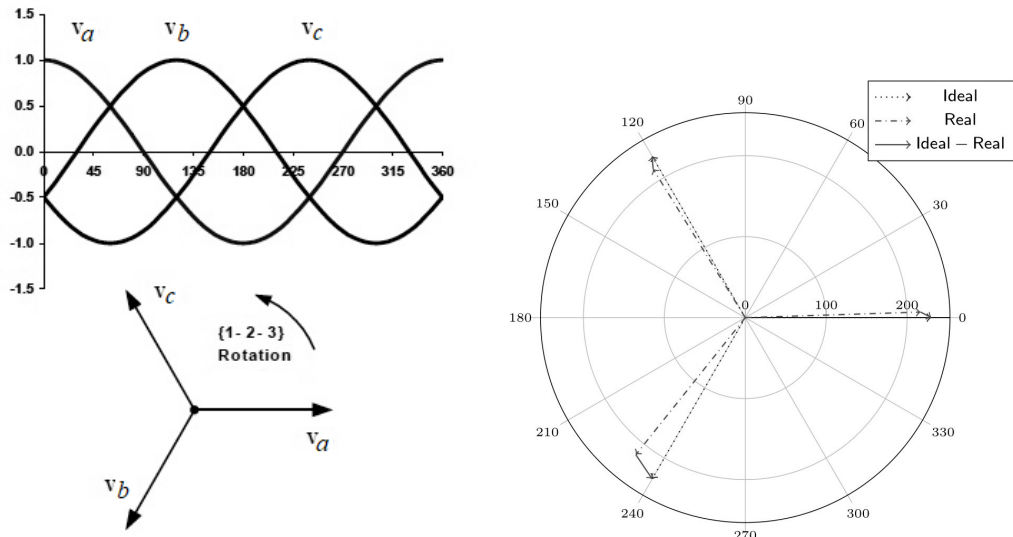
usually well balanced. Transformers may be wired in a way that they have a four-wire secondary but a three-wire primary while allowing unbalanced loads and the associated secondary-side neutral currents [22].

2.2.1 Phenomena of voltage unbalance

In a domestic network, three-phase electric power systems have at least three conductors carrying alternating voltages that are offset in time by one-third of the period. A three-phase system may be arranged in delta or star. A star system allows the use of two different voltages from all three phases, such as a 230/400 V system which provides 230 V between the neutral (center hub) and any one of the phases, and 400 V across any two phases displayed on Fig.(2.1a). The definition is the following:

$$\begin{aligned}\vec{V}_a &= \hat{V} \sin(\theta) \\ \vec{V}_b &= \hat{V} \sin(\theta + \frac{4}{3}\pi) \\ \vec{V}_c &= \hat{V} \sin(\theta + \frac{2}{3}\pi),\end{aligned}\quad (2.1)$$

where \vec{V}_a , \vec{V}_b , \vec{V}_c are the phase voltage vectors, \hat{V} is the voltage peak, and θ is the phase angle. Voltage unbalance a phenomena where the three phase voltages differ in amplitude normal 120 degree phase relationship shown in Fig.(2.1b). In most cases both are happening at the same time. This includes unequal voltage magnitudes at the fundamental frequency, either under, or over voltage, at the fundamental phase angle deviation.



(a) Three phase sine wave of network voltage.
 (b) The three phase voltage phasor with Ideal and Real voltage vectors.

This is observed as a frequently cited power quality issue in low-voltage domestic distribution networks and in systems that supply large single phase loads distributed unevenly among the phases. Effects of voltage unbalance are complex, but can be categorized as structural or functional. The former refers

to the asymmetry in the three-phase impedances of transmission lines, cables, transformers, etc. It occurs because it is neither economical nor necessary to maintain distribution system with perfectly symmetrical impedances. The latter refers to uneven distribution of power consumption over the three phases. Although the term voltage unbalance is unambiguous, the root phenomenon may be various as well as the standard norms used to measure unbalance. All of these different indicators measure voltage unbalance but each of them does it in a different way. In this section a detailed explanation is presented about the types of currently used method for indication.

2.2.2 Types of voltage deviations and norms

Voltage unbalance is not a straightforward term. To understand the concept, unbalance is when on a given frequency (mostly fundamental frequency) voltage vectors (phase or line depending on the definition) deviating from the ideal in terms of length or angle. The first fall in to the category of unbalance, namely any kind of phase deviations, and unbalanced amplitude deviations, and balanced amplitude deviations, like under-voltage. There are many different technological causes with more or less practical importance. The following conditions are examined and tested in the sequel:

Single phase under-voltage unbalance If there is a single phase uncompensated overload in the system, the voltage in the overloaded phase will be lower than the other two.

Two phase under-voltage unbalance Two of the three phases are overloaded without compensation, the two overloaded phases will have higher voltage drop than the third phase. Balanced three phase under-voltage] The loads of all three phases are overloaded in an unbalanced manner.

Unbalanced single phase angle If the three phase voltage amplitudes are balanced but the relative angles between them (ideally it should be equal to ± 120 degree). It is assumed, that V_a would be the reference. If one of the other two phase angles is deflected, unequal displacement.

Unbalanced two phase angles displacement Similar to the single phase angle unbalance, if the other two phase angles are both deflected, then unequal angle displacement in two phase angles occurs.

An indicator of the voltage unbalance is supposed to measure the extent of unbalance but it is not expected to classify between the above types.

2.2.3 Non standardized approximation formulas

Up to now, the following definitions have not been adopted by any standard or rule to indicate the degree of voltage unbalance, but used by various manufacturers. Firstly based on [23] recommended by the CIGRE (International Council on Large Electric Systems, in French: Conseil International des Grands Réseaux Électriques), the voltage unbalance is determined with:

$$VUFactor = \frac{\sqrt{1 - \sqrt{3-6 \frac{V_{ab}^4 + V_{bc}^4 + V_{ca}^4}{(V_{ab}^2 + V_{bc}^2 + V_{ca}^2)^2}}}}{1 + \sqrt{3-6 \frac{V_{ab}^4 + V_{bc}^4 + V_{ca}^4}{(V_{ab}^2 + V_{bc}^2 + V_{ca}^2)^2}}} \quad (2.2)$$

where, $\{V_{ab}, V_{bc}, V_{ca}\}$ are the line-to-line voltages. Note, that the CIRGE variant has no distinct notation, as such it would be indicated as *VUFactor* in this thesis. Moreover, the author of [24] recommends two more variants, based on manufacturer recommended "standards":

$$VU = \frac{82 \cdot \sqrt{(V_{ab} - V_{avgline})^2 + (V_{bc} - V_{avgline})^2 + (V_{ca} - V_{avgline})^2}}{V_{avgline}} \times 100 \quad (2.3)$$

$$VUR = \frac{\max(|V_{ab} - V_{bc}|, |V_{bc} - V_{ca}|, |V_{ca} - V_{ab}|)}{V_{avgline}} \times 100, \quad (2.4)$$

where the mean of line voltages is noted by $V_{avgline} = \frac{V_{ab} + V_{bc} + V_{ca}}{3}$. This formulas were created with the intention to avoid the use of the complex algebra in symmetrical components and give a good approximation of the later described *VUF* standard. With the indicator of (2.3), and as well as (2.4). It is worth noticing, that only the voltage magnitude unbalance is reflected, completely ignoring Fortescue's method of symmetrical components [25] (shall presented later in the thesis), which considers negative sequence components as harmful on electric equipment and yield. Later it will be shown that other methods try to push the same methodology, until the currently used norm (*VUF*) is used.

2.2.4 LVUR

One of the first voltage unbalance in percent is defined by the National Electrical Manufacturers Association (NEMA) [26] is defined as the ratio of the maximum voltage deviation from the average line voltage magnitude to the average line-voltage magnitude.

$$LVUR = \frac{\max(|V_{ab} - V_{avgline}|, |V_{bc} - V_{avgline}|, |V_{ca} - V_{avgline}|)}{V_{avgline}} \times 100 \quad (2.5)$$

The LVUR assumes that the average voltage is always equal to the rated value, which is 480 volts for the US three-phase systems, and it works only with magnitudes. Phase angles are not considered in this definition.

2.2.5 PVUR

The next phase voltage unbalance in percent described in IEEE standard 141. [27] (derived from [28]), is $PVUR_{IEEE-141}$. It is defined as the ratio of the maximum voltage deviation of phase voltages from the average phase-voltage magnitude to the average phase voltage magnitude. In various fields, LVUR

and $PVUR_{IEEE-141}$ are commonly used to estimate the degree of voltage unbalance due to simplicity of calculation. The two unbalance factors mentioned above cannot completely reflect system voltage unbalance effects, such as the phase displacements of unbalanced voltages.

$$PVUR_{IEEE-141} = \frac{\max(|V_a - V_{avg_phase}|, |V_b - V_{avg_phase}|, |V_c - V_{avg_phase}|)}{V_{avg_phase}} \times 100, \quad (2.6)$$

where the voltages $\{V_a, V_b, V_c\}$ denotes the phase-to-neutral voltages, and $V_{avg_phase} = \frac{V_a + V_b + V_c}{3}$. The second variant is, $PVUR_{IEEE-936}$, mentioned in [29] is defined as the ratio of the difference between the highest and the lowest phase-voltage magnitude to the average phase-voltage magnitude. Therefore, the numerical values of voltage balance quantified by $PVUR_{IEEE-936}$ are generally larger than those of $PVUR_{IEEE-141}$ and LVUR.

$$PVUR_{IEEE-936} = \frac{\max(|V_a|, |V_b|, |V_c|) - \min(|V_a|, |V_b|, |V_c|)}{V_{avg_phase}} \times 100, \quad (2.7)$$

The number of possible combinations of three phase or line voltages that satisfy the definitions of voltage unbalance mentioned above will become infinite as only the magnitudes of voltages are considered.

2.2.6 VUF and CVUF

The voltage unbalance factor (VUF) was defined by the International Electrotechnical Commission [30], [31]. From the theorem of symmetrical components [25], voltage unbalance can be considered as a phenomenon that positive sequence voltage (V_p) is disturbed by negative (V_n) and zero-sequence (V_0) voltages:

$$\begin{bmatrix} V_0 \\ V_p \\ V_n \end{bmatrix} = \frac{1}{3} \begin{bmatrix} 1 & 1 & 1 \\ 1 & v & v^2 \\ 1 & v^2 & v \end{bmatrix} \cdot \begin{bmatrix} V_a \\ V_b \\ V_c \end{bmatrix}, \quad (2.8)$$

Where $v = e^{2j\pi/3}$ is the Fortesque operator. From that the formula of VUF can be expressed as:

$$VUF = \left| \frac{V_n}{V_p} \right| \times 100, \quad (2.9)$$

This norm is currently in use world wide for voltage unbalance indication. The main focus is on the negative sequence component V_n , on which many studies attributes importance of the cause of negative effects the voltage unbalance causes.

As such, three-phase electric loads without path through the neutral, negative-sequence voltage is the primary cause of voltage unbalance. Normally, positive-sequence component of three-phase voltages is very close to rated value. If expressed in per-unit quantities, the positive-sequence voltage will be very close to 1.0 p.u., and the corresponding negative-sequence voltage will be very

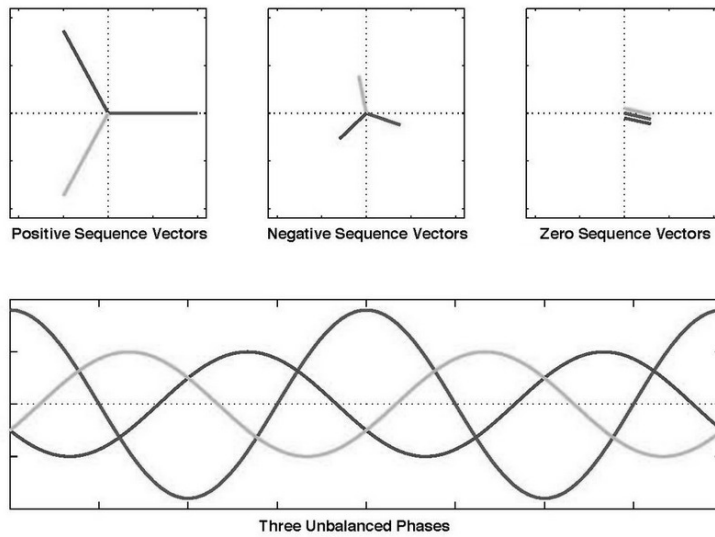


Figure 2.2: Simplified graphical display of symmetrical components.

close to the *VUF*. Thus, the *VUF* can indeed be considered as the negative-sequence component in per-unit. This explains the advantage of using the *VUF* as an index for analyzing the effects of voltage unbalance considering the phase deviations. An extension of the *VUF* is the complex voltage unbalance factor (*CVUF*) that is defined by the ratio of the negative- sequence voltage phasor to the positive-sequence voltage phasor studied in [32], and [33]. The *CVUF* is a complex quantity having the magnitude and the angle. Although the *CVUF* has not yet been widely used by practicing engineers, it has been proposed in some studies (e.g., [34], [35], [36]) due to its richness of information on unbalance. The formula of *CVUF* is similar to *VUF*:

$$k_v = \frac{V_n}{V_p} = k_v \cdot e^{j\theta_v} = k_v \angle \theta_v, \quad (2.10)$$

where k_v is the magnitude and θ_v is the angle of *CVUF*.

It can be observed, that the previously mentioned norms (2.2), (2.3), (2.4), (2.5), (2.6), (2.7), and (2.9) indicate different values for a single case with various correlations. The first two standard indicators, $PVUR_{IEEE-936}$ and $PVUR_{IEEE-141}$, ignore the ± 120 degree phase difference unbalance and only take the amplitudes into account. Additionally, the zero-sequence components never present in the line-to-line voltages regardless of the level of unbalance, only phase-to-neutral voltages. It has been proven, that these components are unelectable in some cases like bridge control of converters [37], or synchronous machine diagnosis [38].

The actual state of the art definition in use, *VUF*, is sensitive to the phase difference unbalance. Lastly *CVUF* considers also phase and magnitude of the voltage unbalance, but the two units are hard to merge together as the optimization cost of a cost function. Moreover, these definitions ignore zero sequence components and harmonic distortion that are always present in three-phase four-wire systems [14].

2.3 Proposed geometrical indicator

As discussed in section 2.2.2, the indicators of voltage unbalance result very different measures for the same circumstance. Additionally most of them are neglecting the phase differences of voltage vectors compared to the ideal, and even the currently used *VUF* calculated by (2.9) is not taking zero sequence components from the Foresque method [25]. There were attempts to close the gap with the CVUF norm shown in (2.10), where the complex component is also considered, but this makes this a clumsy candidate for control design, since two components (real and complex part) shall be weighted and applied. This begs the question, how could voltage unbalance be measured loss-less, but resulting one (conveniently quadratic-like) value, easily applicable for optimization algorithm.

Hence can be stated that every difference between the ideal and the measured voltage in both amplitude phase and sub-harmonics causing a form of voltage deviation. The problem can also be investigated from a geometrical point of view as it is depicted in Figure (2.3). The three-phase voltage system's phasor diagram contains three phase-to-neutral voltage vectors which can be regarded as the points of a triangle (similarly, the three line-to-line vectors can play the role of the edges of the triangle). The two triangles (i.e. the ideal and the actual ones) always intersect except from very extreme and physically meaningless cases. The area where the two triangles do not cover each other (i.e. the difference of their union and intersection) can be used as a norm of voltage quality. In fact it is computationally more demanding compared to the previous methods, but takes every deviation into consideration [P1],[P2]. The calculation of error is given by (2.11).

$$G = \text{Area of } (\Delta_{\text{Ideal}} \cup \Delta_{\text{Real}} - \Delta_{\text{Ideal}} \cap \Delta_{\text{Real}}), \quad (2.11)$$

Δ_{Ideal} indicates the triangle spanned by the ideal voltage vectors and Δ_{Real} the triangle of real voltage vectors. Difference of the ideal and the real triangle's union and intersection defines the norm G . Basically, the algorithm calculates the symmetrical difference of the triangles, stretched from three phase ideal and real voltage vectors.

2.4 The method's novelty compared to VUF

When using a new norm for calculation and cost function it is reasonable to test its usability against the prevalent or regulated method the voltage unbalance factor (*VUF*) defined by the International Electrotechnical Commission, as discussed in section 2.2.6. In this case the geometrical norm's utility (2.11) against the *VUF* value shall be examined.

The geometrical norm was validated experimentally, by investigating the correlation between the regulated and geometrical norms subjected to random, uniformly distributed unbalance on the voltage vector amplitude and phase values with 20 V amplitude and $1/300 \cdot \pi$ rad phase variance (Fig. (2.4), and Fig. (2.5)).

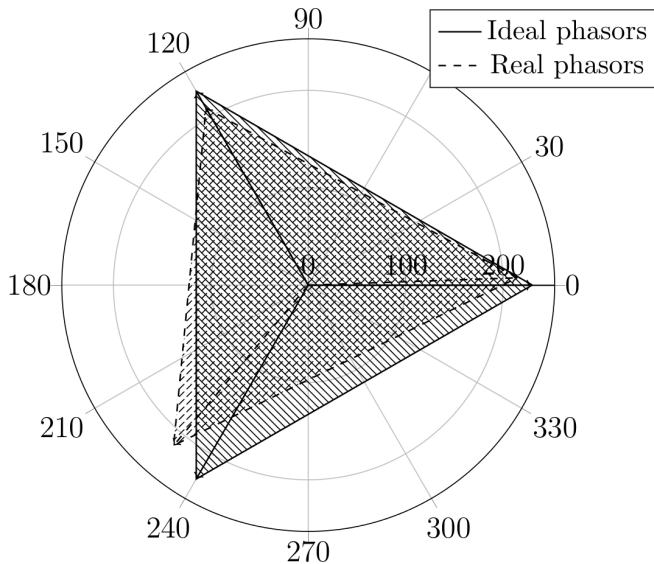


Figure 2.3: The triangles spanned by the ideal and the actual voltage phasors. The extent of voltage deviation on the network can be measured by the sum of areas where the two triangles are not overlapping.

Although there is correlation between the two norm values in the general case, but for some situations the regular method indicates low, while geometrical norm still indicates high value.

On Figure (2.6a) dominant phase deviation can be observed, while Figure (2.6b) shows amplitude deviation but with opposite direction. When there is such deviation on the grid both indicators present almost identical results. On (2.6c) there is still observable unbalance (two phase deviate stronger than the third in terms of amplitude), but the correlation is significantly lower. In the last case in the lowest correlation area, amplitude deviation is present, but the deviation direction is identical on all phases (balanced over-voltage or under-voltage, can be observed on Figure (2.6d)). The regular method indicates very low values. In this case other methods are utilised in parallel in terms of network diagnostics to detect the under-voltage phenomena.[39].

To clarify this, the regular norm's calculation method needs to be investigated. The symmetrical component mutual impedance matrix on a three phase connection point is given by (2.12),

$$\begin{aligned}
 Z_s &= \frac{1}{3} \begin{bmatrix} 1 & 1 & 1 \\ 1 & v & v^2 \\ 1 & v^2 & v \end{bmatrix} \cdot \begin{bmatrix} Z_{aa} & Z_{ab} & Z_{ac} \\ Z_{ba} & Z_{bb} & Z_{bc} \\ Z_{ca} & Z_{cb} & Z_{cc} \end{bmatrix} \cdot \begin{bmatrix} 1 & 1 & 1 \\ 1 & v^2 & v \\ 1 & vv^2 & v \end{bmatrix} = \\
 &= \begin{bmatrix} Z_{00} & Z_{01} & Z_{02} \\ Z_{10} & Z_{11} & Z_{12} \\ Z_{20} & Z_{21} & Z_{22} \end{bmatrix},
 \end{aligned} \tag{2.12}$$

where Z_s is the symmetrical component mutual impedance matrix, and $v = e^{j\frac{2}{3}\pi}$. If there are both negative and zero sequence symmetrical components

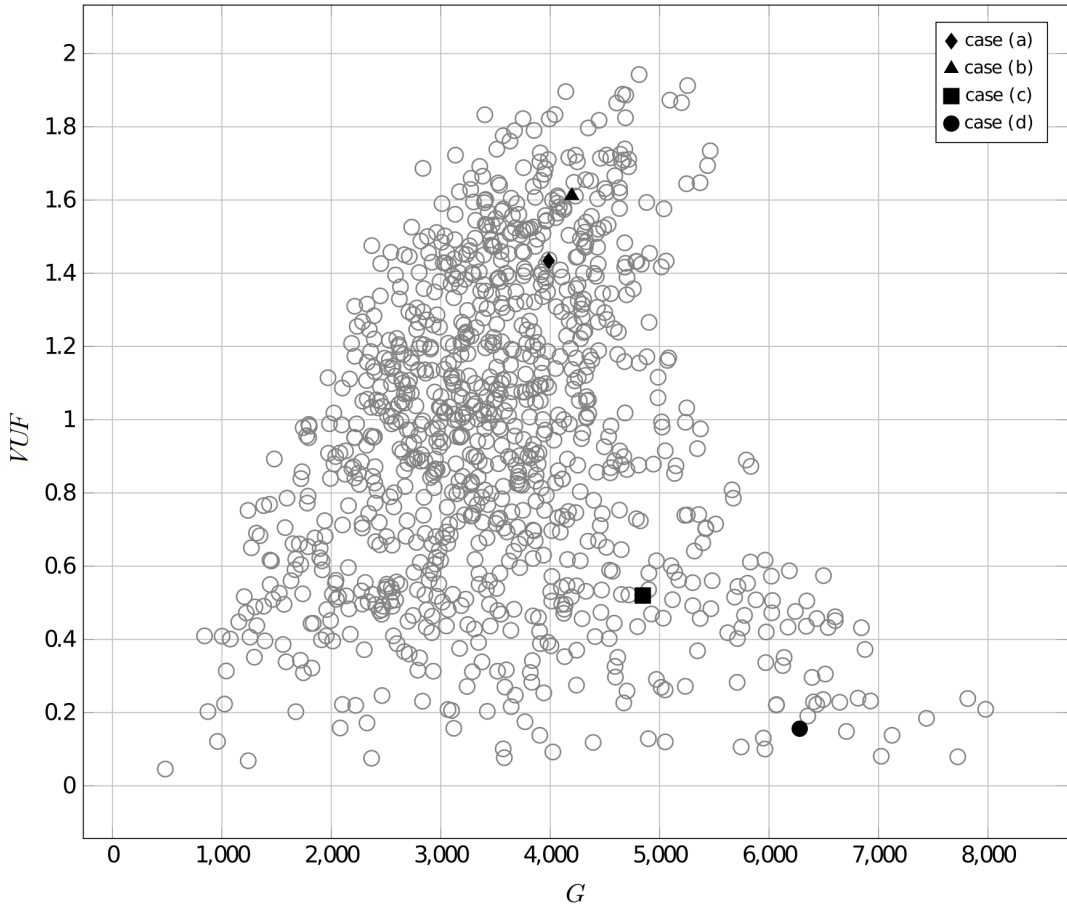


Figure 2.4: Correlation between the geometrical voltage unbalance indicator G and the regulated voltage unbalance indicator VUF using 1000 samples. In every iteration each three phase voltage vector's amplitude and phase values changed randomly, according to uniform distributions with ± 20 V amplitude and $\pm \frac{1}{3}\pi \cdot 10^{-2}$ rad phase variance. It can be seen, that the geometric norm contains more information than the classical one. The four asymmetry cases of Figure (2.6) are denoted by black symbols on the picture. It is apparent, that in case (c), and (d) the G norm holds additional information than the VUF .

present on the network, the dominant part of the voltage drop's negative and zero sequence can be calculated as follows (2.13).

$$\begin{aligned} \Delta U_2 &\approx Z_{21}I_1 + Z_{22}I_2 \\ \Delta U_0 &\approx Z_{01}I_1 + Z_{00}I_0, \end{aligned} \quad (2.13)$$

ΔU_0 , ΔU_1 , ΔU_2 are the voltage drop's zero positive and negative sequence components, I_0 , I_1 , I_2 are the current's drop's zero positive and negative sequence components, and Z_{00} , Z_{01} , Z_{21} , Z_{22} are mutual impedances, respectively. (If there is only positive and negative sequence present, then the right hand side's second term is zero.) As such, the indication of negative and zero sequence present the network calculates (2.14):

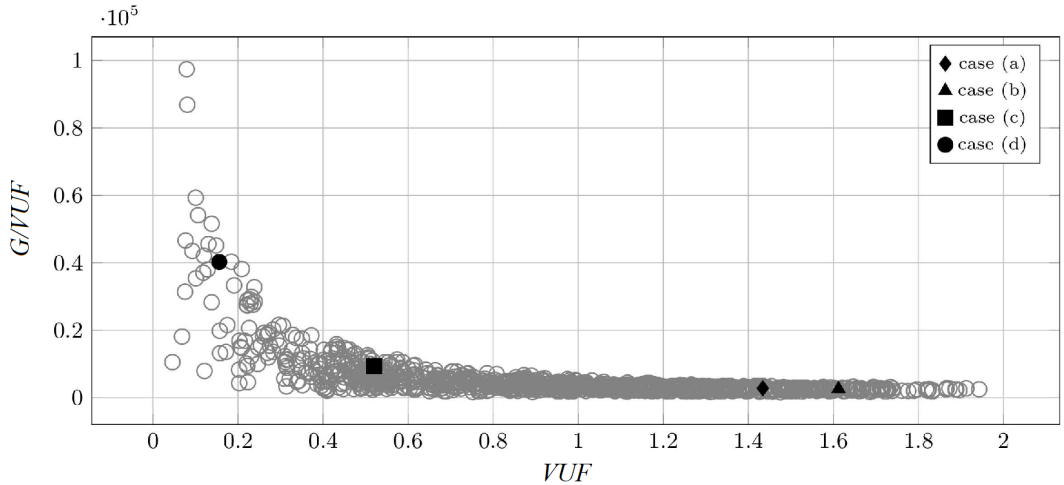


Figure 2.5: Correlation between the regulated unbalance indicator and the fraction of geometrical and regulated indicator. It can be seen that there is a functional connection between the two values.

$$\begin{aligned} m_{21} &= \left| \frac{Z_{21}}{Z_{11}} \right| \times 100 \\ m_{01} &= \left| \frac{Z_{01}}{Z_{11}} \right| \times 100, \end{aligned} \quad (2.14)$$

where m_{21} is the negative sequence factor which is identical to the VUF , and m_{01} is the zero sequence factor.

2.5 Summary

At the previously described balanced over- or under-voltage case the positive sequence value is dominant, so the regular indicator will take considerably lower value. In other words, aside from indicating voltage unbalance, the geometrical method incorporates the balanced deviations as well. In a control design perspective, a general case, where notably highly unbalance values may appear, using VUF as cost function could introduce hidden errors in control due error cancellation. Additionally the geometrical solution checks electrical asymmetry, i.e. the norm of a ± 120 degree rotated version of the ideal three-phase phasor is zero in the geometrical sense. Moreover, the geometrical norm is more sensitive for small scale unbalance, as opposed to the VUF . To summarize, the geometrical indicator a more suitable solution for a more general case indicator, and a good candidate for cost function in optimal control design.

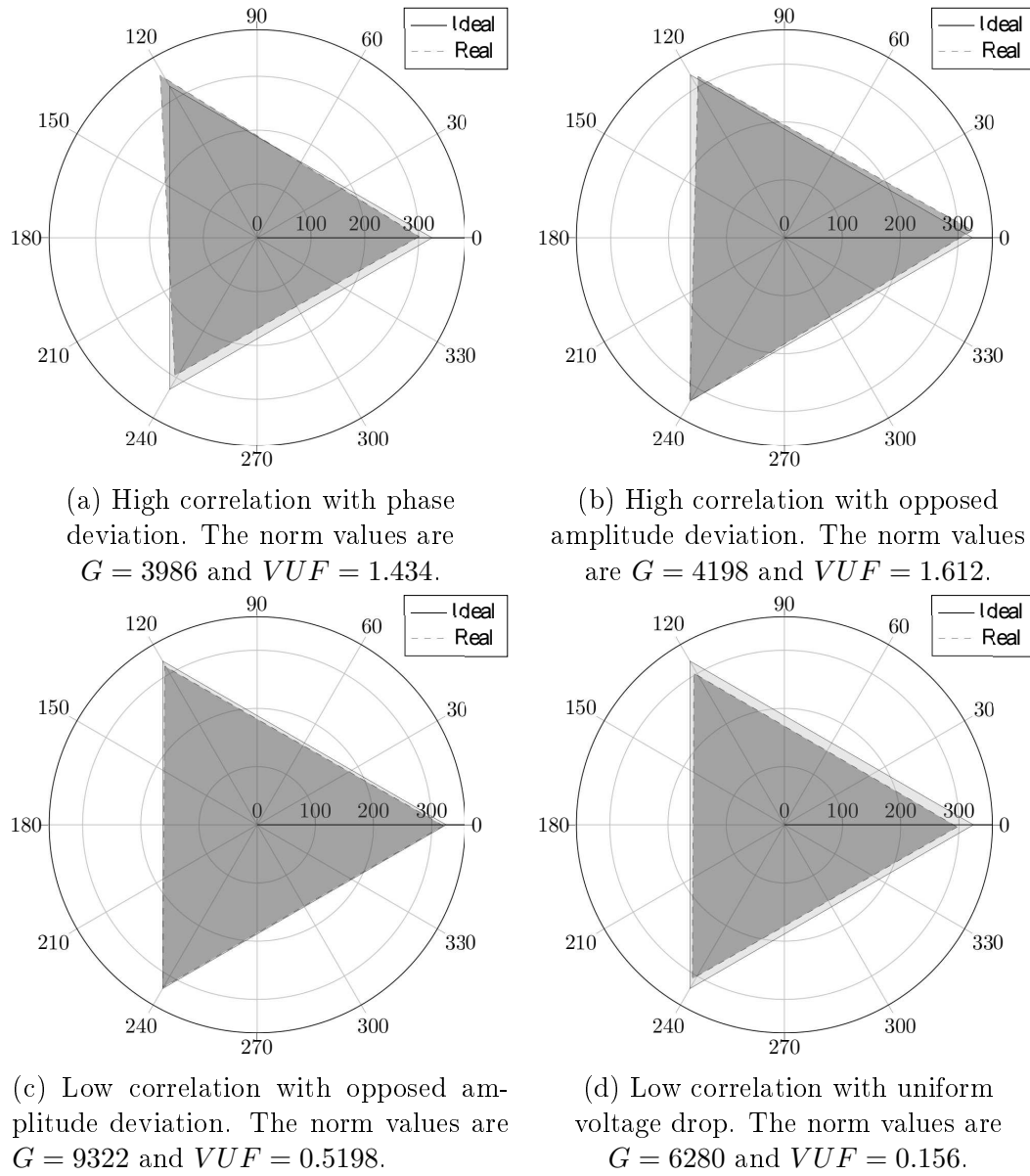


Figure 2.6: Four distinct cases of voltage triangles examining correlation between the regular VUF and geometrical G method.

Notations used in the chapter

$CVUF$	Complex Voltage Unbalance Factor
G	Geometrical voltage unbalance indicator
$I_{0,1,2}$	Zero positive and negative sequence of current drop
k_v	Magnitude of CVUF
$LVUR$	Voltage unbalance notation based on NEMA standard
m_{21}	negative sequence factor, identical to VUF
m_{01}	zero sequence factor
$PVUR_{IEEE-141}, PVUR_{IEEE-936}$	Voltage unbalance notation based on IEEE-141, and IEEE-936 standard
V_{ab}, V_{bc}, V_{ca}	Line-to-line voltages
$V_{avgline}$	Average of line voltages
V_a, V_b, V_c	Phase-to-neutral voltages
$V_{avgphase}$	Average of phase voltages
V_0, V_p, V_n	Zero, negative and positive sequence voltages based on symmetrical components theorem
\hat{V}	Voltage peak
$\vec{V}_a, \vec{V}_b, \vec{V}_c,$	Voltage vectors in the three phase phasor
VUF	Voltage Unbalance Factor
$VUFactor, VU, VUR$	Non standardized voltage unbalance factor based on manufacturer standards
Z	Symmetrical component mutual impedance
ΔU	Zero positive and negative sequence of voltage drop
θ	Angular displacement of the voltage or current vector
θ_v	Angle of CVUF
v	Fortesque operator

Chapter 3

Voltage unbalance compensation with geometrical indicator on a domestic low voltage network

3.1 Literature overview

There are different approaches of lowering the unbalance with different control techniques. Additionally, new computationally efficient control techniques have been presented by [40] to estimate and compensate input voltage unbalance (VU) disturbances for a voltage source converter. These tools are designed to be effective with high power systems with slower PWM switching frequencies of 5 kHz or lower and limited current-controller bandwidth. About the unbalance compensation control aspect, a three-phase IGBT-based static synchronous compensator were proposed for voltage and/or current unbalance compensation by [41]. An instantaneous power theory was used for real-time calculation and control. Three control schemes current control, voltage control and integrated control were proposed to compensate unbalanced voltage, unbalanced current or both. Unbalance phenomena and power quality can be examined with modeling too. A particular modeling method was presented by [42], where a three-phase four-wire grid-interfacing power quality compensator were modeled. During voltage unbalance, the compensator, used a shunt with a series four phase inverter, could enhance both the quality of power within the microgrid and the quality of currents flowing between the microgrid and utility system. In this case a microgrid is a group of interconnected loads and distributed energy resources within clearly defined electrical boundaries that acts as a single controllable entity with respect to the grid. A microgrid can connect and disconnect from the grid to enable it to operate in both grid-connected or island-mode. The shunt four-leg inverter were controlled to maintain a set of balanced distortion free voltages to regulate power sharing among the parallel-connected distributed generation systems. Simulation studies were carried out by [43] where one of the aims was to develop and test the feasibility of a de-coupled three-phase on-load tap charger in the distribution system with the objective of improving the distribution network power quality. Further con-

trol methods were applied for the solution for balancing of the most sensitive with regard to electric energy quality part of power system by [17], minimizing the active power losses, stabilization of three-phase voltages, enhancement of asynchronous machine performance stability and reduction of errors occurring in power consumption measuring circuits.

In the arsenal of voltage unbalance compensation, current source power electronic devices have a dedicated position. Based on the instantaneous active power theory under unbalanced grid conditions [44] proposes an optimized negative-sequence current references for eliminating the double-frequency oscillations on active power at AC side of a current source converter. The author argues in [45] that a classification of the virtual impedances can greatly benefit an unbalance compensating control structure, with an active stabilization method. In [46] direct control strategy with detailed current converter model is shown which is much simpler than the complicated instantaneous power theory approach. This solution needs less voltage and current sensors for the feedback control, which means that it is a cost-effective solution. An interesting, yet similar approach compared in the paper if a bi-directional current source topology is used like in [47]. This enables to compensate a much larger degree of freedom handing unbalanced conditions with the precaution of unstable operation possibilities.

3.2 Power electronic components for current control

As the introduction suggest the main topic of the thesis is optimal current control. As such for reaching the desired optimum, the necessary actuators are needed for the task. For this, power electric converters are used, all of them based on a simple principle, namely they use controllable switches to set the required voltage level or the conducting current value, required on the load's end.

3.2.1 Galvanic decoupled bi-directional DC-DC converters

In this section a basic galvanic decoupled voltage source DC-DC converter shall be presented. In many DC power supplies, a galvanic isolation between the DC or AC input and the DC output is required for safety and reliability. An economical mean of achieving such an isolation is to employ a transformer version of a DC-DC converter. High-frequency transformers are of small size and weight and provide high efficiency. Their turns ratio can be used to additionally adjust the output voltage level. Generally, electric power generated by renewable energy sources is unstable in nature, thus producing an unwanted effect on the utility grid. This fact motivates research on energy storage and quality systems to smooth out active-power flow.

On the converter Fig.(3.1) has two symmetrical single-phase voltage-source full-bridge converters, allowing a bi-directional power flow. Thanks to advancement in power device technology over the last decade the DC-DC devices are able to operate at an efficiency as high as $\approx 97\%$ by using the latest trench-gate IGBTs. Therefore this topology has become a promising candidate as a power electronic interface for an energy storage and renewable system [48] [49].

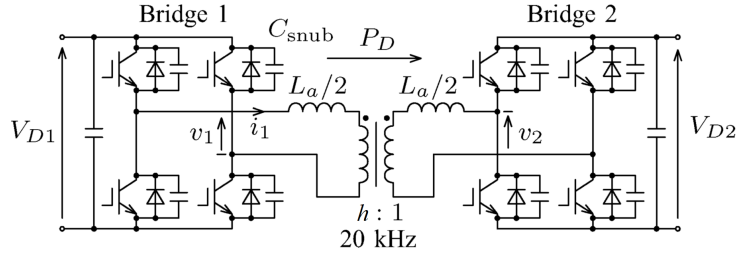


Figure 3.1: Bidirectional isolated DC-DC converter, where V_{D1} , and V_{D2} are the two end's voltage (in- and output depends on the power flow), v_1 and v_2 are the transformer voltages, C_{snub} are to reduce switching loss and to damp out over-voltage, and h is the transformer turn ratio.

The principle of operation of the DC-DC converter is very simple. Two active bridges are interfaced through a transformer and are phase shifted from each other to control the amount of power flow from one DC voltage source to the other. This allows a fixed frequency, square-wave mode of operation and utilization of the leakage inductance of the transformer as the main energy transfer element. The power transfer under idealized conditions is defined as:

$$P_D = \frac{V_{D1}V_{D2}}{\omega L_a} \left(\delta - \frac{\delta^2}{\pi} \right) \quad (3.1)$$

where $\omega = 2\pi f$ is the switching angular frequency of the two single phase full bridge controllers, L_a is the sum of the transformer leakage inductance.

3.2.2 Current source inverters

Single-phase inverter's operating principles are different in each converter. The main features of the different approaches are reviewed and presented in the following. Although these converters cover the low-power range, they are widely used in power supplies or single-phase supplies. For this thesis a domestic current source inverter is considered, which fits into this category. A current source inverter is composed of capacitors, switches, and diodes, where an array of two switches is called inverter leg shown in Fig.(3.2). The capacitors required to provide a neutral point, such that each capacitor maintains a constant voltage.

The inductors required are large, such that the inductors maintain a constant current i_i . Current-source topologies feature a low switching voltage gradient and reliable over-current or short-circuit protection. In order to op-

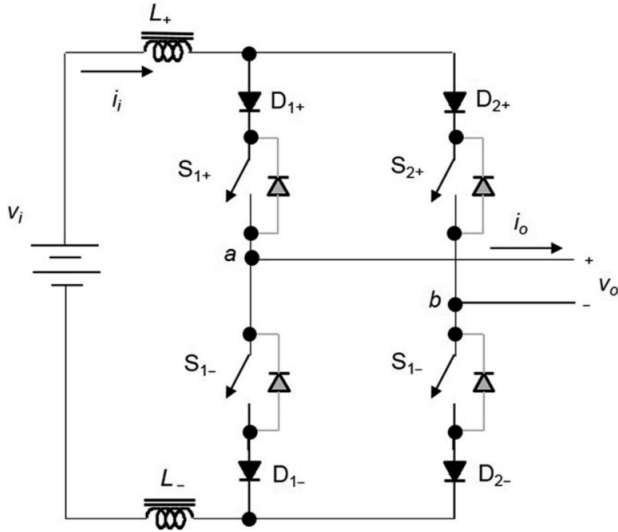


Figure 3.2: Topology of a singly phase current source inverter, where V_i , and V_o are the input and output voltages, i_i , and i_o are the input and output currents respectively. L_+ and L_- are current filter inductances, S_{1+} , S_{2+} , D_{1+} , and D_{2+} are the higher switches (controlled IGBTs for instance) and diodes, and S_{1-} , S_{2-} , D_{1-} , and D_{2-} are the lower switches and diodes respectively.

erate properly the current-source inverter, we need to adhere to the following rules:

- Top or bottom switches of the different legs cannot be off simultaneously, because no current path is provided to the input inductors.
- Diode must be placed in series with each switch, because a short circuit across the output voltage V_o would be produced. If the commercial switch does not include anti- parallel diodes, then the circuit is already complete.
- In practical implementation, an overlapping time must be considered in the control signals of the top or bottom switches of the different legs.

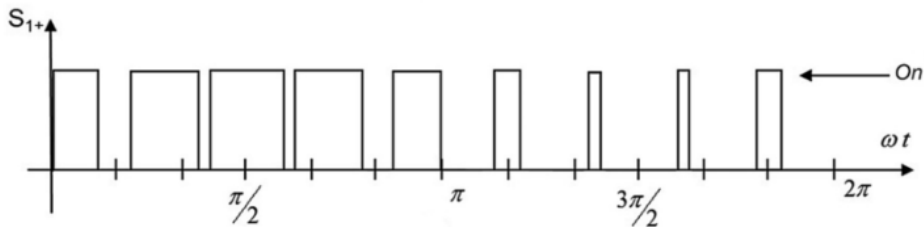
According to the previous rules, it should be noticed that all switches of the inverter leg can be turned on at the same time. This is not possible in voltage source inverters. There are four (1^{st} to 4^{th}) defined states of the switches and one not permitted switching state (5^{th} state) as shown in Table (3.1). The modulating technique should always ensure that at any instant, at least one of the top and bottom switch of the inverter legs is on, otherwise the inverter will be damaged.

The ideal waveforms are shown in Fig.(3.3).

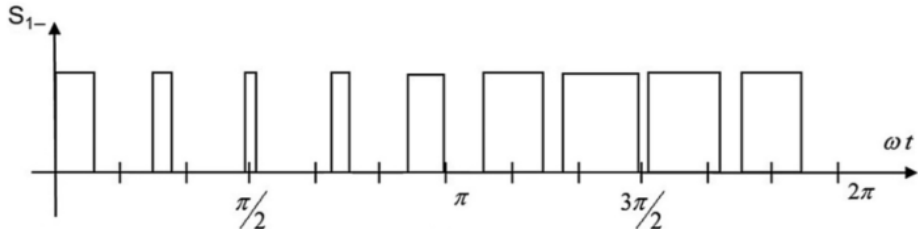
The states for the switches are defined by the modulating technique, which in this case is a carrier-based PWM, but unipolar output is considered. For the CSIs, different output filters may be employed, in order to provide the fundamental component of the output waveform. Depending on the application, it would be desirable to provide a voltage or current output.

Table 3.1: Switching states of the current source inverter, where V_{an} , V_{bn} are the a and b point's potential to ground.

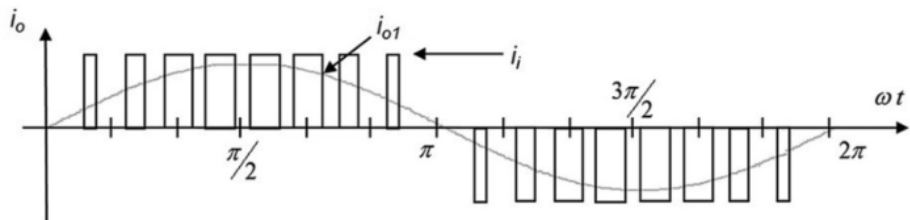
Components conducting				State	Output voltages		
S_{1+}	S_{2+}	S_{1-}	S_{2-}		V_{an}	V_{bn}	V_o
1	0	0	1	1	$V_i/2$	$-V_i/2$	V_i
0	1	1	0	2	$-V_i/2$	$V_i/2$	$-V_i$
1	1	0	0	3	$V_i/2$	$V_i/2$	0
0	0	1	1	4	$-V_i/2$	$-V_i/2$	0
0	-	0	-	5	Not permitted		
-	0	-	0				



(a) The state of switch S_{1+} .



(b) The state of switch S_{2+} .



(c) AC output current.

Figure 3.3: The CSI, ideal waveforms as the result of the modulation.

3.3 Asynchronous parallel pattern search

In the following section, the applied control structure, namely the APPS algorithm shall be discussed in detail. They commonality in this work, is that all of them are designed to search for the optimal control input for a current governing system, should it be voltage unbalance reduction with no applicable network model (due the actors unpredictability), or reaching the fastest reference value with explicit predictive control with the converter's

equation's considered, which shall be discussed in section (4.3.1).

The APPS can rather be described as a linear search program, distributed in a multi-dimensional plane, where it is only a black box model available [50]. These variants of pattern search can solve nonlinear unconstrained problems of the form of:

$$\min_{x \in \mathbb{R}^n} f(x), \quad (3.2)$$

where $f : \mathbb{R}^n \rightarrow \mathbb{R}$. We assume that the evaluation of f is computationally expensive, hence our interest in using either distributed or parallel computing environments to solve the problem. It needs to be concentrated on the parallelization of the search strategy, rather than on the evaluation of f , though the techniques we discuss here can be adapted to handle problems for which the computation of f also can be distributed. Additionally it is assumed that f is continuously differentiable. It can be assumed that the gradient ∇f is unavailable, but the method is applicable as presented in section 3.4.4, where the gradient determines the direction of the next step, further increasing its efficiency. For such problems, pattern search methods are one possible solution technique since they neither require nor explicitly estimate derivatives.

Parallel pattern search

Lets adopt an infinite sequence of iterations $\rho = 0, 1, 2, \dots$, with the last iteration noted as $\rho - 1$ and initialization at 0. It is assumed that the process knows the best point so far as $x^{\rho-1}$, where $f(x^{\rho-1})$ is the global minima of f . Associated with $x^{\rho-1}$ there is a step-length control parameter namely $\Delta^{\rho-1}$. Each $i \in \mathcal{P}$, where $\mathcal{P} = \{1, \dots, p\}$ process ends iteration at $\rho - 1$ by constructing it's trial point and initiating an evaluation of $f(x_i^{\rho-1} + \Delta_i^{\rho-1} d_i)$, where $\mathcal{D} = \{d_1, \dots, d_p\}$ is the finite set of directions applied by each individual process. The simultaneous start of the function evaluations at the trial points on each of the p processes signals the start of iteration ρ . When all of the participating processes are finished with their evaluation of f , they communicate these values to each other and determine the new values of x^ρ , and Δ^ρ . If there exists an $i \in \mathcal{P}$, such that $f(x_i^{\rho-1} + \Delta_i^{\rho-1} d_i) < f(x^{\rho-1})$, then $\rho \in \mathcal{S}$, where \mathcal{S} denotes the successful iterations.

Adding asynchronicity

With said above, the general strategy for asynchronous parallel pattern search, from the perspective of a single process $i \in \mathcal{P}$ can be outlined:

1. Evaluate $f(x_i^{best} + \Delta_i^{best} d_i)$.
2. If $f(x_i^{best} + \Delta_i^{best} d_i) < f(x_i^{best})$, then broadcast result to all other processes.
3. Update local values x_i^{best} and Δ_i^{best} based on the current local information.

4. Repeat.

The price payed is that each process has its own notion of the best known point seen so far, as well as its own value for Δ^i . Any success on one process is communicated to all other processes participating in the search, but the successful process carries on from its new best point without waiting for a response from the other processes. By adding a few mild conditions, the global convergence of the search can be still ensured [50]. Instead of indexing based on a notion of iterations, we switch from ρ to indexing based on discrete time instance, letting the set $\mathcal{Q} = \{1, 2, \dots, q\}$ denote the index of steps. Thus x_i^q 's used for the best point known to process i at time step q , and similarly, Δ_i^q . So if process i starts a function evaluation at time step q , the trial point at which the function evaluation will be made at $x_i^q + \Delta_i^q d_i$. Further worth mention, that time steps are assumed to be of fine enough resolution so that at most one function evaluation finishes per process per time step.

Lets define two sets that satisfy $\mathcal{Q} = \mathcal{S}_i \cup \mathcal{U}_i$, , and $\mathcal{S}_i = \mathcal{I}_i \cup \mathcal{E}_i$, where \mathcal{S}_i is the set of all time successful steps on process i , \mathcal{I}_i is the set if internal successes, \mathcal{E}_i is the set of external successes, and \mathcal{U}_i consists the unsuccessful steps respectfully. An internal success, where the process finds itself the minima, the external success is where the process is updated externally by the minima. Further $\mathcal{C}_i \in \mathcal{U}_i$ is defined as the set of time steps where Δ_i^t is reduced. All the above cases ($\mathcal{U}_i \setminus \mathcal{C}_i$) no action is performed.

The updating functions allow us to give the following general definitions for x_i^q and Δ_i^q . For every $q \in \mathcal{Q}$, $q > 0$, the best point for the i^{th} process defined to be:

$$x_i^q = \begin{cases} x_{\omega_i(q)}^{\tau_i(q)} + \Delta_{\omega_i(q)}^{\tau_i(q)} d_{\omega_i(q)}, & \text{if } q \in \mathcal{S}_i \\ x_i^{q-1}, & \text{otherwise} \end{cases}, \quad (3.3)$$

with the initialisation $x_i^0 = x^0$, where $\omega_i(q)$ is the generating process index for the update time at step q on process i , and $\tau_i(q)$ is the time index for initialization of the function evaluation, that produced the update at time q on process i . For every q the step length control parameter Δ_i^q defined to be:

$$\Delta_i^q = \begin{cases} \lambda_{\omega_i(q)}^{\nu_i(q)} \Delta_{\omega_i(q)}^{\tau_i(q)}, & \text{if } q \in \mathcal{S}_i \\ \theta_i^q \Delta_{\omega_i(q)}^{\tau_i(q)}, & \text{if } q \in \mathcal{C}_i \\ \Delta_i^{q-1}, & \text{otherwise} \end{cases}, \quad (3.4)$$

with the initialization $\Delta_i^0 = \Delta^0$, where $\nu_i(q)$ is time index for the completion of the function evaluation that produced the update at time step q on process i , and θ_i^q and λ_i^q are chosen. With the following pattern followed, the minima of f shall eventually reached, in an undetermined steps.

3.4 Voltage unbalance compensation with optimization based control algorithm and asymmetrical inverter structure

First the networks structure shall be described, the power electrical device is connected to, as a household supplying, renewable utilizing device, followed by the aforementioned device's topology and control shall be presented based on the geometrical voltage unbalance norm (described in section (2.3)), with the performance results on an unbalanced network. It shall be shown, that it is possible to formulate some power quality related aims, or demands for the domestic size generator units implemented in a complex power electrical system, capable of supplying a household, with both renewable and network supplied energy, and lowering voltage unbalance as well, considering a network with unpredictable impedance.

3.4.1 Network structure

The examined network is supposed to be the low voltage local transformer area with regular households, depicted in Figure (3.4). The network structure of Figure (3.4) has been implemented in SimulinkTM environment for simulation based experiments. Most of the households represent a single phase load with resistive inductive and capacitive properties while some of them are symmetric three phase ones. There might also be some households with domestic power plant, they are not only loads but also represents distributed generators. Furthermore, it is assumed that the households located on a domestic size grid tie inverter are also provided with battery storage capacities. Commercially available inverters are capable of optimizing the working point and charging current of the system, while the ability of power quality improvement is far not typical - it is in experimental phase in some cases, e.g. [15].

3.4.2 Problem statement

The voltage and current unbalance presents in the three phase low voltage transformer area causes additional power loss inside the medium voltage/low voltage transformer and in the transportation line wires too. It also has undesired effects in certain three phase loads, mainly rotating machines where it causes torque reduction and pulsating torque effect. Large scale unbalance can activate automatic protection functions of electricity dispatch system causes power outage. This is unpleasant for the customers and adds maintenance cost to the service provider. These negative effects lower the electric power quality and rises the cost of electrical energy and rises the carbon footprint of our everyday life. The aim to propose a model and control for a three phase instrumentation, which can compensate these undesirable effects, lower or eliminate the voltage and current unbalance to lower the power losses and the CO₂ emission and increase power quality not only at the connection point but in the whole low voltage transformer area. *It is important to note, that*

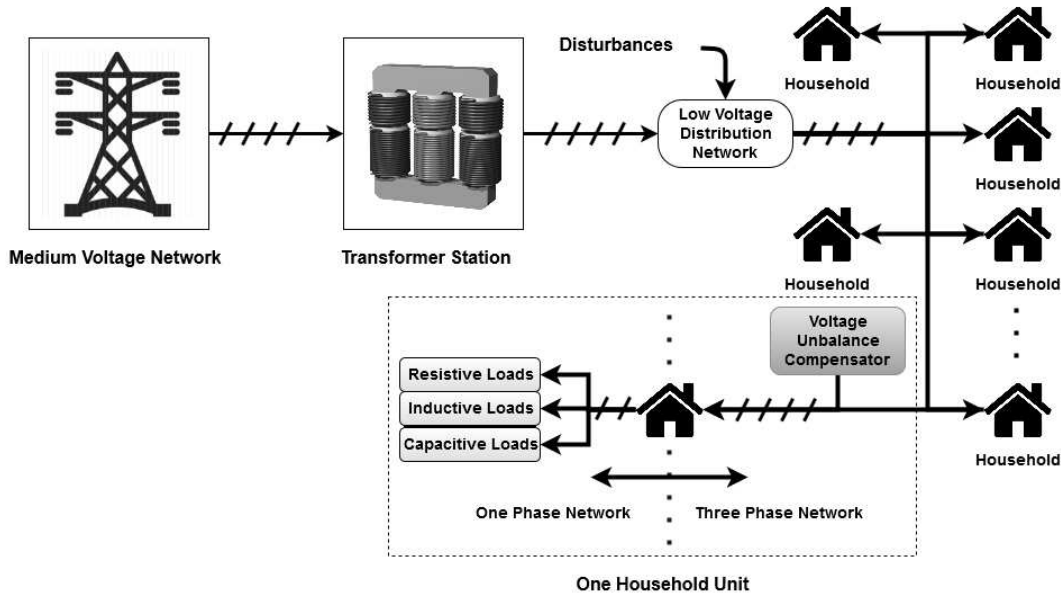


Figure 3.4: The simplified structure of a three phase four wire low voltage network. The transformer station acts as transition from the medium voltage power grid to the low voltage network. The several regular households are representing the main loads of the network. The transformer and the loads are connected with power line sections infected by inductive and resistive disturbances and capacitive couplings. Domestic powerplants can connect to any connection point within the low voltage network, via an appropriate inverter - either to the three phase sections using a three phase inverter or to a single phase using a single phase inverter.

this power quality improvement can be achieved without any significant added cost. The future aim is to integrate this function into an existing three phase photovoltaic inverter device connected to the low voltage grid, and a complex energetic system is able to inject the renewable energy to the transportation network, can store the electrical energy from stochastic renewable sources in electrical vehicle batteries or feed the grid from the charged batteries in energy deficit and high demand simultaneous situations. The novelty is the integrated control algorithm which can highly lower or eliminate the observed unbalance of the network.

3.4.3 Control problem

The above problem statement partially specifies the solution space together with the solution method. The system of interest is the power grid with all the stochastic and nonlinear phenomena present in it mentioned in section 3.4.1. The input to the system are current signals (one current in the single phase case and three in the three phase setup), which are naturally constrained by the available energy of the household, stored in a battery pack or momentarily generated by the wind or solar generator unit. The response of the system can be either the current or the voltage measured at the connection point

of the inverter unit, however, the general legal regulations only allow voltage measurement for consumers. The difficulty of the control problem comes from the fact, that there are no mathematically tractable models of the network can be generated because of its unpredictable and nonlinear features. This means, that in these conditions only black-box methods can be applied for this system. For the control aim it is a natural choice to minimize the actual voltage unbalance of the low voltage local transformer area measured (or calculated) at the connection point of the inverter. Several optimization based methods are available for such kind of optimal control problems, e.g. [15] where the only bottleneck is the computational efficiency since the implemented controller has to run on the commercial inverter's hardware (digital signal processor unit).

Asymmetrical inverter structure

For the sake of completeness an asymmetrical inverter was developed in simulation environment, which is capable of carrying out the specified control task. The renewable energy injection is realized increasingly, and applied directly to the three phase low voltage grid with a domestic size photovoltaic power plant as source of power. This can reduce the voltage and current unbalance caused by the stochastic power production of wind and solar sources. More and more manufacturers produce three phase grid synchronized inverters from 5 kW size. These equipments implement accurate symmetrical current feed with a standard three phase full bridge structure, consists of six Isolated Gate Bipolar Transistors (IGBT). The demand is to employ a current source single phase structure with aforementioned controllable switches in section 3.2.2. This is a standard structure suitable for symmetric harmonic current injection. It has limited capacities to inject not totally symmetric 3 phase current time functions, but Kirchhoff's current law permits only constant zero-sum current time functions injected with this structure. There are examples with this type of asymmetric current injections in the literature [40].

This type of current injection has limited compensation capacity and this is not enough in most asymmetric production and load cases. In our case we need more general, not specific asymmetric current waveforms, because the proposed control aim assumes the ability of injecting non zero-sum currents. This needs special inverter design structure. We need zero line connection for the differential current. One of the possible solution is to use 3 different full bridge single phase current inverters to supply each phase of low voltage transportation lines [51]. This way it is most sufficient to use bi-directional power flow, with galvanic decoupling, but with a current controlled fashion (shown in section 3.2.2).

This isolation can be reached with using isolation transformers in the supply side. But we prefer to use it a complex energetic system with specific inside true DC bus system fed from Photovoltaic panel or batteries. We have to isolate at least 2 full bridges with two way DC-DC converters (described in section 3.2.1). This can complicate the physical realization but easy to simulate with two controlled power source. Other possible easy to realize solution to isolate the full bridge outputs connected to three phase lines with isolat-

ing transformers. It is recommended due to electric shock protection reasons. Our distant aim to compensate other operational type line failures, such zero current appearing. This isolation method doesn't allow to produce DC current components, that's why we are looking for other design. Possible elegant solution to supplement the standard three phase inverter design with a fourth half bridge for Zero line, building a specific four leg inverter design [52].

Only drawback of this solution is the complex difficult control method of the half bridges, to keep the current sum in zero values in each moment, and to provide the correct current paths inside the inverter. This structure has the lowest production cost, but in the phase of proofing the asymmetry compensation we chose the DC-DC isolated full bridge design for simulation purpose because of the simple control during simulation.

As a further generalization step, the injection of no harmonic current shapes will be necessary in order to decrease the extant Total Harmonic Distortion (THD) of the network. These expectations yield an inverter with new structure suitable for arbitrary current injections without limitations. The design lends similar elements like in [15] by means of battery charge, renewable power point tracking, intermediate voltage, and IGBT bridge control, but in this case the problem requires a three phase solution for the voltage unbalance reduction. The applied structure based on a full bridge IGBT structure used in single phase current injection. Three different IGBT full bridge were connected at the output point, thus our structure has three phase and neutral connection too, to carry out any current form. The disadvantage of this structure is that it needs 12 IGBTs in the output stage as opposed to the 6 IGBTs needed for a classical full bridge structure and needs three galvanically isolated direct current (DC) voltage source for feeding.

The other standard elements, that the inverter design consists:

- Standard maximum power point tracking (MPPT) input stage, to inject the maximum available power from the renewable source to the intermediate voltage capacitor with a simple controlled boost converter
- A half bridge current controller to charge or deploy the battery pack connected to the complex energetic system for energy storage and energy unbalance compensation
- Intermediate voltage controller
- Universal three phase output stage with 3 single phase full bridge IGBT current injector and 2 high current DC-DC converter

This is suitable to inject any necessary current shape to the low voltage three phase grid even DC currents too. Later a power loss and production cost analysis will be necessary if the built structure will be suitable for asymmetric compensation of low voltage transformer area.

Of course there is a possibility that there is no renewable power available for a longer period of time and the battery completely loses its charge. In this case the system should work merely with the power of the connection

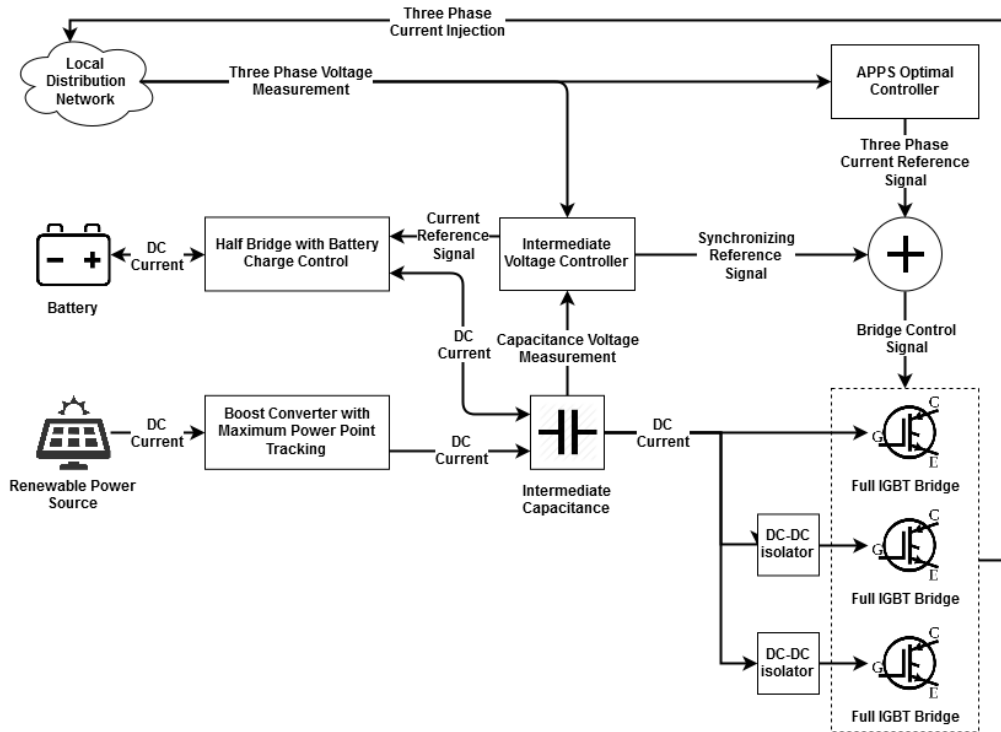


Figure 3.5: The asymmetrical inverter design, which applies three single phase full bridge IGBT current injector to create the injected asymmetrical current shapes for voltage unbalance compensation.

point but with zero energy balance. This states to operate two controller with semi-opposite control goals. The optimization based controller requires current injection while the intermediate voltage controller (Figure (3.5)) keeps the inverters energy balance. *Although for this operation some of the control's performance should be sacrificed, unbalance compensation could be achieved even without external renewable power, and energy storage at a minimum power requirement.*

Measurements from a real unbalanced network

The measurements took place at the campus building's power electronics laboratory, where a common 400 V connection point was investigated as the behaviour of the network. The three phase 230 V line-to-ground voltages has been transformed to 6 V to be effectively measurable in time domain with high performance NI-USB DAQ on 10 ksample/s. Because of the limited computational capacity only a 10 second measurement was made in every hour. The measurements then has been merged and smoothed to eliminate the inter-measurement transients.

Afterwards, the measurement data has been used as the input of a micro-grid segment of the Matlab/Simulink model, to test the controller and inverters structure's performance in quasi-realistic circumstances. The controllers performance on the simulated microgrid's network loss reduction can be observed on Figure (3.10) and Figure (3.11). The measurement output is connected

to a modeled three phase load and network system, consisting of symmetrical loads and network segments between them. Further artificial load unbalance is not necessary since the network's unbalance is already present. This structure enables to show that any point the inverter is connected, could restore power quality with a certain degree such unbalance compensation at this case. The future plan is to set up multiple devices on different connection points.

3.4.4 Optimization based control algorithm

Unfortunately the difficulty from optimization point of view is that the exact mathematical relation is hard to formulate because the nonlinear, and highly time variant and stochastic loads of the network. As such a kind of control strategy should be used to cope this nonlinear and time variant energy system. For this purpose we chose an asynchronous parallel pattern search method (APPS) which could be able to control our scenario [53]. The methodology and formulation of the APPS method is described in section 3.3. We applied a variant of the gradient method that is a first-order optimization (minimization) algorithm for a multivariate function $f(\mathbf{x})$. The point \mathbf{x}^q corresponding to the local minimum can be calculated from the negative gradient $\nabla f(\mathbf{x})$, that gives the value and direction of the corresponding step in the parameter space. The next step is made in the direction of gradient with the proper sign. This sequence of steps, ideally, converges to local multivariate extreme value \mathbf{x}^q of the function (3.5).

$$\mathbf{x}^{(q)} = \mathbf{x}^{(q-1)} - t_q \nabla f(\mathbf{x}^{(q-1)}), \quad (3.5)$$

where $q \in \mathbb{N}$, and t_q resembles the step time of the algorithm.

The controlled electrical system is described by multivariate non-linear differential equations, the optimization of which is infeasible to derive using the differentiation of an error function. Therefore, the optimization methods based on direct differentiation are not applicable. In such cases, when high computational power is needed for performing long time-consuming simulations, the APPS method can utilized. The search pattern p is based on the sampling of the error function (selected norm) on a "grid", and it corresponds to variables or subsets of variables in each point in the independent variable or parameter space easily. At the same time, the norm values at these points can be calculated independently if $\Delta_q > 0$, using (3.6).

$$\begin{aligned} \mathbf{x}^{(q+1)} &= \mathbf{x}^{(q)} + \Delta_q d_i \\ \text{if } &f(\mathbf{x}^{(k)} + \Delta_q d_i) \leq f(\mathbf{x}^{(q)}), \end{aligned} \quad (3.6)$$

The parameter is $\mathbf{x}^q \in \mathbb{R}^n$, and the search pattern $\mathbf{p} \in \mathcal{D} = d_1, \dots, d_n$ is taken from a predefined finite set. In this case, the error function values should be calculated for each pattern \mathbf{p} in the set \mathcal{D} . If the error function is not decreasing in any of the directions, then the step size should be reduced (e.g. by half). As the competing directions are different, if there is not enough computing power available for direction vector \mathbf{p} , synchronization should not be maintained. In this case we are talking about the asynchronous case . In the

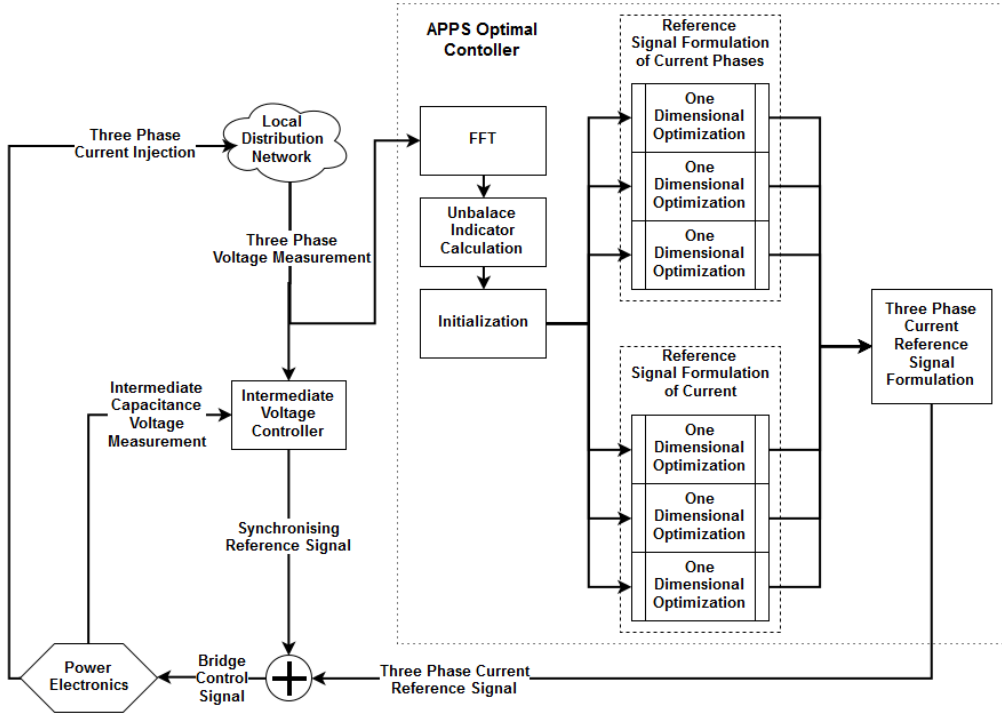


Figure 3.6: The optimization algorithm implemented for current control. A one dimensional linear optimization step is being solved in each dimension of the six dimensional parameter space, iteratively.

case of our controller, an individual \mathbf{p} vector is defined for each output variable, and the optimization was performed in each direction asynchronously and shifted in time. Most likely, the error function has a single local minimum as a symmetric amplitude and phase values. Approaching the minimal value of norm, the controller uses adaptive increments that are proportional to the norm itself. Because of the complex interactions between the components of the controller, only one parameter is changed at a time, even if the values of the amplitude and phase components in specific time slot changes. The algorithm moves along the six axes of six separate time slots close to the local minimum of the error function.

Unlike other similar approaches, e.g. [54], the explained optimal controller does not rely on a measured current signal (which varies according where the measurement took place on the grid and renders the global optimization unreliable) but rather measuring and analyzing the voltage unbalance via the proposed indicator and optimizes the voltage shape, the latter of which depends on the nonlinear distortion of the whole low-voltage transformer area and determines additional power losses. The controller's performance was compared to a non compensated network, and a network consisting synchronized symmetric power intake from a regular inverter.

In each iteration only one physical value is changing on the six dimensional parameter field, which consists of the three amplitude and three phase values. If the change effects with cost function reduction (the reference norm's normalized value), the controller holds the new value of amplitude or phase for

the controlled current sources (Figure (3.6)). The advantage of this controller structure that is not necessary to know the controlled value's behavior well, like we could not determine the number and type of the other loads on the network [P1]. There are however two disadvantages. First is the low speed of control, due to the several necessary iterations (depending on the circumstances) to find the optimal directions in the parameter space, and the serial nature of interventions and norm calculations. The second comes from the method itself since the controller may stuck in local minima.

3.5 Discussion

3.5.1 Dynamical simulation based experiments

In order to be able to investigate the proposed optimization based unbalance reduction control structure with the three phase inverter on a low voltage local grid, all the elements of this complex electrical system (including the photovoltaic source, the inverter, the battery and the nonlinear local grid with different types of loads) has been modeled in Matlab/Simulink environment. The primary aim of the simulation based experiments were to serve as a proof of concept for the proposed complex control structure.

3.5.2 Performance analysis

The aim of performance analysis is twofold. First of all, the proposed voltage unbalance indicator has to be investigated in the control structure as the cost function of the optimization based controller, and on the other hand, the control structure itself has to be exposed against engineering expectations.

The results of the first experiment can be seen in Figure (3.7) where the geometrical norm (2.11) has been used as the voltage unbalance indicator and the cost function for the optimizer. The dashed line represents the examined low voltage local network's unbalance norm (G) without the proposed controller implemented in the inverter unit of the domestic powerplant while the solid line represents the compensated network's norm value. The performance of the controller with this norm is apparent, it was able to decrease the network voltage unbalance by approximately 85 %. In this experimental setup the controller has enough input energy due to the batteries and the available solar power.

A slightly more challenging situation is investigated in Figure (3.8) where the controller had to operate without photovoltaic source and batteries. This is called zero moving average balance operation mode when the energy obtained from the network is reinjected in such a way that the unbalance indicators decrease. It can be seen that the performance of the controller is modest than that of Figure (3.7), but it is still acceptable.

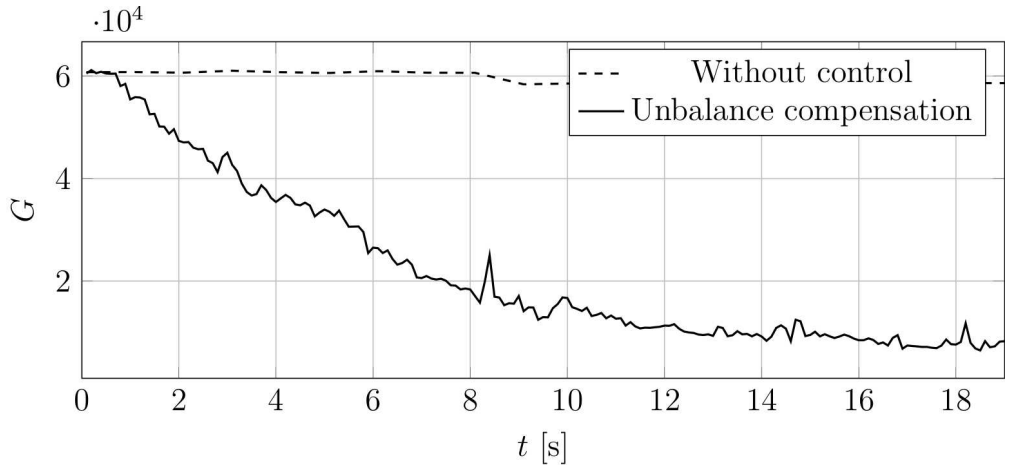


Figure 3.7: Unbalance reduction control system performance with half charged battery and photovoltaic power source available. The underlying unbalance norm is the geometrical one (G) in this experiment. After starting the controller at $t = 0.1\text{s}$ the unbalance measure G of the network significantly decrease.

Robustness analysis

The robustness of the proposed control structure is an important qualitative property with respect to the time dependent loads present on the network. The robustness of the proposed controller had to be tested via simulation when different types of loads (inductive, capacitive, resistive) had been varied in step changes representing the on/off switching the different types of household appliances (motors, switching mode power supplies, electric heaters, etc.). In the experiment depicted in Figure (3.9), a load change has been introduced to the network in every 15 seconds causing the voltage unbalance to jump to a different value (measured in the geometrical norm (2.11)). As it can be seen in the figure the controller successfully compensates the unbalance after each transient.

3.5.3 Environmental effect

The favorable effects of the proposed unbalance reduction control algorithm, i.e. increase power quality not only at the connection point but in the whole low voltage transformer area, which causes a reduction of the effective power loss and the reduction in the CO₂ emission.

Power loss reduction on the network

Network loss reduction due to the unbalance reduction compensation control is investigated on Figure (3.10) where the simulation experiment was carried out in the circumstance when the renewable source was not shut down (e.g. insufficient amount of sunlight) and additionally the battery was drained completely [P1], [P2].

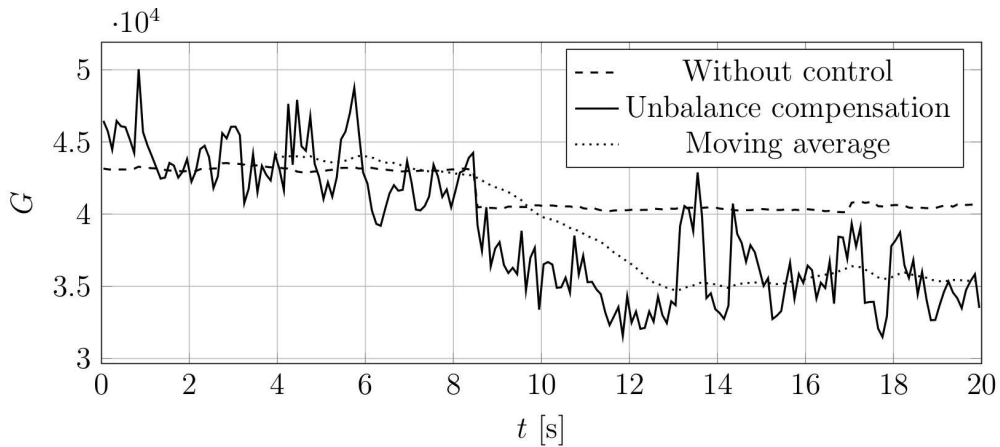


Figure 3.8: Unbalance reduction control system performance without battery and renewable source (zero energy balance operation). The performance reduction is clearly observable compared to the case when external power source is available (Figure (3.7)), but as result the voltage unbalance indicator G reduced by the average value of 14.78%.

The results show that despite of the negative cross effects of the intermediate voltage controller and the unbalance reduction controller it was possible to find the trade-off between the control goals of the different controllers (maintain zero energy balance for the inverter and decrease the unbalance on the network). The estimated loss reduction in the experimental setup is 6.5%.

CO₂ footprint

The fact that this controller enables the reactive power reduction has a favourable consequence, i.e. the power loss or equivalently CO₂ emission and the carbon footprint can also be decreased. The estimated environmental effects of voltage asymmetry compensation can be calculated. Let us assume 3000 kWh for the yearly electric energy consumption an average household and 9.173% for the loss of the distribution network at 2013 [55] and 7.654% at 2018 [56]. Using the controller the losses on the simulated network are reduced by 6.5%. The calculation follows (3.7):

$$\begin{aligned} P_{loss} &= 3000 \text{ kWh} \cdot 7.654\% \\ P_{loss}^{comp} &= 3000 \text{ kWh} \cdot (7.654 \cdot 0.93)\% \\ \Delta P_{loss} &= P_{loss} - P_{loss}^{comp} \end{aligned} \quad (3.7)$$

where P_{loss} is the assumed network loss per household and P_{loss}^{comp} is the assumed network loss with unbalance compensation control and ΔP_{loss} is the saved energy. According to (3.7), unbalance compensation results in an energy savings of 19.26 kWh in 2013 and 16.07 kWh in 2018. Taking into account the proportion of power currently generated by fossil fuels (coal 17.3%, gas 38.3% at 2013 [55], [15] and coal 13.1%, gas 51.4% at 2018 [56]) and the rate of CO₂ emission during electric energy production (1,000 g/kWh from coal and 430 g/kWh from gas), it can be concluded that voltage unbalance compensation

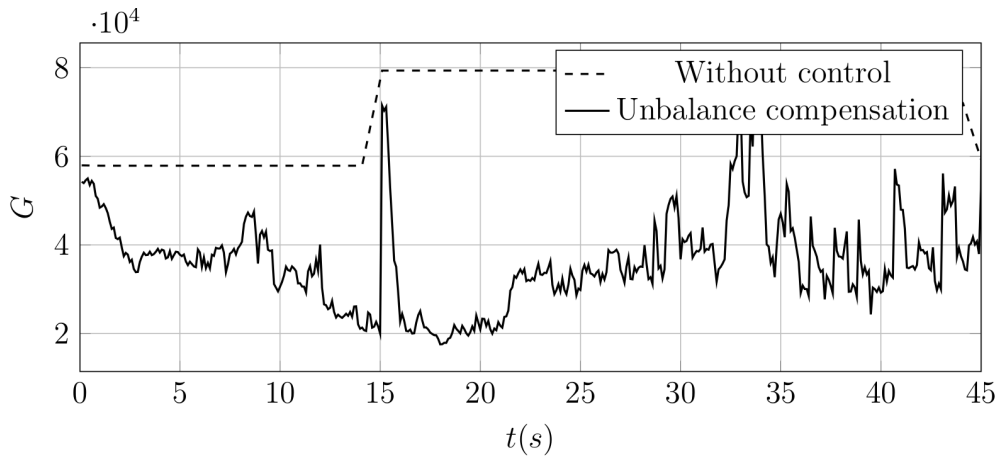


Figure 3.9: Robustness analysis with respect to step type changes in the network load (and voltage unbalance). The unbalance reduction controller successfully compensates the changes in the network voltage unbalance norm (G) value.

could reduce CO₂ emissions by 6504.9 g a year in 2013 and 5656.96 g in 2018 in an average household. Note that this result reflect only the proof of concept, due the neglected power losses of the inverter and the artificial load of the network.

3.6 Conclusion

Currently used measures of voltage unbalance (see section 2.2.2) has been extended in this chapter with a new norm candidate, namely a geometrical norm, where the magnitude of voltage unbalance are evaluated by the symmetrical difference of the voltage phasor triangles. It is more demanding from the computational point, of view but has an interesting feature namely it checks electrical asymmetry, i.e. the norm of a ±120 degree rotated version of the ideal three-phase phasor is zero in the geometrical sense.

This way, the defined norm is applied as a cost function in the asymmetry reducing controller structure utilizing an asynchronous parallel pattern search (APPS) algorithm also presented in the thesis. Simulations, performed in Matlab/Simulink environment show that the geometrical based indicator can serve as a basis of further research. The suggested controller structure enables the residential users owning a grid synchronized domestic power (renewable) plant to reduce voltage unbalance measurable at the connection point. The fundamental element of the system is a modified three phase inverter that is capable of the asymmetric current injection of any current waveforms to the network, via decoupled bi-directional DC-DC converters. The optimization-based control algorithm injects the available energy (as current waveform) in such a way, that the voltage unbalance decreases. This is an optimization problem which is constrained by the available renewable energy supplied by the power plant, or energy storage unit.

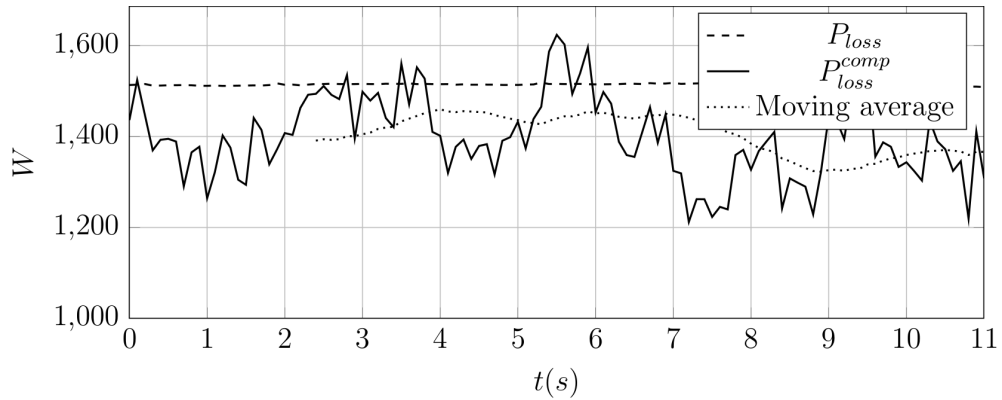


Figure 3.10: Compensation control's loss reduction during zero energy balance operation on the modeled network, where P_{loss} indicates the effective power losses and P_{loss}^{comp} effective power losses during control of the network. As result the network losses reduced by mean 6.5%.

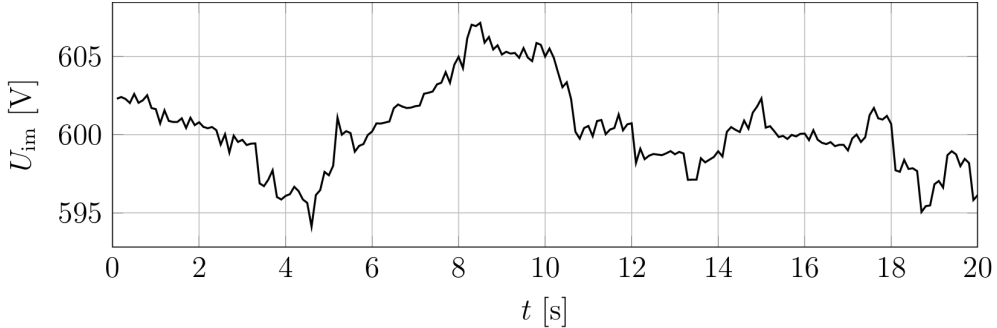


Figure 3.11: Intermediate puffer capacitance's voltage within boundaries (600 ± 10 V), during zero energy balance operation mode of the voltage unbalance compensation controller. U_{im} indicates intermediate the capacitance's voltage.

The control structure has been tested on a low voltage network model in a dynamical simulation environment consisting of the models of the electrical grid, a domestic power plant, an asymmetrical inverter circuit, and different types of loads. Different simulation experiments have been run for each norm and for both the power constrained and unconstrained case. The preliminary results show that this structure can serve as a residential level voltage quality improvement method for the three phase low voltage network also indirectly reduces the CO₂ emission due facilitating more effective energy usage.

3.7 Notations used in the chapter

C_{snub}	Capacitance to reduce switching loss and to damp out over-voltage
C	APPS steps where Δ_i^t is reduced
D_{1+}, D_{2+}	CSI Higher diodes
D_{1+}, D_{2+}	CSI Lower diodes
\mathcal{D}	APPS set of step directions
d_i	APPS direction of active process
\mathcal{E}	APPS set of external successes
$f(\mathbf{x})$	Multivariate function to minimize
G	Geometrical voltage unbalance indicator
h	DC-DC transformer turn ratio
\mathcal{I}	APPS set of internal successes
L_+, L_-	CSI current filter inductors
L_a	DC-DC transformer leakage inductance
\mathcal{P}	APPS set of processes
P_D	DC-DC power transfer under idealized conditions
P_{loss}^{comp}	Lost power per household due to network unbalance
P_{loss}	Assumed network loss with unbalance compensation control
ΔP_{loss}	Saved power with unbalance compensation control
\mathbf{p}	APPS search pattern
p	APPS process index
Q	APPS set of sidestep indices
q	Discrete time step
S_{1+}, S_{2+}	CSI higher switches
S_{1+}, S_{2+}	CSI lower switches
\mathcal{S}	APPS set of successful iterations
s	Dimension of the decision vector
t_q	Timestep of the algorithm at q
\mathcal{U}	APPS set of unsuccessful steps
V_{an}, V_{bn}	Designated point's potential to ground
V_i	Constant input voltage
V_o	Alternating output voltage
V_{D1}, V_{D2}	Two end's voltage on the DC-DC converter
VUF	Voltage Unbalance Factor
v_1, v_2	DC-DC transformer voltages
\mathbf{x}^q	Local multivariate state at the q^{th} timestep
x_i^{best}	APPS best reached state, where x_i^{best} is a minima
α	Fortesque operator
Δ	APPS step length control parameter
Δ_i^{best}	APPS best reached step size
δ	DC-DC modulation coefficient
Δ_q	Step size at q
λ	APPS system specific tunable parameter
θ	APPS system specific tunable parameter
$\nu_i(q)$	Time index for the completion of the function evaluation that produced the update at time step q on process i
ρ	APPS infinite sequence iterator
$\tau_i(q)$	Time index for initialization of the function evaluation, that produced the update at time q on process i
ω	Angular velocity of output sinusoidal voltage or current
$\omega_i(q)$	Generating process index for the update time at step q on process i
\triangle_{Ideal}	Triangle of Ideal voltage vectors
\triangle_{Real}	Triangle of real voltage vectors

Chapter 4

Explicit model predictive control of a current source buck-type rectifier

4.1 Literature overview

Current source rectifiers (CSR) are widely used in front-end power electronic converter for the uncontrollable or controllable DC-bus in industrial and commercial applications. They have maintained their position through many applications, with uses such as medium-voltage high-power drives [57], [58] STATCOMs [59] and renewable systems [60], [61]. They have a plain and reliable circuit structure, which makes them attractive for simple control design. The CSRs are traditionally controlled by state feedback, or classic cascaded linear control loops such as PI controllers. These simple control applications are suitable for induction motor control [62], and other electromechanical actuators [63], and unusual topologies [P3]. Also, worth mentioning of self-tuning variants of PI controllers [64].

In the past, the modulation methods used were trapezoidal pulse width modulation techniques (TPWM), or application of pulse patterns calculated off-line for selective harmonic elimination (SHE). More recently, current space vector modulation (SVM) has been used for the synthesis of the transistor control signals [65]. Even so, AC-side harmonic elimination could still be an issue at lower switching frequencies where LCL filtering (inductive-capacitive-inductive) would be advised [66].

In terms of the amplitude of the grid and DC-link voltages, CSRs exhibit a step-down conversion. When used as DC voltage source, the rectifier can output a lower DC voltage without the need of a grid-side transformer, as is usually employed in voltage source rectifiers (VSR). Because of their current source behavior, CSRs can easily be paralleled and provide inherent short-circuit protection, representing an excellent potential in DC power supply applications [67], [68].

There are several control strategies in addition to classical PI control for applications in this domain. Self-adapting control methods are on the rise with

more sophisticated algorithms in the field of fuzzy logic [69]. They are capable of handling increasingly more complicated models and systems with high dynamics and accuracy [70], [71], and even without establishing and validating classical state-space models [72]. The other field is the sliding mode control, which can achieve good dynamic performance and handle non-linearity. Still, they might also introduce chattering, which can be very undesirable when applied to real-life systems like in [73] and [74]. Additionally in [75] the validity of an MPC-based, digital pulse width modulation control strategy for single-phase voltage source rectifiers is discussed, further confirming the validity of this method in control systems.

In the linear domain implicit model predictive control (IMPC or MPC) is a fair solution due its effectiveness in power electronics because of its configurable cost function and such scalable nature [76], [75]. In this field also finite-state solutions are present which can be considered also predictive control, where the modulation scheme's defined states serve as optimization potential [77], [78]. As a further step adaptive application was established to tackle parameter estimation problems for better performance [79]

Recently, beside implicit, finite-state, and adaptive predictive control, explicit model predictive control has emerged in the field of power electronics [80]. Establishing the MPC cost function can range widely depending on the expected dynamics, degree of noise cancellation, and model complexity. Additionally, the current limitation can also be implemented introducing constraints in the modulation algorithm.

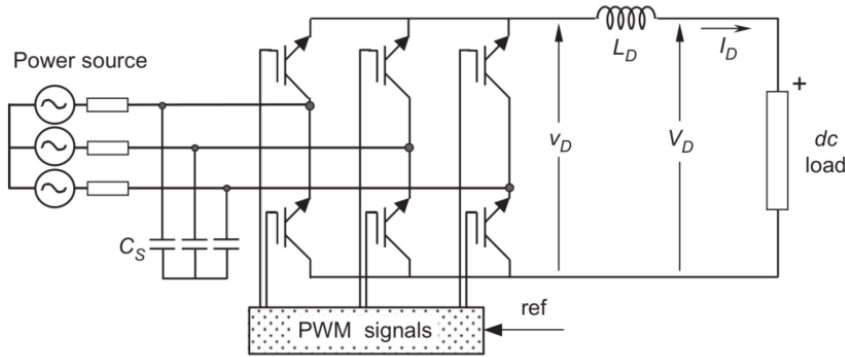
4.2 Three-phase buck-type rectifiers

Three-phase controlled rectifiers have a wide range of applications, from small rectifiers to large high-voltage direct-current transmission systems. They are used e.g. at electrochemical processes, many kinds of motor drives, traction equipment, controlled power supplies. In this thesis only force commuted rectifiers are examined, which are built with semiconductors (IGBTs in this case) with gate-turn-off capability. The gate-turn-off capability allows full control of the converter, because valves can be switched ON and OFF whenever is required. This allows the commutation of the valves, hundreds of times in one period that is not possible with line-commutated rectifiers, where IGBTs are switched ON and OFF only once a cycle. This has the following advantages:

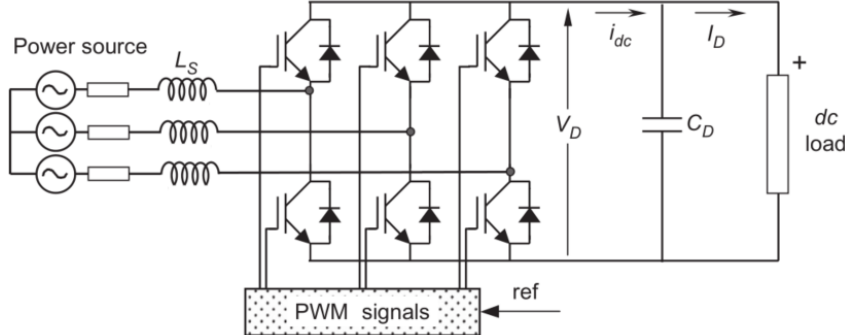
- The current or voltage can be (pulse width) modulated, generating less harmonic contamination.
- The power factor (ratio of the real and reactive power) can be controlled and even it can be made leading, signifies that the load is capacitive, as the load “supplies” reactive power.
- They can be built as voltage-source or current-source based on the required application.

- The reversal of power in switching rectifiers is by reversal of voltage at the DC link. This allows force commutated rectifiers can be implemented for both, reversal of voltage or reversal of current.

There are two ways to implement force commutated three phase rectifiers, as a current-source rectifier (Fig.(4.1a)), where power reversal is by DC voltage reversal, and as a voltage-source rectifier (Fig.(4.1b)), where power reversal is solved by current reversal at the DC link.



(a) Current source rectifier with capacitive filtering and choke inductance.



(b) Voltage source rectifier with inductive filtering and DC voltage smoothing capacitance.

Figure 4.1: Basic topologies of force commuted rectifiers.

As general case be a front-end converter power supply (e.g. lighting or telecommunications) shall be designed such that it should have approximately these general characteristics: sinusoidal main currents, unity power factor, high power density and simplicity of the power circuit structure. Two structures are most fitted for the task. First a boost-type input rectifier (e.g., Vienna rectifier, [81]), that typically features two 400 V output voltages with a three-level isolated DC-DC converter or two isolated DC-DC output stage (see Fig. (4.4) in Ch.5.). The second candidate is the buck-type input rectifier (or current source rectifier (CSR)) (conventionally six-switch topologies as proposed in [82], [83]) with only one two-level isolated DC-DC converter output stage. Also the input stage can be realized as a three-switch topology with considerably lower system complexity as compared to the boost-type structure. In

particular, the number of utilized active and passive components is much lower. Furthermore, there is no middle-point that has to be stabilized, as this is the case for the boost-type structures, making control and active filter design less complex. Further system advantages are the potential of direct start-up and the implicit over current protection in case of an output short circuit. Therefore, these topologies of high interest for many safety critical applications as such future electric aircraft, or automotive applications or as power supplies for process technology [84]. The three-switch buck rectifier topology was first proposed in [85]. In [86] and [87], aspects of the system modulation and control have been treated. The application of the topology used as an active filter is discussed in [88]. The addition of a DC-DC output boost-stage has been proposed in [89] in order to maintain 400 V output voltage for a wide input voltage range and for the case of unbalanced mains as, e.g., the loss of one phase.

Basic operation principles

For the derivation of the relative on-times of the three buck transistors S_i with the following assumptions are made for clarity and facilitation of calculations:

- The AC-side filter capacitor voltages (v_{cp} , where $p \in \{1, 2, 3\}$) at the input of the CSR are sinusoidal and in phase with the main harmonic component of voltage.

$$\begin{aligned} v_{c_1} &= \hat{v}_c \cos(\omega t) \\ v_{c_2} &= \hat{v}_c \cos(\omega t - 2\pi/3) \\ v_{c_3} &= \hat{v}_c \cos(\omega t + 2\pi/3), \end{aligned} \quad (4.1)$$

where ω is the network voltage's angular velocity.

- The mains currents are assumed to be equal to the fundamental component of the rectifier input currents.
- The current in the DC output inductor L_D is not affected by the high frequency ripple due to the switching operation.

For achieving ohmic mains behavior also in case of unbalanced fundamental harmonics conditions the explained modulation method can still be utilized, however, additionally the control structure presented in [90] has to be employed.

The waveforms of the phase and line-to-line mains voltages are divided into twelve sectors of $\frac{\pi}{6}$ rad wide shown in Fig.(4.2). The following calculations are based on the analysis of the first sector which is characterized by the voltage harmonic phase relation. For the remaining sectors the calculations can be accomplished in a similar manner [84].

Accordingly, on AC side, if conditions are favorable, inductor current can appear in an instant of time either in two out of three phases or in none. In

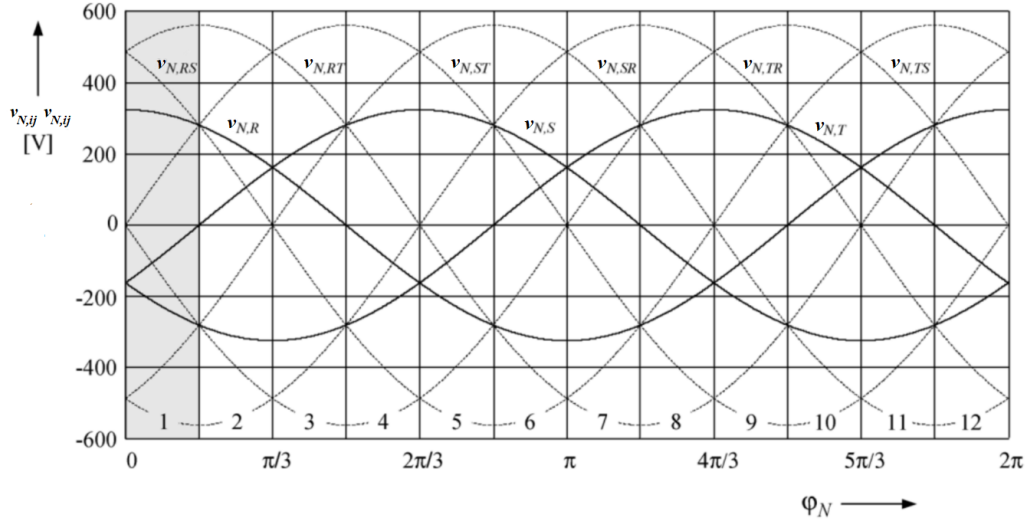


Figure 4.2: Phase voltages v_i , where line-to-line voltages $v_{N,ij} = v_{N,i} - v_{N,j}$, $(i, j) \in \{R, S, T\}$ and sectors 1 to 12 being defined by the different relations of the instantaneous values of the mains phase voltages for $v = 400V$

this modulation technique, the switches in each converter leg can conduct only one at the time (aside from zero states, where both upper and lower switches are conducting). When the upper leg is conducting it is indicated by ‘1’, when the lower ‘−1’ and when neither ‘0’. As such the choice whether upper or lower switch of the leg conducts current depends of the reference current vector’s sector location. According to the actual switch combination the DC link current shaped by the choke inductance, and distributed to two of the input phases or the freewheeling diode. With this, the input current space vectors can be calculated for each of the before-mentioned switching states. Generally the space vector of three-phase quantities (e.g., for the rectifier input current) are described as:

$$\vec{i} = \frac{2}{3} \left(\vec{i}_a + \vec{i}_b e^{\frac{j\pi}{3}} + \vec{i}_b c^{\frac{4j\pi}{3}} \right). \quad (4.2)$$

Based on (4.2) the corresponding active space vectors in the first sector can be obtained as:

$$\begin{aligned} \vec{i}_{(1,0,-1)} &= \vec{i}_1 &= 2i_{dc} e^{j\pi/6} / \sqrt{3} \\ \vec{i}_{(0,1,-1)} &= \vec{i}_2 &= 2i_{dc} e^{j\pi/2} / \sqrt{3} \\ \vec{i}_{(-1,1,0)} &= \vec{i}_3 &= 2i_{dc} e^{j5\pi/6} / \sqrt{3} \end{aligned} \quad (4.3)$$

The resulting discrete space vectors can be used to synthesize desired current space vector \vec{i}_{ref} .

The modulation methods were evaluated in and chosen for this paper based on [91], which ensures minimum switching-losses, minimum ripple values of the input capacitor voltages and of the output inductor current. According to this modulation, each pulse interval comprises two active states and a freewheeling

state, arranged symmetrically about the middle of the pulse interval (see Table (4.3)). For more in depth functional description see section (4.4.3).

4.2.1 Coordinate transformations

In section (4.4.1) the three phase current source rectifier's (CSR) equations are converted to different coordinate spaces.

Clarke transformation

In electrical engineering, Clarke transformation is a mathematical transformation employed to simplify the analysis of three-phase circuits. Conceptually it is similar to the Park transformation. One very useful application is the generation of the reference signal used for space vector modulation control of three-phase inverters. The transformation follows:

$$\mathbf{i}_{\alpha\beta\gamma}(t) = T_{Clarke} \mathbf{i}_{abc}(t) \begin{bmatrix} 1 & -\frac{1}{2} & -\frac{1}{2} \\ 0 & \frac{\sqrt{3}}{2} & -\frac{\sqrt{3}}{2} \\ \frac{1}{2} & \frac{1}{2} & \frac{1}{2} \end{bmatrix} \begin{bmatrix} i_a(t) \\ i_b(t) \\ i_c(t) \end{bmatrix}, \quad (4.4)$$

where \mathbf{i}_{abc} is the generic three phase current sequence, and $\mathbf{i}_{\alpha\beta\gamma}$ is given by the transformation.

Park transformation

The Park transformation is a tensor that rotates the reference frame of a three-element vector or a three-by-three element matrix in an effort to simplify analysis. The transform can be used to rotate the reference frames of AC waveforms such that they become DC signals. Simplified calculations can then be carried out on these dc quantities before performing the inverse transform to recover the actual three-phase ac results. As an example, the Park transform is often used in order to simplify the analysis of three-phase synchronous machines or to simplify calculations for the control of three-phase inverters. In analysis of three-phase synchronous machines the transformation transfers three-phase stator and rotor quantities into a single rotating reference frame to eliminate the effect of time-varying inductances. The transformation follows:

$$\mathbf{i}_{dq0}(t) = T_{Park} \mathbf{i}_{abc}(t) \sqrt{\frac{2}{3}} \begin{bmatrix} \cos(\theta) & \cos(\theta - \frac{2\pi}{3}) & \cos(\theta + \frac{2\pi}{3}) \\ -\sin(\theta) & -\sin(\theta - \frac{2\pi}{3}) & -\sin(\theta + \frac{2\pi}{3}) \\ \frac{\sqrt{2}}{2} & \frac{\sqrt{2}}{2} & \frac{\sqrt{2}}{2} \end{bmatrix} \begin{bmatrix} i_a(t) \\ i_b(t) \\ i_c(t) \end{bmatrix}, \quad (4.5)$$

where θ is instantaneous angular position of an arbitrary frequency.

4.3 Model based predictive control

4.3.1 Quadratic optimization and predictive control

Philosophically MPC reflects human behavior whereby we select control actions which we think will lead to the best predicted outcome (or output) over some limited horizon. To make this selection we use an internal model of the process in question, and constantly update our decisions as new observations become available. Hence a predictive control law has the following components:

- The control law depends on predicted behavior.
- The output predictions are computed using a process model.
- The current input is determined by optimizing some measure of predicted performance.
- The receding horizon: the control input is updated at every sampling instant.

Most control laws, say PID (proportional, integral and derivative) control, does not explicitly consider the future implication of current control actions. To some extent this is only accounted by the expected closed-loop dynamics. MPC on the other hand implicitly (or explicitly) computes the predicted behavior over some horizon. One can therefore restrict the choice of the proposed input trajectories to those that do not lead to difficulties in the future.

In order to predict the future behavior of a process, we must have a model of how the process behaves. In particular, this model must show the dependence of the output on the current measured variable and the current/future inputs. This does not have to be linear (e.g. transfer function, state-space) and in fact can be just about anything. A precise model is not always required to get tight control, because the decisions are updated regularly. This will deal with some model uncertainty in a fairly fast time scale. The decision on the best control is thus continually updated using information from this comparison [92].

This way, model based predictive control methods are optimal regulators, with a defined cost function on a defined and encompassed prediction horizon with restrictions [93], [94], [95], [96]. The control signal is calculated over a defined horizon, but from the sequence of applicable control signals only the first one is used in the next sample. This procedure is repeated according to the principle of the moving horizon, using new iterations, as such provides the reaction in each sample. The method was developed for systems with physical restrictions, in the first stage for the control of chemical processes in the oil industry, then it was applied to various rapid processes from automotive or power electronics industry [97] , [98]. By default the optimization problem can be solved, for each sample, or explicitly using the multi-parameter programming techniques (mp-LP, mp-QP).

Linear quadratic optimal control

In practice most MPC algorithms use linear models because the dependence of the predictions on future control choices is then linear and this facilitates optimization as well as off-line analysis of expected closed-loop behavior. However, nonlinear models can be used where the implied computational burden is not a problem and linear approximations are not accurate enough. It is also important to note here the comment fit for purpose. In predictive control, the model is used solely to compute system output predictions, so the model is fit for purpose if it gives accurate enough predictions. The effort and detail put into modeling stage should reflect this. Let us assume that the system is linear and time-invariant (LTI):

$$\mathbf{x}(q+1) = \mathbf{A}\mathbf{x}(q) + \mathbf{B}\mathbf{u}(q), \quad (4.6)$$

where $\mathbf{x}(q) \in \mathbb{R}^n$ and $\mathbf{u}(q) \in \mathbb{R}^m$ are the state and input vectors respectively. We define a quadratic cost function over a finite horizon of N steps:

$$J_0(\mathbf{U}_0, \mathbf{x}(0)) = \mathbf{x}'_N \mathbf{P} \mathbf{x}_N + \sum_{k=0}^{N-1} \mathbf{x}'_k \mathbf{Q} \mathbf{x}_k + \mathbf{u}'_k \mathbf{R} \mathbf{u}_k \quad (4.7)$$

where $\mathbf{U}_0 = [\mathbf{u}'_0, \dots, \mathbf{u}'_{N-1}] \in \mathbb{R}^s$, $s = m \cdot N$ is the decision vector (with m dimensional input vector) constraining all future inputs, also $\mathbf{P} = \mathbf{P}' \succeq 0$, $\mathbf{Q} = \mathbf{Q}' \succeq 0$, $\mathbf{R} = \mathbf{R}' \succeq 0$, and \mathbf{x}_k denotes the state vector at time k obtained from $\mathbf{x}_0 = \mathbf{x}(0)$. We also apply the system model based on (4.6):

$$\mathbf{x}_{k+1} = \mathbf{A}\mathbf{x}_k + \mathbf{B}\mathbf{u}_k, \quad (4.8)$$

From the above a finite optimal control problem can be considered:

$$\begin{aligned} J_0^*(\mathbf{x}(0)) &= \min_{\mathbf{U}_0} J_0(\mathbf{U}_0, \mathbf{x}(0)) \\ \text{subj. to } &\mathbf{x}_{k+1} = \mathbf{A}\mathbf{x}_k + \mathbf{B}\mathbf{u}_k \\ &\mathbf{x}_0 = \mathbf{x}(0) \\ &k = 0, 1, \dots, N-1 \end{aligned} \quad (4.9)$$

The first step is to write the equality constraints to express all future states and inputs from the initial state \mathbf{x}_0 until the end of horizon N :

$$\underbrace{\begin{bmatrix} \mathbf{x}(0) \\ \mathbf{x}_1 \\ \vdots \\ \mathbf{x}_N \end{bmatrix}}_{\mathcal{X}^x} = \underbrace{\begin{bmatrix} \mathbf{I}_0 \\ \mathbf{A}_1 \\ \vdots \\ \mathbf{A}^N \end{bmatrix}}_{\mathcal{S}^x} \mathbf{x}(0) + \underbrace{\begin{bmatrix} 0 & \cdots & \cdots & 0 \\ \mathbf{B} & 0 & \cdots & 0 \\ \mathbf{AB} & \ddots & \ddots & \vdots \\ \vdots & \ddots & \ddots & \vdots \\ \mathbf{A}^{N-1}\mathbf{B} & \ddots & \ddots & \mathbf{B} \end{bmatrix}}_{\mathcal{S}^u} \underbrace{\begin{bmatrix} \mathbf{u}_0 \\ \vdots \\ \mathbf{u}_N \end{bmatrix}}_{\mathcal{U}^u}. \quad (4.10)$$

Here all future states are explicit functions of the state $\mathbf{x}(0)$ and the future inputs of $\mathbf{u}_0, \mathbf{u}_1$ only. By defining appropriate quantities, we can rewrite (4.10) in a compact form:

$$\mathcal{X}^x = \mathcal{S}^x(0) + \mathcal{S}^u \mathbf{U}_0. \quad (4.11)$$

Using the same notation the object function can be rewritten as:

$$J(\mathbf{x}_0, \mathbf{U}_0) = \mathcal{X}' \bar{\mathbf{Q}} \mathcal{X} + \mathbf{U}_0' \bar{\mathbf{R}} \mathbf{U}_0, \quad (4.12)$$

where $\bar{\mathbf{Q}} = \text{diag}\{\mathbf{Q}, \dots, \mathbf{Q}, \mathbf{P}\}$, and $\bar{\mathbf{R}} = \text{diag}\{\mathbf{R}, \dots, \mathbf{R}\}$. Substituting (4.11) into the objective function (4.12) yields:

$$\begin{aligned} J(\mathbf{x}_0, \mathbf{U}_0) &= (\mathcal{S}^x(0) + \mathcal{S}^u \mathbf{U}_0)' \bar{\mathbf{Q}} (\mathcal{S}^x(0) + \mathcal{S}^u \mathbf{U}_0) + \mathbf{U}_0' \bar{\mathbf{R}} \mathbf{U}_0 \\ &= \mathbf{U}_0' \underbrace{(\mathcal{S}^{u'} \bar{\mathbf{Q}} \mathcal{S}^u + \bar{\mathbf{R}})}_{\mathbf{H}} \mathbf{U}_0 + \\ &\quad + 2\mathbf{x}'(0) \underbrace{(\mathcal{S}^{x'} \bar{\mathbf{Q}} \mathcal{S}^u)}_{\mathbf{F}} \mathbf{U}_0 + \\ &\quad + \mathbf{x}'(0) \underbrace{(\mathcal{S}^{x'} \bar{\mathbf{Q}} \mathcal{S}^x)}_{\mathbf{Y}} \mathbf{x}(0) \\ &= \mathbf{U}_0' \mathbf{H} \mathbf{U}_0 + 2\mathbf{x}'(0) \mathbf{F} \mathbf{U}_0 + \mathbf{x}'(0) \mathbf{Y} \mathbf{x}(0). \end{aligned} \quad (4.13)$$

Because $\bar{\mathbf{R}} \succ 0$, and $\mathbf{H} \succ 0$, thus $J(\mathbf{x}_0, \mathbf{U}_0)$ is a positive definite quadratic function of \mathbf{U}_0 , therefore its minimum can be found by computing its gradient and setting it to zero, which yields the optimal vector of future inputs:

$$\begin{aligned} \mathbf{U}_0^*(\mathbf{x}(0)) &= -\mathbf{H}^{-1} \mathbf{F}' \mathbf{x}(0) \\ &= -(\mathcal{S}^{u'} \bar{\mathbf{Q}} \mathcal{S}^u + \bar{\mathbf{R}})^{-1} \mathcal{S}^{u'} \bar{\mathbf{Q}} \mathcal{S}^x \mathbf{x}(0). \end{aligned} \quad (4.14)$$

With (4.14) applied and calculated \mathbf{U}_0 the cost is the optimal following:

$$\begin{aligned} \mathbf{J}_0^*(\mathbf{x}(0)) &= -\mathbf{x}(0)' \mathbf{F} \mathbf{H}^{-1} \mathbf{F}' \mathbf{x}(0) \\ &= \mathbf{x}(0)' [\mathcal{S}^{x'} \bar{\mathbf{Q}} \mathcal{S}^x - \mathcal{S}^{x'} \bar{\mathbf{Q}} \mathcal{S}^u (\mathcal{S}^{u'} \bar{\mathbf{Q}} \mathcal{S}^u + \bar{\mathbf{R}})^{-1} \mathcal{S}^{u'} \bar{\mathbf{Q}} \mathcal{S}^x] \mathbf{x}(0). \end{aligned} \quad (4.15)$$

Note that the optimal vector of future inputs $\mathbf{U}_0^*(\mathbf{x}(0))$ is a linear function of (4.14) of the initial state $\mathbf{x}(0)$ and the optimal cost $J_0^*(\mathbf{x}(0))$ is a quadratic function (4.15) of the initial state $\mathbf{x}(0)$.

Alternatively the formulation can be done in a recursive manner. The optimal cost can be defined as $J_j^*(\mathbf{x}_j)$ for the j^{th} for the $N - j$ step problem starting from state \mathbf{x}_j as:

$$J_j^*(\mathbf{x}_j) = \min_{\mathbf{u}_j, \dots, \mathbf{u}_{N-1}} \mathbf{x}_N' \mathbf{P} \mathbf{x}_N + \sum_{k=0}^{N-1} \mathbf{x}_k' \mathbf{Q} \mathbf{x}_k + \mathbf{u}_k' \mathbf{R} \mathbf{u}_k. \quad (4.16)$$

The optimal "one step cost to go" can be obtained as:

$$\begin{aligned} J_{N-1}^*(\mathbf{x}_{N-1}) &= \min_{\mathbf{u}_{N-1}} \mathbf{x}_N' \mathbf{P}_N \mathbf{x}_N + \mathbf{x}_{N-1}' \mathbf{Q} \mathbf{x}_{N-1} + \mathbf{u}_{N-1}' \mathbf{R} \mathbf{u}_{N-1}. \\ \text{subj. to } & \mathbf{x}_N = \mathbf{A} \mathbf{x}_{N-1} + \mathbf{B} \mathbf{u}_{N-1} \\ & \mathbf{P}_N = \mathbf{P}, \end{aligned} \quad (4.17)$$

where $J_{N-1}^*(\mathbf{x}_{N-1})$ is a positive quadratic function of the decision variable \mathbf{u}_{N-1} . Writing (4.17) as the objective function:

$$\begin{aligned} J_{N-1}^*(\mathbf{x}_{N-1}) &= \min_{\mathbf{u}_{N-1}} \{ \mathbf{x}'_{N-1} (\mathbf{A}' \mathbf{P}_N \mathbf{A} + \mathbf{Q}) \mathbf{x}_{N-1} + \\ &+ 2\mathbf{x}'_{N-1} \mathbf{A}' \mathbf{P}_N \mathbf{B} \mathbf{u}_{N-1} + \\ &+ \mathbf{u}'_{N-1} (\mathbf{B}' \mathbf{P}_N \mathbf{B} + \mathbf{R}) \mathbf{x}_{N-1} \}. \end{aligned} \quad (4.18)$$

The optimal input can be found by setting the gradient to zero:

$$\mathbf{u}_{N-1}^* = \underbrace{-(\mathbf{B}' \mathbf{P}_N \mathbf{B} + \mathbf{R})^{-1} \mathbf{B}' \mathbf{P}_N \mathbf{A}}_{\mathbf{F}_{N-1}} \mathbf{x}_{N-1}, \quad (4.19)$$

and the optimal one step optimal cost:

$$J_{N-1}^*(\mathbf{x}_{N-1}) = \mathbf{x}'_{N-1} \mathbf{P}_{N-1} \mathbf{x}_{N-1}, \quad (4.20)$$

where \mathbf{P}_{N-1} can be defined recursively as:

$$\mathbf{P}_{N-1} = \mathbf{A}' \mathbf{P}_N \mathbf{A} + \mathbf{Q} - \mathbf{A}' \mathbf{P}_N \mathbf{B} (\mathbf{B}' \mathbf{P}_N \mathbf{B} + \mathbf{R})^{-1} \mathbf{B}' \mathbf{P}_N \mathbf{A}. \quad (4.21)$$

The next stage is to write down the "two step" problem based on (4.17):

$$\begin{aligned} J_{N-2}^*(\mathbf{x}_{N-2}) &= \min_{\mathbf{u}_{N-2}} \mathbf{x}'_{N-2} \mathbf{P}_{N-1} \mathbf{x}_{N-1} + \mathbf{x}'_{N-2} \mathbf{Q} \mathbf{x}_{N-2} + \mathbf{u}'_{N-2} \mathbf{R} \mathbf{u}_{N-2}. \\ \text{subj. to } \mathbf{x}_{N-1} &= \mathbf{A} \mathbf{x}_{N-2} + \mathbf{B} \mathbf{u}_{N-2} \end{aligned} \quad (4.22)$$

We since (4.22) has the same form as (4.17) we can apply the same solution seen at (4.19):

$$\mathbf{u}_{N-2}^* = \underbrace{-(\mathbf{B}' \mathbf{P}_{N-1} \mathbf{B} + \mathbf{R})^{-1} \mathbf{B}' \mathbf{P}_{N-1} \mathbf{A}}_{\mathbf{F}_{N-2}} \mathbf{x}_{N-2}, \quad (4.23)$$

where the "two step" cost:

$$J_{N-2}^*(\mathbf{x}_{N-2}) = \mathbf{x}'_{N-2} \mathbf{P}_{N-2} \mathbf{x}_{N-2}, \quad (4.24)$$

where \mathbf{P}_{N-2} can be defined recursively as:

$$\mathbf{P}_{N-2} = \mathbf{A}' \mathbf{P}_{N-1} \mathbf{A} + \mathbf{Q} - \mathbf{A}' \mathbf{P}_{N-1} \mathbf{B} (\mathbf{B}' \mathbf{P}_{N-1} \mathbf{B} + \mathbf{R})^{-1} \mathbf{B}' \mathbf{P}_{N-1} \mathbf{A}. \quad (4.25)$$

Continuing in this manner at some arbitrary time k the optimal control action is:

$$\mathbf{u}^*(k) = \underbrace{-(\mathbf{B}' \mathbf{P}_{k+1} \mathbf{B} + \mathbf{R})^{-1} \mathbf{B}' \mathbf{P}_{k+1} \mathbf{A}}_{\mathbf{F}_k} \mathbf{x}_k, \quad (4.26)$$

where $k = 0, 1, \dots, N-1$ and:

$$\mathbf{P}_k = \mathbf{A}' \mathbf{P}_{k+1} \mathbf{A} + \mathbf{Q} - \mathbf{A}' \mathbf{P}_{k+1} \mathbf{B} (\mathbf{B}' \mathbf{P}_{k+1} \mathbf{B} + \mathbf{R})^{-1} \mathbf{B}' \mathbf{P}_{k+1} \mathbf{A}. \quad (4.27)$$

and the optimal starting cost starting from the measured state:

$$J_k^*(\mathbf{x}(k)) = \mathbf{x}'(k) \mathbf{P}_k \mathbf{x}(k). \quad (4.28)$$

Equation (4.27) is called the discrete Riccati equation [99], or Riccati difference equation, which is initialised with $\mathbf{P}_n = \mathbf{P}$ and solves backwards. It is worth noting that from (4.26) the optimal control action $\mathbf{u}^*(k)$ is obtained in the form of feedback law as linear function of the measured state $\mathbf{x}(k)$ at time instance k , and the optimal cost is (4.28).

Constrained optimal control

In constrained optimal control for any input action with a given initial state the control action can be computed with quadratic programming but with respect to pre described constraints. As displayed, the linear quadratic approach requires a numerical definition so that a precise calculation can be made, that is, which optimal input trajectory gives the lowest numerical value to the cost. The main requirement is that the cost depends on the batch or recursive input sequence and that low values of cost imply good closed-loop performance good being defined for the process. Of course the choice of the cost affects the complexity of the implied optimization and this is also a consideration.

With considering an LTI system such as (4.6), let us assume that it is subject to constraints:

$$\mathbf{x}(q) \in \mathcal{X}^x, \quad \mathbf{u}(q) \in \mathcal{U}^u, \quad \forall t \geq 0, \quad (4.29)$$

where the set of inputs $\mathcal{U}^u \subseteq \mathbb{R}^m$ and states $\mathcal{X}^x \subseteq \mathbb{R}^n$ are polyhedra. when Euclidian norm is used with the cost as (4.7) with $\mathbf{P} \succeq 0$, $\mathbf{Q} \succeq 0$, and $\mathbf{R} \succ 0$ we define the constrained optimal control problem as:

$$\begin{aligned} J_0^*(\mathbf{x}(0)) &= \min_{\mathbf{U}_0} J_0(\mathbf{x}(0), \mathbf{U}_0) \\ \text{subj. to } &\mathbf{x}_{k+1} = \mathbf{A}\mathbf{x}_k + \mathbf{B}\mathbf{u}_k, k = 0, 1, \dots, N-1 \\ &\mathbf{x}_N \in \mathcal{X}_f, \mathbf{x}_k \in \mathcal{X}^x, \mathbf{u}_k \in \mathcal{U}^u \\ &\mathbf{x}_0 = \mathbf{x}(0), \end{aligned} \quad (4.30)$$

where $\mathbf{x}_N \subseteq \mathbb{R}^n$ is the terminal polyhedral region, and $\mathbf{U}_0 = [\mathbf{u}'_0, \dots, \mathbf{u}'_{N-1}]' \in \mathbb{R}^s$ with $s = m \cdot N$ is the optimization vector. We denote $\mathcal{X}_0 \subset \mathcal{X}^x$ as the set of initial states $\mathbf{x}(0)$ for which the optimal control problem is feasible such as:

$$\begin{aligned} \mathcal{X}_0 &= \{\mathbf{x}_0 \in \mathbb{R}^n : \exists \mathbf{U}_0, \\ &\text{s.t. : } \mathbf{x}_k \in \mathcal{X}^x, \mathbf{u}_k \in \mathcal{U}^u, \mathbf{x}_N \in \mathcal{X}_f, \\ &\text{where } \mathbf{x}_{k+1} = \mathbf{A}\mathbf{x}_k + \mathbf{B}\mathbf{u}_k, k = 0, \dots, N-1\}. \end{aligned} \quad (4.31)$$

We denote \mathcal{X}_i as the set of states \mathbf{x}_i at time $i = 0, 1, \dots, N$ which is feasible for (4.30). The sets \mathcal{X}_i are independent of the cost function as long as it guarantees the existence of a minima and the algorithm used to compute

the solution. There are also ways to define and compute \mathcal{X}_i . With the batch approach is as follows:

$$\begin{aligned} \mathcal{X}_i = & \{\mathbf{x}_i \in \mathbb{R}^n : \exists \mathbf{U}_i, \\ & s.t. : \mathbf{x}_k \in \mathcal{X}^x, \mathbf{u}_k \in \mathcal{U}^u, \mathbf{x}_N \in \mathcal{X}_f, \\ & \text{where } \mathbf{x}_{k+1} = \mathbf{A}\mathbf{x}_k + \mathbf{B}\mathbf{u}_k, k = 0, \dots, N-1\}. \end{aligned} \quad (4.32)$$

This definition requires, that for any initial $\mathbf{x}_i \in \mathcal{X}_i$ state there exists a feasible $\mathbf{U}_i = [\mathbf{u}_i, \dots, \mathbf{u}_{N-1}]$ which keeps the state evolution in the feasible set \mathcal{X}^x at future time instants k and forces \mathbf{x}_N into \mathcal{X}_f at $k = N$.

Next we show how to compute \mathcal{X}_i for $i = 0, \dots, N-1$. It is stated that the state \mathcal{X}^x , \mathcal{X}_f and input \mathcal{U}^u sets are \mathcal{H} -polyhedra [99], and $\mathbf{A}_x \leq \mathbf{x}\mathbf{b}_x$, $\mathbf{A}_f\mathbf{x}_N \leq \mathbf{b}_f$, are the set of equality and inequality constraints for the states and the terminal state and $\mathbf{A}_u\mathbf{u} \leq \mathbf{b}_u$ are the set of equality and inequality constraints on inputs respectively. We define the set of constraints as polyhedron \mathcal{P}_i^c at time instance i as:

$$\mathcal{P}_i^c = \{(\mathbf{U}_i, \mathbf{x}_i) \in \mathbb{R}^{m \cdot (N-i)+n}, s.t. : \mathbf{G}_u \mathbf{U}_i - \mathbf{E}_i \mathbf{x}_i \leq \mathbf{w}_i\}, \quad (4.33)$$

where \mathbf{G}_i , \mathbf{E}_i , and \mathbf{w}_i as the matrices of inequality and equality constraints are defined as:

$$\mathbf{G}_i = \begin{bmatrix} \mathbf{A}_u & 0 & \cdots & 0 \\ 0 & \mathbf{A}_u & \cdots & 0 \\ \vdots & \vdots & \ddots & \vdots \\ 0 & 0 & \cdots & \mathbf{A}_u \\ 0 & 0 & \cdots & 0 \\ \mathbf{A}_x \mathbf{B} & 0 & \cdots & 0 \\ \mathbf{A}_x \mathbf{A} \mathbf{B} & \mathbf{A}_x \mathbf{B} & \cdots & 0 \\ \vdots & \vdots & \ddots & \vdots \\ \mathbf{A}_f \mathbf{A}^{N-i-1} \mathbf{B} & \mathbf{A}_f \mathbf{A}^{N-i-2} \mathbf{B} & \cdots & \mathbf{A}_f \mathbf{B} \end{bmatrix} \quad \mathbf{E}_i = \begin{bmatrix} 0 \\ 0 \\ \vdots \\ 0 \\ -\mathbf{A}_x \\ -\mathbf{A}_x \mathbf{A} \\ -\mathbf{A}_x \mathbf{A}^2 \\ \vdots \\ -\mathbf{A}_f \mathbf{A}^{N-i} \end{bmatrix} \quad \mathbf{w}_i = \begin{bmatrix} \mathbf{b}_u \\ \mathbf{b}_u \\ \vdots \\ \mathbf{b}_u \\ \mathbf{b}_x \\ \mathbf{b}_x \\ \vdots \\ \mathbf{b}_x \\ \vdots \\ \mathbf{b}_f \end{bmatrix}. \quad (4.34)$$

Also, the set \mathcal{X}_i is a polyhedron serves as the projection of \mathcal{P}_i^c in (4.33) and in (4.34).

Next the previously mentioned terms are implemented with using the Euclidian norm case. For this we start with the constrained control problem (4.30) with the assumption of $\mathbf{Q} = \mathbf{Q}' \succeq 0$, $\mathbf{R} = \mathbf{R}' \succ 0$, and $\mathbf{R} = \mathbf{R}' \succeq 0$. As such the constrained control problem with euclidian norm:

$$\begin{aligned} J_0^*(\mathbf{x}(0)) = & \min_{\mathbf{U}_0} J_0(\mathbf{x}(0), \mathbf{U}_0) = \mathbf{x}'_N \mathbf{P} \mathbf{x}_N + \sum_{k=0}^{N-1} \mathbf{x}'_k \mathbf{Q} \mathbf{x}_k + \mathbf{u}'_k \mathbf{R} \mathbf{u}_k \\ \text{subj. to } & \mathbf{x}_{k+1} = \mathbf{A}\mathbf{x}_k + \mathbf{B}\mathbf{u}_k, k = 0, 1, \dots, N-1 \\ & \mathbf{x}_N \in \mathcal{X}_f, \mathbf{x}_k \in \mathcal{X}^x, \mathbf{u}_k \in \mathcal{U}^u \\ & \mathbf{x}_0 = \mathbf{x}(0). \end{aligned} \quad (4.35)$$

As shown in the unconstrained case (4.35) can be rewritten as:

$$\begin{aligned}
 \min_{\mathbf{U}_0} J_0(\mathbf{x}(0), \mathbf{U}_0) &= \mathbf{U}'_0 \mathbf{H} \mathbf{U}_0 + 2\mathbf{x}(0) \mathbf{F} \mathbf{U}_0 + \mathbf{x}(0) \mathbf{Y} \mathbf{x}(0) \\
 &= [\mathbf{U}'_0 \mathbf{x}'(0)] \begin{bmatrix} \mathbf{H} & \mathbf{F}' \\ \mathbf{F} & \mathbf{Y} \end{bmatrix} [\mathbf{U}'_0 \mathbf{x}'(0)]' \quad (4.36) \\
 \text{subj. to } \mathbf{G}_0 \mathbf{U}_0 &\leq \mathbf{w}_0 + \mathbf{E}_0 \mathbf{x}(0),
 \end{aligned}$$

with \mathbf{G}_0 , \mathbf{w}_0 , and \mathbf{E}_0 are defined in (4.34) and \mathbf{H} , \mathbf{F} , and \mathbf{Y} are defined in (4.13), additionally as $J_0(\mathbf{x}(0), \mathbf{U}_0) \geq 0$ it follows that $\begin{bmatrix} \mathbf{H} & \mathbf{F}' \\ \mathbf{F} & \mathbf{Y} \end{bmatrix} \succeq 0$.

To obtain problem (4.36) elimination of equality constraints can be obtained by successive substitution of $\mathbf{x}_{k+1} = \mathbf{A}\mathbf{x}_k + \mathbf{B}\mathbf{u}_k$, so only an input sequence as decision variables of $\mathbf{U}_0 = [\mathbf{u}_0, \dots, \mathbf{u}_{N-1}]$ and $\mathbf{x}(0)$ is left as a parameter vector. In general, it might be more efficient to solve the problem the equality and inequality constraints, so that sparsity can be exploited. To aim this, for this lets define the set of inputs and states as $\tilde{\mathbf{z}} = [\mathbf{x}'_1, \dots, \mathbf{x}'_N, \mathbf{u}'_0, \dots, \mathbf{u}'_{N-1}]$ and rewrite (4.35) as:

$$\begin{aligned}
 J_0^*(\mathbf{x}(0)) &= [\mathbf{U}'_0 \mathbf{x}'(0)] \begin{bmatrix} \mathbf{H} & \mathbf{F}' \\ \mathbf{F} & \mathbf{Y} \end{bmatrix} [\mathbf{U}'_0 \mathbf{x}'(0)]' \quad (4.37) \\
 \text{subj. to } \mathbf{G}_{0,eq} \tilde{\mathbf{z}} &= \mathbf{E}_{0,eq} \mathbf{x}(0) \\
 \mathbf{G}_{0,in} \tilde{\mathbf{z}} &\leq \mathbf{w}_{0,in} + \mathbf{E}_{0,in} \mathbf{x}(0),
 \end{aligned}$$

where $\mathbf{G}_{0,eq}$, and $\mathbf{E}_{0,eq}$, are the equality constraint matrices, and $\mathbf{G}_{0,in}$, $\mathbf{E}_{0,in}$, and $\mathbf{w}_{0,in}$ are the inequality constraint matrices respectively:

$$\begin{aligned}
 \mathbf{G}_{0,eq} &= \left[\begin{array}{cc|ccccc} \mathbf{I} & & -\mathbf{B} & & & & \\ -\mathbf{A} & \mathbf{I} & & -\mathbf{B} & & & \\ & & & & \ddots & & \\ & & & & & \ddots & \\ & & & & & & -\mathbf{B} \\ -\mathbf{A} & & & & & & \end{array} \right], \mathbf{E}_{0,eq} = \begin{bmatrix} \mathbf{A} \\ 0 \\ \vdots \\ 0 \end{bmatrix}, \\
 \mathbf{G}_{0,in} &= \left[\begin{array}{cc|ccccc} 0 & 0 & 0 & & & & \\ \mathbf{A}_x & 0 & 0 & 0 & & & \\ & \mathbf{A}_x & & & \ddots & & \\ & & \ddots & & & \ddots & \\ & & & \mathbf{A}_x & & 0 & 0 \\ & & & & \mathbf{A}_f & & \\ \hline 0 & 0 & \mathbf{A}_u & & & & \\ & \ddots & & \mathbf{A}_u & & & \\ & & 0 & & \ddots & & \\ & & & 0 & & \mathbf{A}_u & \mathbf{A}_u \\ & & & & & & \end{array} \right], \mathbf{w}_{0,in} = \begin{bmatrix} \mathbf{b}_x \\ \mathbf{b}_x \\ \vdots \\ \mathbf{b}_x \\ \mathbf{b}_f \\ \mathbf{b}_u \\ \mathbf{b}_u \\ \vdots \\ \mathbf{b}_u \\ \mathbf{b}_u \end{bmatrix}, \\
 \mathbf{E}_{0,in} &= \begin{bmatrix} -\mathbf{A}'_x & 0 & \dots & 0 \end{bmatrix}, \quad (4.38)
 \end{aligned}$$

and the constructed cost matrix \mathbf{H} as:

$$\bar{\mathbf{H}} = \left[\begin{array}{c|c} \mathbf{Q} & \\ \vdots & \mathbf{Q} \\ \hline & \mathbf{P} \end{array} \middle| \begin{array}{c} \\ \\ \hline \mathbf{R} \\ \vdots \\ \mathbf{R} \end{array} \right]. \quad (4.39)$$

In the following the state feedback solution starting from the presumed initial state for one minimizing instance $J_0^*(\mathbf{x}(0))$ shall be displayed for the constrained quadratic control problem (4.35) as (4.37), with $\mathbf{G}_0, \mathbf{E}_0, \mathbf{w}_0$ as the constraint describing matrices as defined in (4.34) starting from $\mathbf{x}(0)$, and \mathbf{H} , \mathbf{F} , and \mathbf{Y} as the substitute matrices described in (4.13), to acquire the optimal solution.

We view the initial state $\mathbf{x}(0)$ as the vector of parameters as our goal to solve (4.35) for all values of the set of initial states $\mathbf{x}(0) \in \mathcal{X}_0$ and make this dependence explicit, with the computation of \mathcal{X}_0 in terms of feasibility, described in (4.32).

For convenience let us define the substitutive term \mathbf{z} as:

$$\mathbf{z} = \mathbf{U}_0 + \mathbf{H}^{-1}\mathbf{F}'\mathbf{x}(0), \quad (4.40)$$

where $\mathbf{z} \in \mathbb{R}^s$ and with this transform (4.35) to obtain the equivalent control problem:

$$\begin{aligned} \hat{J}^*(\mathbf{x}(0)) &= J_0^*(\mathbf{x}(0)) - \mathbf{x}(0)'(\mathbf{Y} - \mathbf{F}\mathbf{H}^{-1}\mathbf{F}')\mathbf{x}(0) \\ &= \min_{\mathbf{z}} \mathbf{z}'\mathbf{H}\mathbf{z} \\ \text{subj. to } &\mathbf{G}_0\mathbf{U}_0 \leq \mathbf{w}_0 + \mathbf{S}_0\mathbf{x}(0), \end{aligned} \quad (4.41)$$

where $\mathbf{S}_0 = \mathbf{E}_0 + \mathbf{G}_0\mathbf{H}^{-1}\mathbf{F}'$. In this transformed problem the initial parameter vector $\mathbf{x}(0)$ appears only on right hand side of constraints. In this case (4.41) is a multi parametric constrained quadratic optimal program that can be solved explicitly by using geometrical means described first by the authors in [100]. This shall be discussed in section (5.4).

Receding horizon control

All this said, even if we calculate the best optimal step sequence for solving the constrained control problem, there are still uncertainties for the future. Optimization over a finite horizon has the following disadvantages:

- Unforeseen problems may occur after the fixed optimization horizon, which may cancel the sequence of order for the calculated finished horizon.
- After reaching the time defined by the horizon, the law of command is no longer optimal.

- Finite horizon optimization is usually used because of the limited computing power is available, and not for theoretical reasons

To prevent this problem, the notion of optimization is introduced on a moving horizon. In each sample k , an optimization problem is solved over a defined horizon $k, \dots, k + N$ to calculate the appropriate command sequence, and only the first command is applied. This results in a moving optimization horizon, which eliminates the issues listed before displayed on Fig.(4.3).

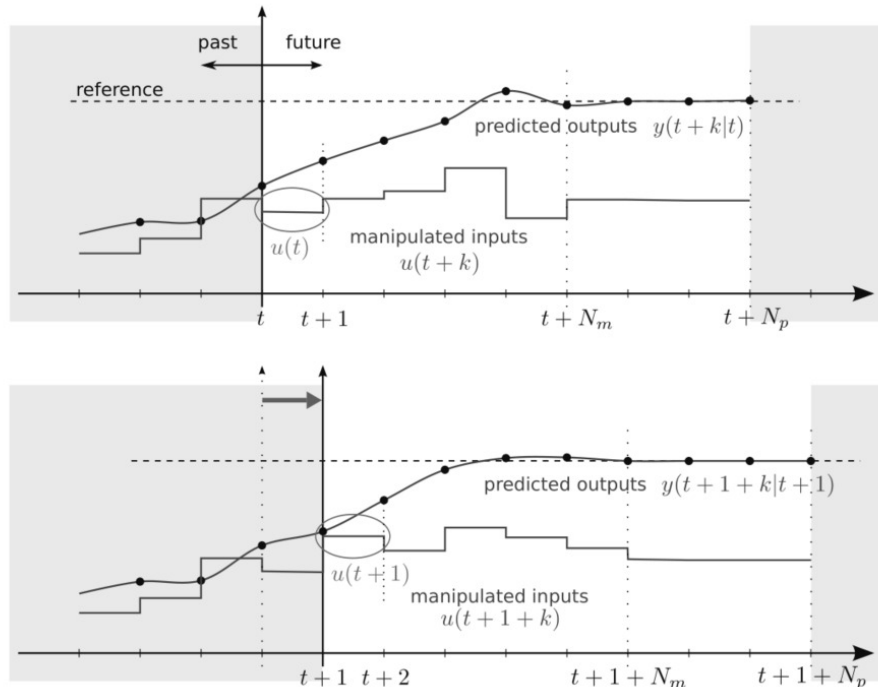


Figure 4.3: Graphical display of receding horizon control (RHC) idea [99].

The Formulation of the optimal control problem with moving horizon [101] in the system (4.6) with input and output constraints as mentioned in (4.29) with the cost function to minimize:

$$\begin{aligned}
 J(\mathbf{U}, \mathbf{x}(q)) &= \min_{\mathbf{U}_{q \rightarrow q+N|q}} J_q(\mathbf{x}(q), \mathbf{U}_{q \rightarrow q+N|q}) \\
 &= \mathbf{x}'_{q+N_y|q} \mathbf{P} \mathbf{x}_{q+N_y|q} + \sum_{k=0}^{N_y-1} \mathbf{x}'_{q+k|q} \mathbf{Q} \mathbf{x}_{q+k|q} + \mathbf{u}'_{q+k} \mathbf{R} \mathbf{u}_{q+k}, \\
 \text{subj. to } &\mathbf{x}_N \in \mathcal{X}_f, \mathbf{x}_k \in \mathcal{X}^x, \mathbf{u}_k \in \mathcal{U}^u \\
 &\mathbf{x}_{q|q} = \mathbf{x}(q), \\
 &\mathbf{x}_{q+k+1|q} = \mathbf{A} \mathbf{x}_{q+k|q} + \mathbf{B} \mathbf{u}_{q+k}, \\
 &\mathbf{u}_{q+k} = -K \mathbf{x}_{q+k|q}, N_u \leq k \leq N_y,
 \end{aligned} \tag{4.42}$$

where $\mathbf{Q} = \mathbf{Q}' \geq 0$, $\mathbf{R} = \mathbf{R}' \geq 0$, $\mathbf{P} \geq 0$, (\mathbf{C}, \mathbf{A}) is observable, and $N_u \leq N_y$, $N_c \leq N_y - 1$. One trivial possibility to choose $K = 0$ and \mathbf{P} to satisfy the Lyapunov equation:

$$\mathbf{P} = \mathbf{A}'\mathbf{P}\mathbf{A} + \mathbf{Q} \quad (4.43)$$

This means that after N_u samples the control stops and the system is evolving to an open loop form. It is obvious that the choice only makes sense if the open loop system is stable. The second option would as described with the method (4.27), but this involves to use an unconstrained control for N_u LQR samples. As a result, the MPC law calculates the optimal command sequence:

$$\mathbf{U}^*(q) = \{\mathbf{u}_q^*, \dots, \mathbf{u}_{q+N_u-1}^*\}, \quad (4.44)$$

and only the first control input is applied:

$$\mathbf{u}(q) = \mathbf{u}_q^*. \quad (4.45)$$

The optimal control inputs estimated for future samples are not taken into account and the algorithm is repeated on the basis of new measurements or a new estimation of the states.

Stability of MPC

The problem of closed system stability with the predictive control has been extensively studied e.g. in [102], [103]. In the first generation of model based controllers, stability was achieved more experimentally by choosing parameters based on previous studies and experiences. In 1988 the Lyapunov stability method for discrete systems were introduced [104], and in 1990 for continuous systems [105] also for continuous systems.

While asymptotic convergence $\lim_{k \rightarrow \infty} \mathbf{x}_k = 0$ is a desirable property, it is generally not sufficient in practice. We would also like a system to stay in a small neighborhood of the origin when it is disturbed by a little. Formally this is expressed as Lyapunov stability.

For the autonomous system:

$$\mathbf{x}_{k+1} = g(\mathbf{x}_k) \quad (4.46)$$

where $g(0) = 0$. The definition of Lyapunov stability is for the equilibrium point $\mathbf{x} = 0$ of system (4.46) is:

- stable if, for each $\epsilon > 0$, there is a $\varphi > 0$ such that:

$$\|\mathbf{x}_0\| < \varphi \text{ s.t.: } \|\mathbf{x}_k\| < \epsilon, \forall k \geq 0. \quad (4.47)$$

- unstable if not stable
- asymptotically stable if in the set $\Omega \subseteq \mathbb{R}^n$ if its stable and:

$$\lim_{k \rightarrow \infty} \mathbf{x}_k = 0, \forall \mathbf{x}_0 \in \Omega. \quad (4.48)$$

- globally asymptotically stable if it is asymptotically stable and $\Omega = \mathbb{R}^n$

- exponentially stable if it is stable and there exist constants $\chi > 0$ and $\psi \in (0, 1)$ such that:

$$\|\mathbf{x}_0\| < \varphi \text{ s.t.: } \|\mathbf{x}_k\| \leq \chi \|\mathbf{x}_0\| \psi^k, \quad \forall k \geq 0. \quad (4.49)$$

Usually to show Lyapunov stability of the origin for a particular system one constructs a so called Lyapunov function, i.e., a function satisfying the conditions of the following theorem:

Consider the equilibrium point $\mathbf{x} = 0$ of system (4.46). Let $\Omega \subset \mathbb{R}^n$ be a closed and bounded set containing the origin. Assume there exists a function $V : \mathbb{R}^n \rightarrow \mathbb{R}$ continuous at the origin, finite for every $\mathbf{x} \in \Omega$ and such that:

$$V(0) = 0 \quad (4.50a)$$

$$V(\mathbf{x}) > 0, \quad \forall \mathbf{x} \in \Omega \setminus \{0\} \quad (4.50b)$$

$$V(\mathbf{x}_{k+1}) - V(\mathbf{x}_k) \leq -\chi(\mathbf{x}_k), \quad \forall \mathbf{x} \in \Omega \setminus \{0\}, \quad (4.50c)$$

where $\chi : \mathbb{R}^n \rightarrow \mathbb{R}$ is a continuous positive definite function, then $\mathbf{x} = 0$ is asymptotically stable. As such a function satisfying (4.50) is called a Lyapunov function.

A similar theorem can be derived for global asymptotic stability i.e.: $\Omega = \mathbb{R}^n$: Consider the equilibrium point $\mathbf{x} = 0$ of system (4.46). Let $\Omega \subset \mathbb{R}^n$ be a closed and bounded set containing the origin. Assume there exists a function $V : \mathbb{R}^n \rightarrow \mathbb{R}$ continuous at the origin, finite for every $\mathbf{x} \in \Omega$ and such that:

$$\|\mathbf{x}\| \rightarrow \infty, \text{ s.t.: } V(\mathbf{x}) \rightarrow \infty \quad (4.51a)$$

$$V(0) = 0 \quad (4.51b)$$

$$V(\mathbf{x}) > 0, \quad \forall \mathbf{x} \neq 0 \quad (4.51c)$$

$$V(\mathbf{x}_{k+1}) - V(\mathbf{x}_k) \leq -\chi(\mathbf{x}_k), \quad \forall \mathbf{x} \neq 0, \quad (4.51d)$$

where $\chi : \mathbb{R}^n \rightarrow \mathbb{R}$ is a continuous positive definite function, then $\mathbf{x} = 0$ is globally asymptotically stable.

For linear systems a simple and effective Lyapunov function can be:

$$V(\mathbf{x}) = \mathbf{x}' \mathbf{P} \mathbf{x}, \quad \mathbf{P} \succ 0, \quad (4.52)$$

In order to test the satisfaction of the last point of (4.51), we compute:

$$\begin{aligned} V(\mathbf{x}_{k+1}) - V(\mathbf{x}_k) &= \mathbf{x}'_{k+1} \mathbf{P} \mathbf{x}_{k+1} - \mathbf{x}'_k \mathbf{P} \mathbf{x}_k \\ &= \mathbf{x}'_k (\mathbf{A}' \mathbf{P} \mathbf{A}) \mathbf{x}_k - \mathbf{x}'_k \mathbf{P} \mathbf{x}_k \\ &= \mathbf{x}'_k (\mathbf{A}' \mathbf{P} \mathbf{A} - \mathbf{P}) \mathbf{x}_k, \end{aligned} \quad (4.53)$$

therefore, if (4.52) holds true then:

$$\mathbf{A}' \mathbf{P} \mathbf{A} - \mathbf{P} = -\mathbf{Q}, \quad \mathbf{Q} \succ 0, \quad (4.54)$$

which is referred as discrete time Lyapunov equation.

4.4 Constrained, explicit predictive control for current source buck-type rectifiers

As mentioned in section 4.1 current source rectifiers (CSR) play a major role in industrial instrumentation. They are invaluable, in the fields of direct power control, torque control, or power injection is required.

In the third thesis, I propose an explicit model based predictive control scheme realised on a classic CSR (or buck-type rectifier) control structure. The device as the name suggests utilizes three phase alternating current waveform, obtained from domestic three phase source, to create a steady direct current on the output poles. This structure was described in section 4.2, where the topology and waveform formulation is written in detail. Also worth mention that the modelled devices's equations (described in section 4.4.1) are not entirely in the linear domain.

The employed control structure (section 4.4.2) is unique in a sense, since classic model based predictive control was not part of the power electronic domain recently. The high frequency switching periods and dynamical demand renders classic MPCs ineffective due to they massive calculation demand. However, if the control space is mapped and an effective search pattern is utilized, the feasibility could be guarantied. Also since the control structure relies on physical parameters the structure of choice supports embedded constraint handling(described in section 4.3.1) which is essential in electric power conversion realisations.

The goal of the control is two fold. On one hand the goal is to reach the steady state current reference, with minimal overshoot, at the output poles as fast as possible with a resistive load assumed. On the other, the reactive power and process noise on the network's side shall be also minimized.

4.4.1 Modeling

Understandably, model based controllers require the system's model the ought to control, or supervise. In this case the most common structure of a CSR is chosen, with inductive and capacitive filtering on both ends. The differential equations are constructed based on Kirchoff's law and then presented as a state space model for further examination.

Mathematical modeling of the CSR

The structure of the classical three phase buck-type current source rectifier (CSR) is presented in (4.4). The purpose of such a device is provide a continuous direct current at the output (i_{dc}) but instead of the widely used boost type counterparts, the voltage can be consideraby lower, making ideal for high current operations like induction heating. The device's detailed contexture can be observed in section 4.2. Basically, a finite configuration of switching states with high enough frequency consists a continuous current flow of direct- at the

output poles and alternating current at the input poles. This is reached via filtering the high dynamic ripples with low pass filtering realised with LC components. In continuous current mode, the differential equations corresponding to the CRS's inductor currents and capacitor voltages (obtained straightforwardly via Kirchoff's law.) are the following:

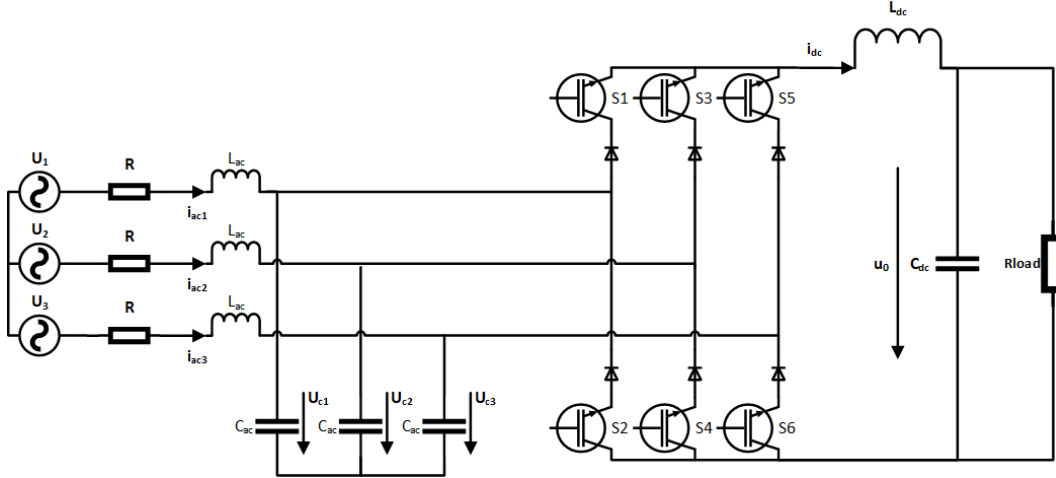


Figure 4.4: Circuit diagram of the three-phase buck-type rectifier with insulated gate bipolar transistors (IGBTs).

$$\begin{aligned} \dot{L_{ac} i_{ac_p}} &= u_p - u_{c_p} - R i_{ac_p} \\ \dot{C_{ac} u_{c_p}} &= i_{ac_p} - \delta_p i_{dc} \\ \dot{L_{dc} i_{dc}} &= (\sum_{p=1}^3 \delta_p u_{c_p}) - u_0 \\ \dot{C_{dc} u_0} &= i_{dc} - \frac{u_0}{R_{load}} \end{aligned} \quad (4.55)$$

where $p \in \{1, 2, 3\}$ is the index of three phases and δ_p describes the conduction state of the rectifier leg p (4.56).

$$\delta_p = \begin{cases} 1 & \text{if the upper transistor is ON} \\ -1 & \text{if the lower transistor is ON} \\ 0 & \text{if both are ON or OFF} \end{cases} \quad (4.56)$$

Converting the components in the stationary (Clarke) frame (displayed in section 4.2.1) of the space phasors of the three-phase quantities, from (4.55) it results:

$$\begin{aligned} \dot{L_{ac} i_{ac_\alpha}} &= u_\alpha - u_{c_\alpha} - R i_{ac_\alpha} \\ \dot{L_{ac} i_{ac_\beta}} &= u_\beta - u_{c_\beta} - R i_{ac_\beta} \\ \dot{C_{ac} u_{c_\alpha}} &= i_{ac_\alpha} - \delta_\alpha i_{dc} \\ \dot{C_{ac} u_{c_\beta}} &= i_{ac_\beta} - \delta_\beta i_{dc} \\ \dot{L_{dc} i_{dc}} &= 1.5(\delta_\alpha u_{c_\alpha} + \delta_\beta u_{c_\beta}) - u_0 \\ \dot{C_{dc} u_0} &= i_{dc} - \frac{u_0}{R_{load}} \end{aligned} \quad (4.57)$$

Equation (4.57) is transformed to the synchronous reference (Park) frame (displayed in section 4.2.1) rotating with the u_{c_d} capacitor voltage space vector. The resulting mathematical model is thus:

$$\begin{aligned}
 L_{ac}\dot{i}_{ac_d} &= u_d - u_{c_d} - Ri_{ac_d} + \omega_s L_{ac}i_{ac_q} \\
 L_{ac}\dot{i}_{ac_q} &= u_d - u_{c_q} - Ri_{ac_q} - \omega_s L_{ac}i_{ac_d} \\
 C_{ac}\dot{u}_{c_d} &= i_{ac_d} - \delta_d i_{dc} + \omega_s C_{ac}u_{c_q} \\
 C_{ac}\dot{u}_{c_q} &= i_{ac_q} - \delta_q i_{dc} - \omega_s C_{ac}u_{c_d} \\
 L_{dc}\dot{i}_{dc} &= 1.5(\delta_d u_{c_d} + \delta_q u_{c_q}) - u_0 \\
 C_{dc}\dot{u}_0 &= i_{dc} - \frac{u_0}{R_{load}}
 \end{aligned} \tag{4.58}$$

where ω_s represents the network voltage vector's angular velocity.

Model simplification

Notice, that the sixth-order ODE model (4.58) is bilinear in its states and inputs because of the product terms (e.g.: $\delta_d i_{dc}$). As such, using design methods for linear systems is not straightforward. The high complexity given by the system's order is another problem to tackle. For designing classic MPC, linear, low-order equation systems are favorable. Hence simplification of the model would bring noteworthy benefits, making the MPC design more straightforward, when a linear system resulted. Since the three phase alternating current (AC) and the direct current (DC) side's time constants differ significantly (as in the AC: $\omega_{ac} = \frac{1}{\sqrt{L_{ac}C_{ac}}} \cong 5.7 \cdot 10^3$ rad/s, and on the DC: $\omega_{dc} = \frac{1}{\sqrt{L_{dc}C_{dc}}} \cong 2.8 \cdot 10^2$ rad/s, see Table (4.1). for reference). Thus, the differential equations can be separated into two sets, and the control of the AC and DC sides can be decoupled as described in [75]. The AC side model results as follows:

$$\begin{bmatrix} \dot{i}_{ac_d} \\ \dot{i}_{ac_q} \\ \dot{u}_{c_d} \\ \dot{u}_{c_q} \end{bmatrix} = \begin{bmatrix} -\frac{R}{L_{ac}} & \omega & -\frac{1}{L_{ac}} & 0 \\ -\omega & -\frac{R}{L_{ac}} & 0 & -\frac{1}{L_{ac}} \\ \frac{1}{C_{ac}} & 0 & 0 & \omega \\ 0 & \frac{1}{C_{ac}} & -\omega & 0 \end{bmatrix} \begin{bmatrix} i_{ac_d} \\ i_{ac_q} \\ u_{c_d} \\ u_{c_q} \end{bmatrix} + \begin{bmatrix} \frac{u_d}{L_{ac}} \\ \frac{u_q}{L_{ac}} \\ -\frac{\delta_d i_{dc}}{C_{ac}} \\ -\frac{\delta_q i_{dc}}{C_{ac}} \end{bmatrix} \tag{4.59}$$

Looking at the state matrix it can be further stated that there are only weak couplings between the d and q synchronous reference frame components. This allows to handle them separately, and later to design separate control for each. The equation system describing the DC side dynamics is the following:

$$\begin{bmatrix} \dot{i}_{dc} \\ \dot{u}_0 \end{bmatrix} = \begin{bmatrix} 0 & -\frac{1}{L_{dc}} \\ \frac{1}{C_{dc}} & -\frac{1}{R_{load}C_{dc}} \end{bmatrix} \begin{bmatrix} i_{dc} \\ u_0 \end{bmatrix} + \begin{bmatrix} \frac{1.5}{L_{dc}}(\delta_d u_{c_d} + \delta_q u_{c_q}) \\ 0 \end{bmatrix} \tag{4.60}$$

It can be noticed that, with the AC and DC model separation, bilinearity disappears, since the binding coefficients are present only in the input (\mathbf{u}) of the DC state space model (4.60). Consequently, all equations are linear and with a considerably lower order, making control design much easier and allowing for the application of linear design methods. For the DC side dynamics, the linear time invariant differential equation system's matrices can be identified for predictive control design purposes:

Table 4.1: The applied parameters in model and controller design

Parameter	Value
R	0.3 Ω
Rload	10 Ω
Lac	1 mH
Ldc	30 mH
Cac	30 μF
Cdc	400 μF
f	50 Hz
fpwm	20 kHz
Un	400 V

$$\begin{aligned}
 \mathbf{x} &= \begin{bmatrix} i_{dc} \\ u_0 \end{bmatrix}, \\
 \mathbf{u} &= (\delta_d u_{cd} + \delta_q u_{cd}), \\
 \mathbf{y} &= u_0, \\
 \mathbf{A} &= \begin{bmatrix} 0 & -\frac{1}{L_{dc}} \\ \frac{1}{C_{dc}} & -\frac{1}{R_{load} C_{dc}} \end{bmatrix}, \\
 \mathbf{B} &= \begin{bmatrix} i_{dc} \\ u_0 \end{bmatrix}, \\
 \mathbf{C} &= [0 \ 1].
 \end{aligned} \tag{4.61}$$

where \mathbf{x} , \mathbf{u} and \mathbf{y} are the state, input and output vectors of the DC-side system, and \mathbf{A} , \mathbf{B} and \mathbf{C} are the state, input and output matrices. The circuit parameters used for the implementation of the control structure based on this model are presented in Table (4.1).

Control structure

With (4.61) in mind the requirements of the closed loop system are the following:

- Minimize THD and reactive power on the AC side, from the network's measurement point (at the voltage sources on the topology).
- Reach the steady state reference of i_{dc} the fastest possible with minimal overshoot on the resistive load's poles.

Using the separation of the AC side and DC side controllers, the control structure depicted in Fig. (4.5). is proposed.

The controllers operate in the synchronous frame of the AC filter capacitor voltages $u_{c(1,2,3)}$, and the rectifier input currents $i_{r(1,2,3)}$ are in phase with the capacitor voltages. The current reference $i_{\alpha\beta}^*$ supplied to the space vector modulation unit in the stationary frame, is obtained by coordinate transformation $[D(-\Theta)]$ (or Park to Clarke transformation) of the current reference (4.62) delivered by the current controllers in the synchronous frame.

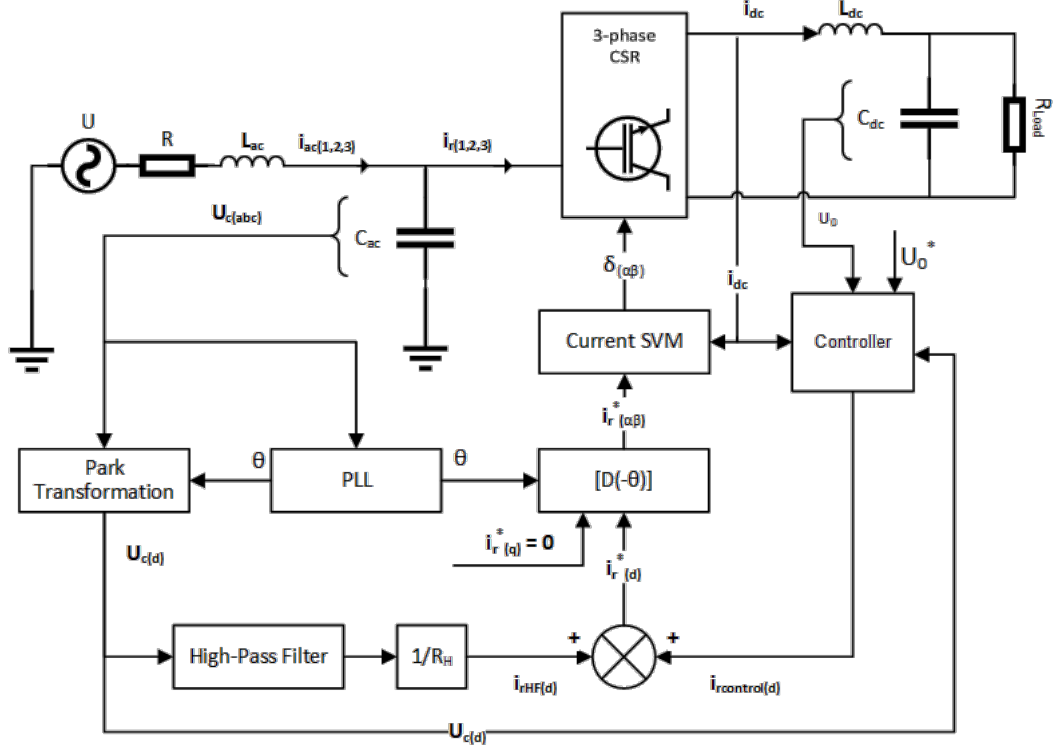


Figure 4.5: Block diagram of the control structure.

$$\begin{cases} i_{rd}^* = i_{rcontrol_d} + i_{rHF_d} \\ i_{rq}^* = 0 \end{cases} \quad (4.62)$$

In (4.62), $i_{rcontrol_d}$ represents the output of the DC voltage controller, while i_{rHF_d} represents the damping current, proportional with the high frequency component of the filter capacitor voltage (the fundamental component of the capacitor voltage in the stationary frame becomes a DC component in the synchronous frame). The DC and AC side control units are explained in more detail in the following sections, and the performance of the control structure is evaluated.

4.4.2 Control

In this section the model based control algorithm is explained, used on the DC side, followed by a simpler AC side active damping.

DC-side explicit model predictive control

Model predictive control (MPC) is an efficient and systematic method for solving complex multi-variable constrained optimal control problems [57]. The basic notions of MPC is explained in section 4.3.1, where the MPC control law is explained, namely, is based on the “receding horizon formulation”, where the model’s assumed behavior is calculated for a number of N steps, where N

stands for the horizon's length. Only the first step of the computed optimal input is applied in each iteration. The remaining steps of the optimal control input are discarded and a new optimal control problem (explained in section 4.3.1) is solved at the next sample time. Using this approach, the receding horizon policy provides the controller with the desired feedback characteristics, although with high order systems the computational effort is considerably demanding since all the steps should be taken in to account on the specified horizon in every iteration.

With Explicit MPC (EMPC), the discrete time constrained optimal control problem is reformulated as multi-parametric linear or quadratic programming. As explained in section 4.3.1, the optimization problem can be solved off-line, making it much more feasible from the perspective of the optimal control task. The optimal control law is a piecewise affine function of the states, and the resulting solution is stored in a pre-calculated lookup table. The parameter space, or the state-space is partitioned into critical regions. The real-time implementation consists in searching for the active critical region, where the measured state variables lie, and in applying the corresponding piecewise affine control law to achieve the desired dynamics. In order to introduce the MPC implementation, let us consider a linear discrete time system (4.63) derived with the discretisation of system (4.60) with zero-order hold method, where control inputs are assumed piecewise constant over the simulation sample time $T_s = \frac{1}{f_s}$:

$$\begin{aligned} \mathbf{x}(t+1) &= \mathbf{A}_d \mathbf{x}(t) + \mathbf{B}_d \mathbf{u}(t) \\ \mathbf{y}(t) &= \mathbf{C}_d \mathbf{x}(t) \end{aligned} \quad (4.63)$$

where \mathbf{A}_d , \mathbf{B}_d , \mathbf{C}_d are the matrices of the discretised system derived from (4.61). With system (4.63) is linear and time invariant, MPC design can be followed. The following constraints have to be satisfied:

$$\begin{aligned} \mathbf{y}_{min} \leq \mathbf{y}(t) \leq \mathbf{y}_{max}, \\ \mathbf{u}_{min} \leq \mathbf{u}(t) \leq \mathbf{u}_{max} \end{aligned} \quad (4.64)$$

where $t > 0$, $\mathbf{x} \in \mathbb{R}^n$, $\mathbf{u} \in \mathbb{R}^m$, $\mathbf{y} \in \mathbb{R}^p$. The MPC solves the following constrained optimization problem [77]:

$$\min_{U=\{u_t \dots u_{t+N_u-1}\}} J(\mathbf{u}, \mathbf{x}(t)) = \sum_{k=0}^{N_y-1} (\mathbf{x}_{t+N_y|t}^T \mathbf{Q} \mathbf{x}_{t+N_y|t} + \mathbf{u}_{t+k}^T \mathbf{R} \mathbf{u}_{t+k}) \quad (4.65)$$

subject to:

$$\begin{aligned} \mathbf{x}_{min} \leq \mathbf{x}_{t+k|t} \leq \mathbf{x}_{max}, & k = 1, \dots, N_c - 1 \\ \mathbf{u}_{min} \leq \mathbf{u}_{t+k|t} \leq \mathbf{u}_{max}, & k = 1, \dots, N_c - 1 \\ \mathbf{x}_{t|t} = \mathbf{x}(t), \mathbf{u}_{t|t} = \mathbf{u}(t) \\ \mathbf{x}_{t+k+1|t} = \mathbf{A}_d \mathbf{x}_{t+k|t} + \mathbf{B}_d \mathbf{u}_{t+k|t} \\ \mathbf{y}_{t+k|t} = \mathbf{C}_d \mathbf{x}_{t+k|t} \\ \mathbf{u}_{t+k|t} = -K \mathbf{x}_{t+k|t}, & k \geq 0 \end{aligned} \quad (4.66)$$

There the formulation of such problem is described in detail in chapter (4.3.1). This problem is solved at each time instant t , where $\mathbf{x}_{t+k|t}$ denotes the state vector predicted at time $t+k$, obtained by applying the input sequence $\mathbf{u}_{t|t} \dots \mathbf{u}_{t|t+1}$ to model (4.69), starting from the state $\mathbf{x}_{t|t}$. Further, it is assumed that Q and R , are symmetric positive semidefinite ($\mathbf{Q}_w = \mathbf{Q}_w^T \geq 0$, $\mathbf{R}_w = \mathbf{R}_w^T > 0$) and K is a feedback gain. Further, N_y, N_u, N_c are the output, input and constraint horizons, respectively. Using the model for predicting the future behavior of the system and with some appropriate substitution and variable manipulation which basic notions showed in section 4.3.1, the problem (4.65),(4.66) can be transformed to the standard multi parametric quadratic programming form, as described in [77]:

$$J^*(\mathbf{x}(t)) = \min_{\mathbf{z}} J(\mathbf{x}, \mathbf{z}) = \frac{1}{2} \mathbf{z}' \mathbf{H} \mathbf{z} \quad (4.67)$$

where subject to:

$$\mathbf{G} \mathbf{z} \leq \mathbf{w} + \mathbf{S} \mathbf{x}(t) \quad (4.68)$$

where the matrices \mathbf{H} , \mathbf{G} , \mathbf{w} , \mathbf{S} result directly from the coordinate transformations described in (4.3.1). The solution of the quadratic optimization problem for each critical region has the form:

$$\mathbf{u}^* = \mathbf{F}_i \mathbf{x} + \mathbf{g}_i \quad (4.69)$$

and the critical region is described by:

$$\mathcal{C}_{reg_i} = \{\mathbf{x} \in \mathbb{R}^n | \mathbf{H}_i \mathbf{x} \leq \mathbf{K}_i\} \quad (4.70)$$

Thus, the explicit MPC controller is completely characterized by the set of parameters:

$$\{\mathbf{F}_i, \mathbf{g}_i, \mathbf{H}_i, \mathbf{K}_i | i = 1 \dots N\} \quad (4.71)$$

In case of the discrete time system resulting from (4.61), for sampling time equal with the switching period $T_s = 5 \cdot 10^{-5}$ s, the problem defined to be solved by MPC is the minimization of the quadratic cost function (4.63) for:

$$\mathbf{R}_w = [1], \mathbf{Q}_w = \begin{bmatrix} 5^{-5} & 0 \\ 0 & 5^{-5} \end{bmatrix}, N_y = N_u = N_c = 4. \quad (4.72)$$

Since N_y, N_u, N_c take the same value, they will be substituted by N . The constraints defined based on the rated power of the CSR $P_n = 2500$ W, are:

$$\begin{aligned} 0 \leq i_{dc} &\leq 50A \\ 0 \leq u_0 &\leq 500V. \end{aligned} \quad (4.73)$$

The state space partition resulting from this problem has 10 critical regions, which can be observed in Fig. (4.6).

From the basis of the discretised model (4.63), the given constraints (4.73), and horizon (4.73) the cost function (4.65) is established via the MPT toolbox

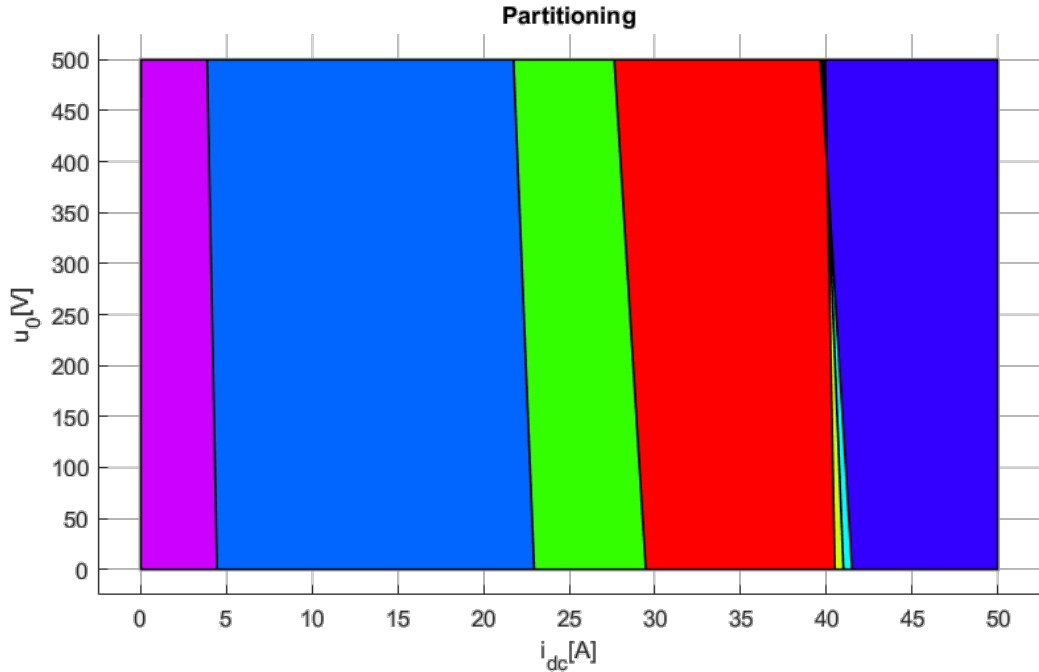


Figure 4.6: State space partitioning over the determined constraints.

[106] and uaastrom2013computeraastrom2013computerzhang2015simplifiedsed in the generated controller for the EMPC design [29], [31]. The controller is created as a compliable S-function in the Matlab/Simulink environment and its place in the control structure can be observed in Fig. (4.7). as the EMPC controller. The output of the MPC controller is the control variable obtained via solving (4.66) and $u_{MPC} = (\delta_d u_{cd} + \delta_q u_{cq})$, from which the current reference can be calculated using (4.73). The quadrature component u_{cq} is zero in the synchronous frame of the filter capacitor voltage.

$$i_{rMPC_d} = \frac{u_{MPC}}{u_{cd}} \cdot i_{dc} \quad (4.74)$$

Active AC-side damping

The CSR requires a voltage supply on the AC side. Taking the inductive character of the mains into consideration, the presence of a three-phase capacitor bank at the input of the CSR is a must. The most convenient is to use three-phase LC filtering with inductors on the lines and star connected capacitors resembling those in Fig. (4.4), although the resonance phenomena between these components can still cause difficult problems.

Let us consider the AC side differential equation of the CSR from (4.59):

$$\begin{bmatrix} \dot{i}_{ac_d} \\ \dot{i}_{ac_q} \\ \dot{u}_{cd} \\ \dot{u}_{cq} \end{bmatrix} = \begin{bmatrix} -\frac{R}{L_{ac}} & \omega & -\frac{1}{L_{ac}} & 0 \\ -\omega & -\frac{R}{L_{ac}} & 0 & -\frac{1}{L_{ac}} \\ \frac{1}{C_{ac}} & 0 & 0 & \omega \\ 0 & \frac{1}{C_{ac}} & -\omega & 0 \end{bmatrix} \begin{bmatrix} i_{ac_d} \\ i_{ac_q} \\ u_{cd} \\ u_{cq} \end{bmatrix} + \begin{bmatrix} \frac{u_d}{L_{ac}} \\ \frac{u_q}{L_{ac}} \\ -\frac{\delta_d i_{dc}}{C_{ac}} \\ -\frac{\delta_q i_{dc}}{C_{ac}} \end{bmatrix}.$$

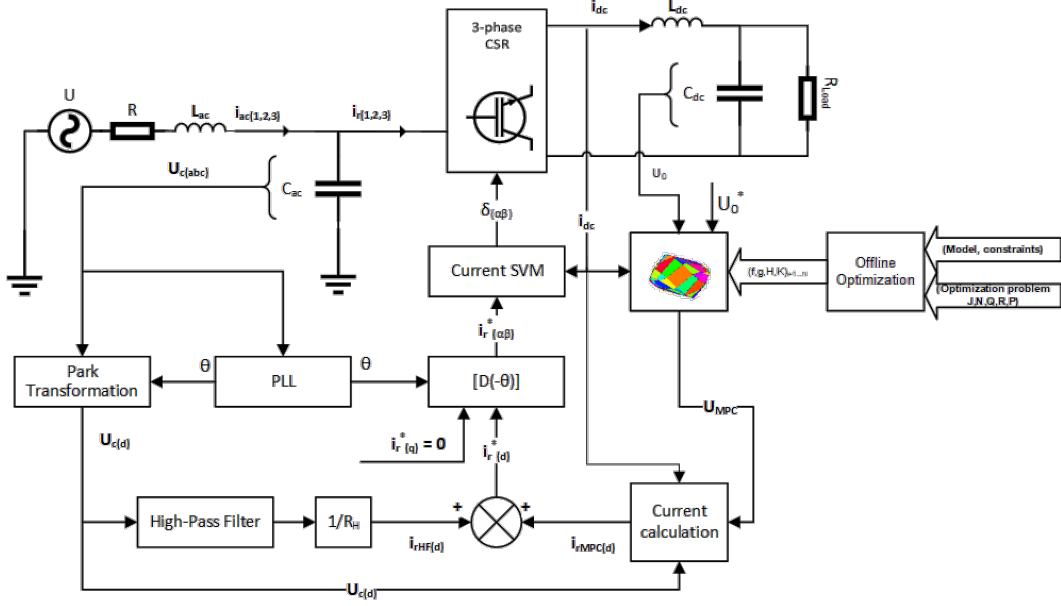


Figure 4.7: The control structure of the CSR, with MPC controller on the DC side.

The above equation set is representing the AC dynamics well, however, since the physical system is compliant to some boundaries, further simplification can be obtained as displayed by [107]. The capacitor's voltage's d-axis can be aligned with the q-axis, as:

$$u_{cq} = 0 \quad (4.75)$$

Since the time constant difference between AC and DC side, described in 4.4.1, and the large difference between L_{ac} and L_{dc} , displayed in Table (4.1). Also i_{dc} can be approximated as an I_{dc} constant (modulated by δ_d), and neglecting small couplings such ωL_{ac} , and ωC_{ac} , the AC side model looks like this:

$$\begin{aligned} L_{ac}\dot{i}_{ac_d} &= u_d - u_{cd} \\ L_{ac}\dot{i}_{ac_q} &= u_q \\ C_{ac}u_{cd} &= i_d - \delta_d I_{dc} \\ 0 &= i_d - \delta_d I_{dc}, \end{aligned} \quad (4.76)$$

Such as in (4.76) the equation along the q-axis is first order and has good stability, in addition, the d-axis can be extended in frequency domain as:

$$u_{cd} = \frac{u_d}{s^2 L_{ac} C_{ac} + 1} - \frac{s L_{ac} I_{dc} \delta_d}{s^2 L_{ac} C_{ac} + 1}, \quad (4.77)$$

where u_d carries potential disturbance due resonance of the LC filter. Hence, equation (4.79) is a second order linear system without any damping, therefore active damping (or resonance suppressing control) can be implemented. The simplest way to dampen the resonance would be to add further damping

resistor across the capacitor [73], to dampen the oscillation. Because these resistors result in high losses, active damping method can be utilised as displayed in [108], which emulate damping resistors by control. This makes the CSR bridge produce an additional high frequency current i_{rHF} , equivalent to the presence of virtual damping resistor R_H connected in parallel with the AC capacitors. The resonance of the AC side LC filter produces harmonics in the capacitor voltage with frequency close to $\omega_{ac} = \frac{1}{\sqrt{L_{ac}C_{ac}}}$, which appears as $\omega_{ac} - \omega$ component in u_{cd} , where $\omega = 2\pi f$. The fundamental component of the capacitor voltage represents a DC component in the synchronous reference frame. Therefore, a high-pass filter (HF) is applied to filter out this DC component, with the transfer function:

$$HF(s) = \frac{s}{s+0.1(\omega_{ac}-\omega)}. \quad (4.78)$$

Adding the HF's transfer function and the virtual resistance, the damped dynamics follows:

$$u_{cd} = \frac{u_d}{s^2 L_{ac} C_{ac} + 1} - \frac{s L_{ac} I_{dc} \delta_d}{s^2 L_{ac} C_{ac} + 1} - \frac{HF(s)}{s C_{ac} R_H}, \quad (4.79)$$

A virtual damping resistance R_H has been defined for calculation of the damping current component i_{rHF} from the HF component of the capacitor voltage, which can be observed in Fig. (4.5), as well as in Fig. (4.7).

4.4.3 Modulation

Modulation is required to govern the CSR device's switching states to realize the control displayed at (4.5). In other words the reference current in Clarke frame $i_{r_{\alpha\beta}}$ needs to be translated into interpretable switching states for the device. In this work this is realised via space vector modulation (SVM), meaning that the current reference is converted to the superposition of the finite set of switching states the converter could realize without malfunction (some states are prohibited e.g. breaking the choke inductor's current flow.) Of course there are other modulation schools for example SHE (mentioned in section 4.1) but they can not translate the control action so easily as SVM. As such they are not in the scope of the thesis.

The chosen modulation strategy is developed in the " $\alpha\beta$ " stationary reference frame, where $i_{r_{\alpha\beta}} = \vec{i}_{ref}$. Based on the notions already mentioned in section 4.2. The structure requires simultaneous conduction of the upper and lower transistors of the bridge, since the current of the L_{dc} choke must not be interrupted. Additionally, the switching devices are considered as ideal.

According to this, one of the upper and one of the lower switches must be closed at all times. This allows nine states, six of which are active. There are three "zero" vectors, corresponding to the switching states, when both devices of one of the bridge legs are in conduction. These current vectors are shown in Table (4.2).

The neighboring space phasors can be formulated as:

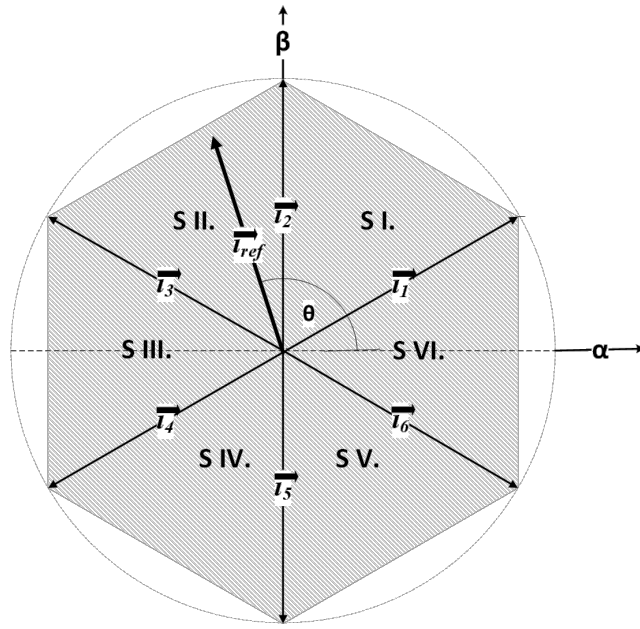


Figure 4.8: The fundamental input current vectors corresponding to the active switching states of the CSR.

$$\begin{aligned}\vec{i}_n &= \frac{2}{\sqrt{3}} i_{dc} e^{j(\frac{n\pi}{3} - \frac{\pi}{6})} \\ \vec{i}_{n+1} &= \frac{2}{\sqrt{3}} i_{dc} e^{j(\frac{n\pi}{3} + \frac{\pi}{6})} \\ n &= 1, 2, \dots, 6,\end{aligned}\quad (4.80)$$

which can be observed in Figure (4.9).

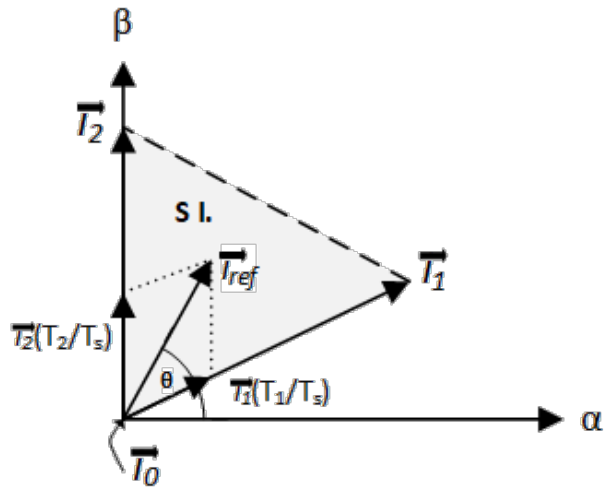


Figure 4.9: Synthesis of \vec{i}_{ref} by \vec{i}_1 , \vec{i}_2 , and \vec{i}_0

The reference current vector is sampled with fixed sampling period T_s . The sampled value of \vec{i}_{ref} is synthesized as the time average of two neighbouring space phasors adjacent to the reference current:

Table 4.2: The fundamental input current vectors corresponding to the active switching states of the CSR.

Name	Switching State						Phase currents			Vector representation
	1	2	3	4	5	6	ia	ib	ic	
\vec{i}_1	1	0	0	0	0	1	i_{dc}	0	$-i_{dc}$	$2i_{dc}e^{j\pi/6}/\sqrt{3}$
\vec{i}_2	0	0	1	0	0	1	0	i_{dc}	$-i_{dc}$	$2i_{dc}e^{j\pi/2}/\sqrt{3}$
\vec{i}_3	0	1	1	0	0	0	$-i_{dc}$	i_{dc}	0	$2i_{dc}e^{j5\pi/6}/\sqrt{3}$
\vec{i}_4	0	1	0	0	1	0	$-i_{dc}$	0	i_{dc}	$2i_{dc}e^{j7\pi/6}/\sqrt{3}$
\vec{i}_5	0	0	0	1	1	0	0	$-i_{dc}$	i_{dc}	$2i_{dc}e^{j3\pi/2}/\sqrt{3}$
\vec{i}_6	1	0	0	1	0	0	i_{dc}	$-i_{dc}$	0	$2i_{dc}e^{j11\pi/6}/\sqrt{3}$
\vec{i}_7	1	1	0	0	0	0	0	0	0	0
\vec{i}_8	0	0	1	1	0	0	0	0	0	0
\vec{i}_9	0	0	0	0	1	1	0	0	0	0

$$T_n \vec{i}_n + T_{n+1} \vec{i}_{n+1} = T_s \vec{i}_{ref} \quad (4.81)$$

T_n and T_{n+1} represent the individual durations of the switching states corresponding to the neighboring vectors. For example, in case of a current reference vector situated in the first sector, T_1 , T_2 and T_0 can be calculated using (4.82).

$$\begin{aligned} T_1 &= T_s \frac{i_{ref\alpha}}{i_{dc}} \\ T_2 &= T_s \frac{\sqrt{3}}{2i_{dc}} (i_{ref\beta} - \frac{i_{ref\alpha}}{\sqrt{3}}) \\ t_0 &= T_s - T_n - T_{n-1} = T_{7,8,9} \end{aligned} \quad (4.82)$$

The complex plane is naturally divided by the fundamental space vectors into six areas, named "sectors".

$$\begin{aligned} x \frac{\pi}{6} + \frac{(n-1)\pi}{3} \leq \theta_n \leq \frac{\pi}{6} + \frac{n\pi}{3} \\ n = 1, 2, \dots, 6 \end{aligned} \quad (4.83)$$

The non-zero space vectors are selected based on the phase angle θ between \vec{i}_{ref} and the real axis. Table (4.3) presents an example of switching pattern in case of a current reference vector situated in Sector I.

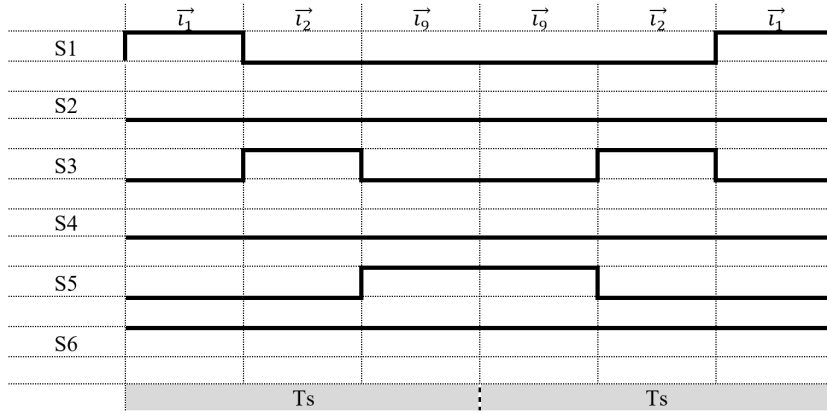
The switching scheme represented in Table (4.2). is aimed at reducing the number of commutations in a switching cycle, resulting in the reduction of the switching losses [91].

Additionally, the implemented modulation logic prevents the reference from applying currents outside the modulation circle of (4.8). This is realised in ((4.84)) resulting from the available magnitudes of the current vectors, is applied to the current reference, on top of the controller constraints in (4.73).

$$0 \leq |i_{ref}| \leq \frac{\sqrt{6}i_{dc}}{\cos\theta + \sqrt{3}\sin\theta} \quad (4.84)$$

The modulation formulation is only meant to apply on the control action in the above mentioned ways (realizing and constraining the reference) since

Table 4.3: Representation of switching sequences for SECTOR I.



the switching frequency $fpwm$ is chosen so high that the controller dynamics match with the SVM state switching frequency. As such no lag or undersampling is assumed, and the system dynamics are already implicit in the controller design.

4.4.4 Discussion

From the continuous AC (4.59), and DC (4.60) model equations described in Ch.X., the controller is formulated from discretised system (4.63), and it is described via the cost function and control problem of (4.65), and (4.66) in Ch.X+1. The evaluated model and control structure are shown on Fig.4. In the following section said EMPC's computational requirements are evaluated, and the Matlab/Simulink simulation results are compared to a classic state feedback controller's dynamic performance.

Lyapunov stability

The systematic finding of Lyapunov functions is described in detail in section 4.3.1 as well as in [99]. The explicit receding horizon control law formulated in section 4.4.2 is mapped according to (4.71), resulting the partitioning of the constrained state space displayed on Fig. (4.6). Considering system (4.63) with the given constraints of (4.73) and RHC law (4.65), the assumption is that a maximal positive-, and control invariant set \mathcal{X}_f can be obtained for the closed loop system, for every defined critical region. For finding and \mathcal{X}_f and the feasibility of constructing the critical region specific Lyapunov function an implemented verification method is available from [106], by searching \mathcal{X}_f for the closed loop autonomous PWA system. Then piece-wise Lyapunov function can be constructed displayed on Fig (4.10).

Computational effort

The binary search tree generated for the control problem presented in Fig. (4.11). The search method and formulation of the tree is described in chapter

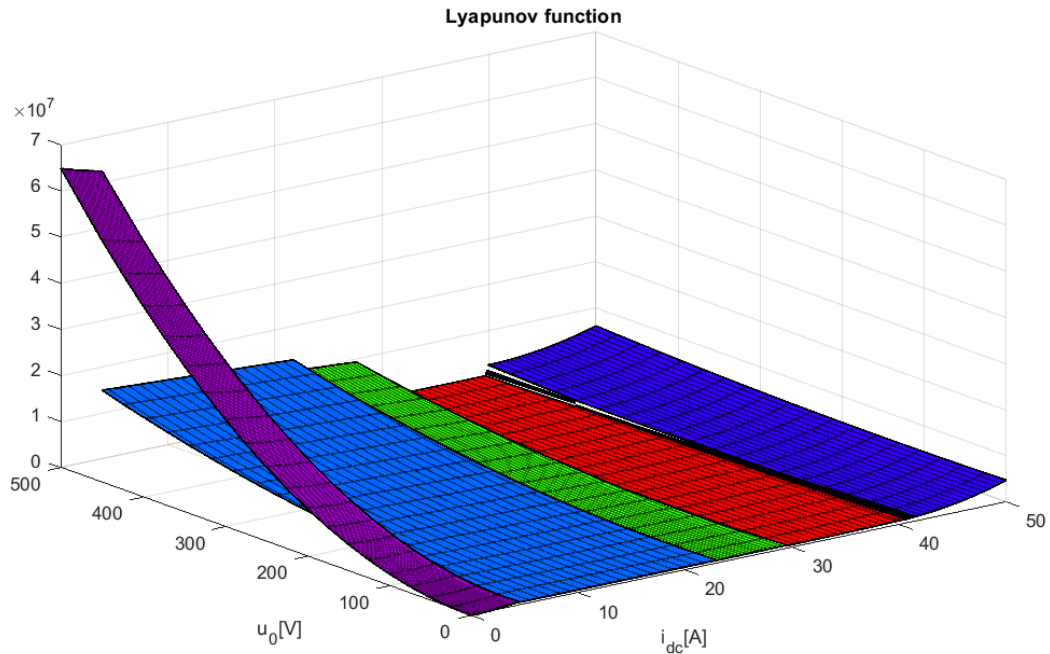


Figure 4.10: Lyapunov function for EMPC every partition.

(5.4.1). The depth of the search tree is 5 and it has a total number of 29 nodes. It is utilized with the MPT toolbox [106], and it can be used for the computationally optimal real-time implementation of the proposed algorithm on low-cost hardware.

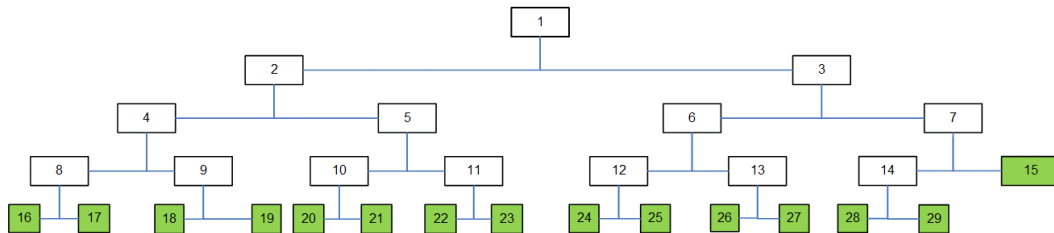


Figure 4.11: Binary search tree of the controller for a horizon of $N = 4$. The leaf nodes are depicted with filled squares. The depth of the tree is 5.

The search for an active critical region starts from the first level and represents the evaluation in each adjacent node of an inequality of the form: $x \leq K$. Thus, in this case a maximum number of 4 inequalities have to be evaluated to reach the active critical region. Implementing the presented algorithm is straightforward on a DSP processor, for instance from the dsPIC33 family by Microchip. Using the MAC (multiply and accumulate) instruction the inequality is evaluated for each node using 4 instructions, thus in 80 ns on a 50 MIPS processor (Fig. (4.12)). The active critical region can be reached in a maximum of 400 ns. Compared to the typical sample rate of 10us in the case of a CSR, the real-time implementation on a DSP processor is possible. More information about storing critical regions can be found in 5.4.1.

More information about storing critical regions can be found in 5.4.1.

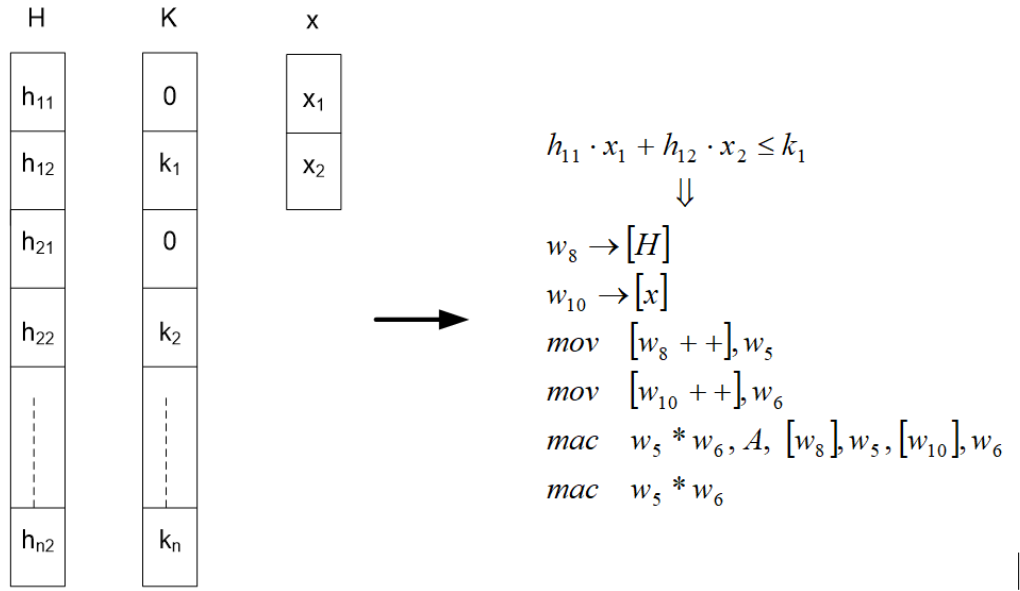


Figure 4.12: Data organization in the data memory of a single core DSP and the evaluation of a 2-dimensional inequality

Horizon performance

With the cost function ((4.65)) employed using ((4.72)), changing the length of the horizon (N) affects the system's complexity illustrated by the partition in the state space shown in Fig. (4.6)., and Fig. (4.13) presents the step response of the controlled system for different lengths of the horizon. It shows, that the response is not affected by the increase of the horizon above $N = 2$, supporting the choice of this value for Matlab Simulink implementation.

Simulation results

The simulation results are produced with Matlab/Simulik. The discrete model's ((4.63)) simulation frequency was 1 MHz, with the model parameters represented in Table (4.1)., and with the control structure shown on Fig. (4.5). The EMPC performance is shown below:

More details about the Matlab simulation are presented in [0].

Comparison with a state feedback control

On the DC side, not only the output voltage u_0 but also the inductor current i_{dc} needs to be controlled. Described in [28], a state feedback control with optimal parameters can be used as a reference based on the model properties listed in Table (4.1), with output voltage u_0 and DC bus current i_{dc} chosen as the state variables. Since u_0 is a DC quantity in steady state, an integrator signal is introduced to diminish the steady-state error. The structure of the controller is represented in Fig. (4.16).

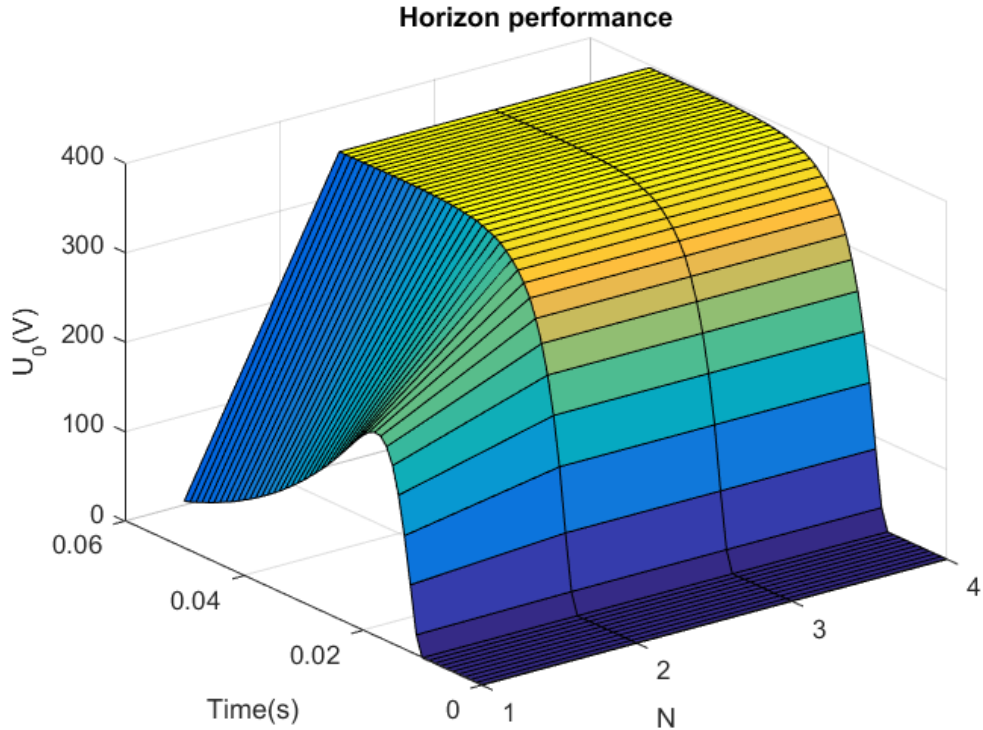


Figure 4.13: Step response of the system as a function of the horizon length (N).

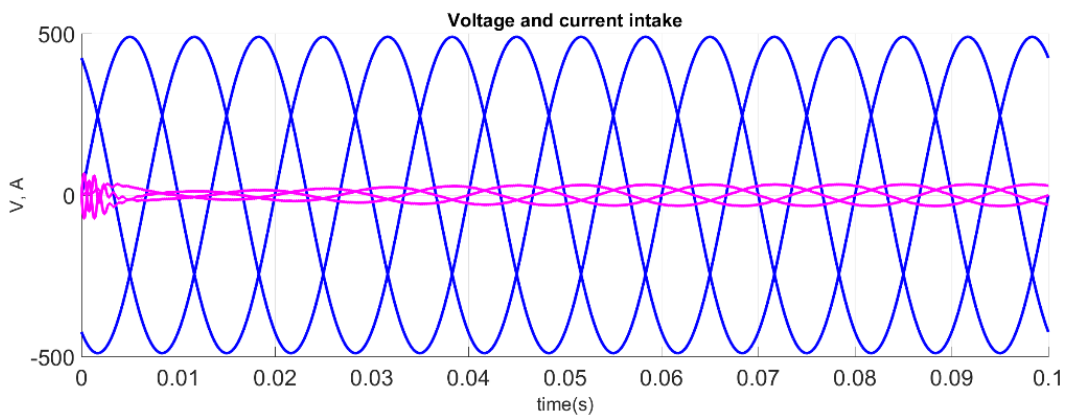


Figure 4.14: Three-phase voltage and current intake of the CSR with EMPC

The tuning constants applied and calculated according to [78] are:

$$k1 = \frac{\omega_n^3}{1.5U_n\omega_{dc}^2}, \quad k2 = \frac{1.9\omega_nL_{dc}}{1.5U_n}, \quad k3 = \frac{2.2\omega_n^2}{1.5U_n(\omega_{dc}^2-1)},$$

where,

$$\omega_n = 1.1, \quad \omega_{ac} = \frac{1}{\sqrt{L_{ac}C_{ac}}}, \quad \omega_{dc} = \frac{1}{\sqrt{L_{dc}C_{dc}}}$$
(4.85)

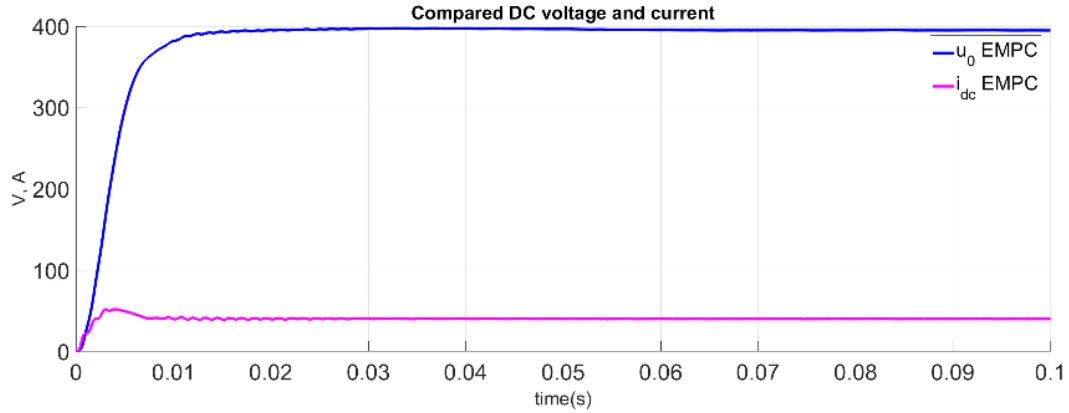


Figure 4.15: Resulting current and voltage trajectories of the CSR with (EMPC).

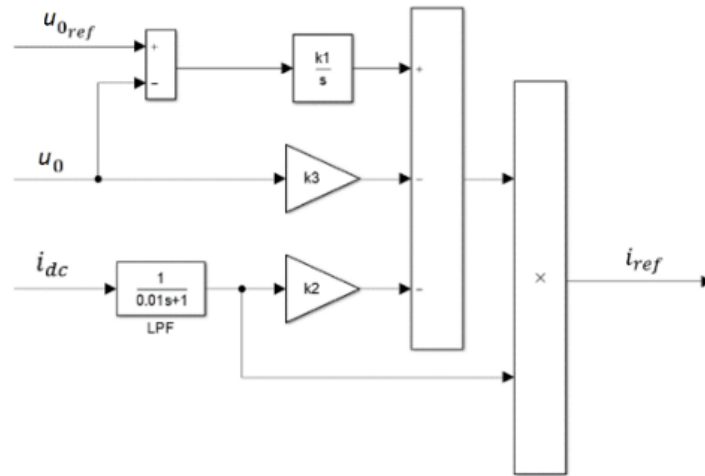


Figure 4.16: Simple DC side state feedback control structure.

The state feedback controllers block on the diagram is taking the controller's place, shown on Fig. (4.5). The independent outputs are the high pass filter's output $i_{rHF(d)}$ and the controller's output $i_{rcontrol(d)}$. The sum of the independent current values is converted to Clarke frame to be able to govern the switching states of the IGBT's. This can be done because $i_{rHF(d)}$ has only high frequency components and $i_{rcontrol(d)}$ has low frequency components due to the differences in LC time constants, as discussed in the second section. Then the control signal governing the switches is applied in the same manner, described at the start of section 4.4.3. The state feedback control's performance in comparison with the EMPC is shown in Fig. (4.17).

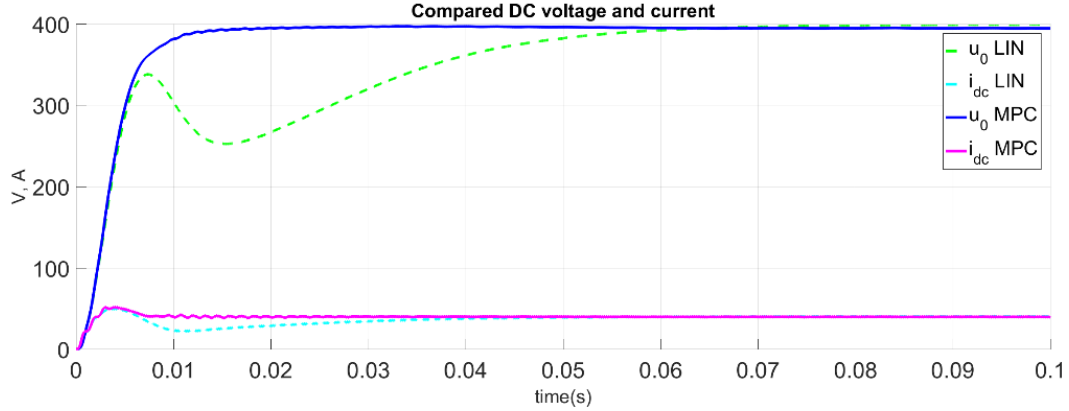


Figure 4.17: Resulting current and voltage trajectories of the CSR with explicit model predictive control (MPC) compared state feedback control (LIN).

4.5 Conclusion

The constrained, model-based optimal control of a current source rectifier has been presented in this dissertation. The dynamic model of a three-phase current source rectifier has been developed in Park frame. The proposed model has been examined from the design and implementation points of view with the purpose of explicit model-based predictive control. It proved to be the case that the regular set of differential equations of the CSR appears to be too complex, and contains non-linearity for such a design approach. To address this issue the usage of separated AC and DC equation sets was suggested to avoid linearization and complexity reduction. This solution eliminates bilinearity and enables the application of linear control design techniques. Current-based SVPWM of the three-phase converter has been used with an emphasis on the reduction of switching losses. Throughout the chapter the explicit model predictive control method is described and the method's effectiveness compared to conventional state feedback control is shown. The implementation and simulation experiments have been performed in Matlab/Simulink environment. Moreover, the proper implementation of the system in a modern DSP chip will result in real-time operation.

4.6 Notations used in the chapter

A	State matrix of the DC side system
A_d	Discretised state matrix of the DC side system
A_x	Constraint state matrix
A_u	Constraint input matrix
A_f	Constraint state matrix at the end of the horizon
A	Set if indices in states where the constraints are active
A^N	Set if indices in states where the constraints are inactive
B	Input matrix of the DC side system
B_d	Discretised input matrix of the DC side system
\bar{C}_{ac}	AC side inductance
C_{dc}	DC side inductance
C	Output matrix of the DC side system
C_d	Discretised output matrix of the DC side system
C_{reg_i}	Critical region
$D(-\Theta)$	Inverse Clarke transformation
E	Unified constraint state matrix
F	State coefficient matrix for calculating the optimal input
f	Network voltage frequency
f_{pwm}	Rectifier switching frequency
f_s	Simulation frequency
f_i	Function of state at the i^{th} step
G	Unified constraint input matrix
g_i	Function of input at the i^{th} step
H	Supplementary quadratic optimizer matrix
$HPF(s)$	High pass filter transfer function
i_{abc}	Generic three phase current
$i_{ac1,2,3}$	AC side inductance current
$i_{ac\alpha,\beta}$	AC side inductance current in Clarke frame
$i_{acd,q}$	AC side inductance current in Park frame
i_{HPF}	AC side damping current
$i_{r1,2,3}$	Rectifier current
i_{rMPC_d}	Direct component of the output of the EMPC controller
$i_{r1,2,3}^*$	Rectifier reference current
$i_{r\alpha,\beta}^*$	Rectifier reference current in Clarke frame
$i_{rcontrol_d}$	Direct component of the output of the DC voltage controller
i_{rHF_d}	Direct component of the damping current of AC noise
i_{dc}	DC side inductance current
$i_{ref\alpha,\beta,\gamma}$	α, β , or γ component of the reference current vector respectively
\vec{i}_{dq0}	Three phase current converted to Park frame
$\vec{i}_{0,...,9}$	Current vector of the phasor
\vec{i}_{ref}	Reference current vector
\mathcal{J}	Set if indices of active constraints
J	Quadratic EMPC cost function
J^*	Optimal cost value
J_0	Cost function to optimize at the initial state
J_0^*	Optimal cost function at the initial state
\mathcal{K}	Set of controller gains respective to critical regions
K	Feedback gain of EMPC controller
$k_{1,2,3}$	State feedback controller's coefficients
L_{ac}	AC side inductance
L_{dc}	DC side inductance
L_S	Input filter inductance of the three phase alternating current in VSR
L_D	Inductor for filtering the output current of the CSR (Choke)
N	Control horizon
N_y, N_u, N_c	Output, input and constraint horizons
n	Current phasor sector indicator
\mathcal{P}^c	Set of all (input and state) constraints at time instance
\mathcal{P}_p	Set of primary feasibility conditions
\mathcal{P}_d	Set of dual feasibility conditions
P_n	Nominal power of the CRS
P	Terminal penalising weight matrix
\mathbf{P}_N	Terminal penalising weight matrix at the end of the horizon
Q	State weight matrix of quadratic MPC cost function
\mathbf{Q}	Batch of state penalising weight matrix
R	Phase resistance
R_H	Virtual damping resistance

R_{load}	Load resistance
\mathbf{R}	Input weight matrix of quadratic MPC cost function
$\bar{\mathbf{R}}$	Batch of input penalising weight matrix
\mathbb{R}	Set of real numbers
S	Current phasor sector
\mathbf{S}	Coefficient constraint matrix
\mathcal{S}^x	Set of all possible future state matrices stepping through the horizon
\mathcal{S}^u	Set of all possible future input matrices stepping through the horizon
T_s	Switching period
$T_{0,...,9}$	Dwell time in the corresponding sector
t	Discrete timestep
U	Set of MPC inputs
U_n	Network line-to-line voltage
\mathbf{U}_0^*	Optimal vector of future inputs starting from the initial state
\mathcal{U}^u	Set of inputs not violating constraints
\mathbf{u}^*	Optimal vector of input
\hat{u}	Peak value of AC-side capacitor voltage
\mathbf{u}	Output vector of the DC side system
$u_{1,2,3}$	AC side phase voltage
$u_{\alpha,\beta}$	AC side phase voltage in Clarke frame
$u_{d,q}$	AC side phase voltage in Park frame
$u_{c1,2,3}$	AC side capacitance voltage
$u_{c\alpha,\beta}$	AC side capacitance voltage in Clarke frame
$u_{cd,q}$	AC side capacitance voltage in Park frame
u_0	DC side voltage on load
u_0^*	DC side voltage reference
u_{MPC}	MPC control variable
\mathbf{u}^*	Optimal input vector
v_D	Output voltage before the choke inductor L_D
$v_{i,j}$	Three phase phase-to-neutral voltage $i, j \in \{R, S, T\}$
$v_{N,RS}$	Three phase line-to-line voltage of R and S
v_{cp}	AC-side capacitor voltage, where $p \in \{1, 2, 3\}$
\hat{v}	Voltage peak
\mathbf{w}	Unified constraint vector
\mathcal{X}^x	Set of all possible future states stepping through the horizon
\mathcal{X}_f	Set of all possible future states at the end of the horizon
\mathcal{X}_0	Set of initial states
\mathbf{x}	State vector of a linear time invariant model
$\bar{\mathbf{x}}$	Minimum state value of the objective function
$\mathbf{x}(0)$	Initial state
\mathbf{y}	Input vector of the DC side system
\mathbf{Y}	Remainder supplementary matrix
\mathbf{z}	Vector of optimization variables
\mathbf{Z}^*	Set of optimizers leading to feasible states
\mathbf{z}	Optimizer of linear multi parametric problem
$\tilde{\mathbf{z}}$	Set of all future states and inputs over the horizon
$\delta_{1,2,3}$	Conduction state leg
$\delta_{\alpha,\beta}$	Conduction state leg in Clarke frame
$\delta_{d,q}$	Conduction state leg in Park frame
θ	Network voltage vector's angular displacement
$\epsilon, \varphi, \chi, \psi$	Constant sets
Ω	Closed and bounded set of states containing the origin
ω	Network voltage vector's angular velocity
ω_{ac}	Ac side LC filter angular velocity
ω_n	Damping angular velocity

Chapter 5

Thesis and Summary

5.1 Summary

The topic of this PhD. dissertation is optimal current control. The aim of the research was to apply and simulate high frequency controllers with optimization purpose of cost functions with the presence of constraints and circumstances, on controlled switch based power electronic devices.

In chapter ??, a current controlled inverter structure was presented, connected to a small, domestic grid, representing the connection of a household with possible renewable (or other) generators, to balance consumption. The examined grid, the phenomena of voltage unbalance was assumed to be present, as the main problem, of which this device was ought to not only handle, but mitigate within the limit of its physical capabilities. For this reason, first an indicator was established, based on a proposed geometrical operation, as a voltage unbalance norm candidate (section 2.3). This norm was calculated from the symmetrical difference between the convex hull of voltage phasor vectors, always present on a three phase network. The idea was, that any deviation from the ideal phasor, (which first vector assumed in phase with the ideal one) introduces sub-optimal behavior, or fault of appliances connected. This way the already present indicators of voltage unbalance was examined (section 2.4). Afterwards found that not only, they vary in result, but ignore phase differences, or the zero-sequence component (based on the Fortescue method), or its ponderous to serve as a cost function need to be minimize. The proposed geometrical norm however considers all of the above, with the addition that since it calculates area, instead of vector length differences, the result is a square-like function, serves as an excellent candidate. The downside is the yet unresolved computational overload, that is method introduces.

In the next phase, the network's unbalance was attempted to be mitigated by designing a power electronic converter for a household, which utilizes an external power source (a photo voltaic source in this case) for counter balance (section 3.4). This way some obstacles needed to be dealt with, first and foremost, the highly stochastic nature of the network. It was assumed, that the device has no external information, rather than the voltage, measured at the network connection point. This way a non-model based asynchronous paral-

lel pattern search (APPS) controller was designed and applied based on the said geometrical norm, which decreases the cost regardless of unknown circumstances. Furthermore, the device needed various subunits, to efficiently handle the power flow in all three phases, namely power-point-tracking, intermediate voltage control, and per-phase current injection was required. The results were tested in Matlab/Simulink environment with simulating the actual device via Simscape, and the unbalanced network, also with experimental measurements. The result was, that the controller could reduce the network's voltage unbalance, based on the network's robustness (how large is the impedance, which created the unbalance), how much control reserve is present as energy source, and physical boundaries (the device can not supply infinite current). Based on this the household's normal operation can withheld even in with unbalanced loads.

Lastly in chapter 4.4 in-depth modeling and predictive control task has been performed, on one power electric component, namely on a buck-type rectifier. This rectifier uses current source operation to supply the load it is connected to. The main goal was to create on the Kirchhoff's law based differential equations a model based predictive controller, suited to reach the reference point with the best dynamics. It was also taken in mind, that an implicit MPC would not be up to the task, since every control rule was to be re-calculated from scratch, implying a very expensive CPU. This gap could be bridged by reaching out for the explicit MPC method, by partitioning the state space, on a pre-defined rule set. This way the control demand could be reduced significantly, however, this is not suited for high rank systems. As such the system's bi-linearity was eliminated by applying on the premise that two dynamics which have highly different fundamental frequencies can operate in superposition. This way the problem was simplified, and explicit MPC could be implemented in DC-side, whilst active damping at the AC-side. The method's efficiency was tested in Matlab/Simulink environment against a conventional state-feedback controller, with good results. Additionally the computational demand was evaluated, with assumed binary search algorithm.

5.2 New scientific results

- I.) **Thesis:** *Geometrical indicator for voltage unbalance in three phase networks*

Related publications: [P2], [P1].

I extended the currently used measures of voltage unbalance with a new norm candidate. I found out that it is more demanding from the computational point of view, but has a new feature namely it checks electrical asymmetry, i.e. the norm of a ± 120 degree rotated version of the ideal three phase phasor is zero in the geometrical sense. I compared my geometrical approach to the standard wide-spread use of voltage unbalance factor (VUF) and found out it carries additional information, whilst retaining its original purpose.

- II.) **Thesis:** *Voltage unbalance compensation with optimization based control algorithm and asymmetrical inverter structure*

Related publications: [P1], [P0], [P3].

I found out that the regular current controlling applications would not fit to the purpose for reducing voltage unbalance whilst only relying on the voltage measurement. As such I developed an asymmetrical current source inverter (ACSI) circuit with combined asynchronous parallel pattern search (APPS) control structure, in Matlab/Simulink environment, and I applied the my geometrical norm as a cost function. I showed with validating simulations, that the geometrical based unbalance indicator can serve as a basis of further research.

The fundamental element of the system is a modified three phase inverter that is capable of the asymmetric injection of any current waveforms to the network. The optimization based control algorithm injects the available energy (as current waveform) in such a way, that the voltage unbalance decreases. The structure enables to show that any point the inverter is connected, could restore power quality with a certain degree such unbalance compensation. This optimization problem is usually constrained by the available renewable energy supplied by the power plant. This suggested controller with combined inverter structure enables the residential users owning a grid synchronized domestic power plant to reduce voltage unbalance measurable at any low voltage domestic the connection point.

I also tested the control structure on a real low voltage network model in a dynamical simulation environment consisting of the models of the electrical grid, a domestic power plant, ACSI, and different types of loads. Different simulation experiments has been run for each norm and for both the power constrained and unconstrained case. I showed with the evaluation that this structure can serve as a residential level voltage quality improvement method for the three phase low voltage network.

- III.) **Thesis:** *Constrained, explicit predictive control for current source buck-type rectifiers*

Related publications: [P0].

I proposed a simplified CSR model, which was derived from the well known CSR structure and was examined from design and implementation points of view with the purpose of explicit model-based predictive control. The regular set of differential equations of the CSR appeared to be too complex for my a design approach, for applying explicit predictive control.

I addressed this issue with the separation AC and DC equation sets was of the CSR to decrease complexity and easy controller design. With this solution I eliminated bi-linearity and enabled the application of linear control design techniques. I used current-based SVPWM the modula-

tion, what has been used with an emphasis on the reduction of switching losses.

For DC side control I implemented explicit model predictive control (EMPC) and I compared this method's effectiveness to conventional state feedback control. I implemented the CSR structure and the proposed controller with EMPC on DC and active damping on the AC side in Matlab/Simulink environment and tested by simulation. Additionally, I tested the proper implementation's computational requirements in a modern DSP chip, which would serve in real-time operation.

Publications not related to the thesis: [P0], [P0], [P0], [P0].

5.3 Applications and future work

In this section the possible applications shall be described based on my thesis. These are not yet scope of current research activities, but can serve as a potential direction and evolution for these results.

5.3.1 Geometrical voltage unbalance norm

As mentioned the geometrical norm's largest weakness is the computational demand. The required areas, computed from the voltage phasors realized with the corresponding Matlab functions, which are not designed for continuous calculation, especially not for time constants for power electronic devices. This can be resolved, via replacing the calculation of the symmetrical difference (difference between the two polygon's union and intersection) with finite-element method, with scalability, where the segmentation's resolution would be adjustable and based on the corresponding simulation's (or system's) time constant and the simulator machine's calculation capabilities. After this, the calculation method shall be phrased in an traditional equation form, using the toolset of set theory, and linear algebra. This way, the norm's calculation could be further reduced, and could be implemented on a cheaper embedded system.

The geometrical norm's usefulness was already proven compared o the regular *VUF* method. However the robustness of the method seems implicitly proven, is shall be tested on real conditions, even in extreme (faulty) situations, and with such hard constrains could be defined, where the algorithm outlives its usefulness. This way, instead of just a resulting number, a full formulation of an optimization problem could be utilized, presented in section (4.3.1), with model based predictive capabilities. This can be further enhanced, with recognizing different scenarios, form general inefficiency, to fault prediction, or handling (like graceful degradation).

5.3.2 Voltage unbalance reducing inverter structure

The inverter structure employ a variety of subsystems, which shall work together in harmony. A global optimum shall be defined (with weighting the various factors) based on external circumstances, and the customers needs. This way, the individual Kirchhoff equations based differential equations shall be established, and controller designed.

This way the system's physical properties shall be scalable (based on a household's needs and its energy producing and storing capabilities), as in designing a real power electric system for implementation. Next actual implementation shall be proceeded, with prototype realization on a test bench, with a simulated domestic network connection. Further step to test the presence of multiple of such devices on the network, and how they could mitigate unbalance in synchronous or asynchronous operation.

The APPS method, however fulfills its optimizing responsibilities very well in such an environment, where changes are expected to be highly stochastic, based on network knowledge, a netwok- and/or device model based optimal control shall be established, where various current and voltage inertias can be taken into account, giving a leverage for prediction.

5.3.3 Explicit model predictive control for buck-type rectifier

From mathematical perspective it is an alternative possibility to take the harder route and take the inherent bilinearity into account. This way, the devices equations should not be partitioned, and a hybrid design can be commenced. This has been performed in the literature, but seldom on three phase systems, for complexity reasons.

The topology could be altered, by removing (or greatly decreasing) some of the device's filtering capabilities, in inductive or capacitive terms (some inductors, like the choke L_{dc} are non-removable), and try to outsource this problems to the controller itself to some degree.

Try the cost function from Euclidean norm to an infinity norm, and also give stricter constrains. The optimum could be power throughput based instead of a specified current. The types of loads can be extended, and merged with the current equation system. This enables to expand the research on electric machinery, where starting/ breaking dynamics can be tested. On the other side, the effects on the supplying network can be taken into consideration, further reducing harmonics, and test conditions in the presence of unbalance. Lastly, experimental results shall be performed on a device, further validating its usefulness, and implement the used S-function from Simulink to an embedded system.

Appendix

5.4 Geometric approach to multi parametric programming

In this section the goal is to explain how to solve multi-parametric optimization problems (mp-OP). By start lets consider the following linear multiparametric problem:

$$J^*(\mathbf{x}) = \min_{\mathbf{z}} J(\mathbf{x}, \mathbf{z}) = \mathbf{c}'\mathbf{z} \quad (5.1)$$

subj. to $\mathbf{G}\mathbf{z} \leq \mathbf{w} + \mathbf{S}\mathbf{x}$,

where $\mathbf{z} \in \mathbb{R}^s$ is the vector of the optimization variables, $\mathbf{x} \in \mathbb{R}^n$ is the vector of parameters, and of course $J(\mathbf{x}, \mathbf{z}) : \mathbb{R}^{s+n} \rightarrow \mathbb{R}$ is the objective or cost function. Additionally $\mathbf{G} \in \mathbb{R}^{m \times s}$, $\mathbf{w} \in \mathbb{R}^m$, $\mathbf{c} \in \mathbb{R}^s$ and $\mathbf{S} \in \mathbb{R}^{m \times n}$ as described in section (4.3.1). Next we define a closed convex parameter set $\mathbf{K} \subset \mathbb{R}^n$ such as:

$$\mathbf{K} = \{\mathbf{x} \in \mathbb{R}^n : \mathbf{T}\mathbf{x} \leq \mathbf{Z}\}, \quad (5.2)$$

where $\mathbf{K}^* \subseteq \mathbf{K}$ is the set where (5.1) is feasible, and $\mathbf{x}^* \in \mathbf{K}^*$ where \mathbf{x}^* is the optimum. It is further assumed that:

1. the constraint $\mathbf{x} \in \mathbf{K}$ is included in the constraints of $\mathbf{G}\mathbf{z} \leq \mathbf{w} + \mathbf{S}\mathbf{x}$.
2. \mathbf{K} is a full dimensional polytope, or the problem can be reformulated to \mathbf{K} to be full dimensional with a smaller set of parameters.
3. \mathbf{S} is on full rank, or the problem can be reformulated to \mathbf{S} to be full rank with a smaller set of parameters.

As such $\mathbf{J}^* : \mathbf{K}^* \rightarrow \mathbb{R}$ is a function which gives the optimum by \mathbf{x} . That said let $\mathbf{Z}^* : \mathbf{K}^* \rightarrow \mathbb{R}^s$ the function which gives the set of optimizers namely $\mathbf{z}^* \in \mathbf{Z}^*$. The task is to find a $\mathbf{K}^* \subseteq \mathbf{K}$ set and a $\mathbf{z}^* \in \mathbf{Z}^*$ optimizer and the value of the optimum.

Beside of the systematic linear and quadratic program solutions [99] there is a direct geometrical solution for the problem which uses critical regions for describing the parameter space. The critical regions are convex subsets of the parameter space where the optimum is constant based on the function of the parameters. Consider the multi parametric program (5.1), and let $\mathcal{I}_c = \{1, \dots, m\}$ be the set of constraint indices. For any $\mathcal{A} \subseteq \mathcal{I}_c$, let $\mathbf{G}_{\mathcal{A}}$, and $\mathbf{S}_{\mathcal{A}}$

be the subsets of \mathbf{G} , and \mathbf{S} , respectively, compromising the rows indexed by \mathcal{A} , and denote with \mathbf{G}_j , \mathbf{S}_j and \mathbf{w}_j , the j^{th} row of \mathbf{G} , \mathbf{S} and \mathbf{w} . We define $\mathcal{C}_{\mathcal{A}}$ as the set of states \mathbf{x} for which the same set \mathcal{A} of constraints is active at the optimum. Formally, the *optimal partition* of \mathcal{I}_c at \mathbf{x} is the optimal partition of $(\mathcal{A}(x), \mathcal{A}^N(x))$, where:

$$\begin{aligned}\mathcal{A} &= \{j \in \mathcal{I}_c : \mathbf{G}_j \mathbf{z}^*(x) - \mathbf{S}_j \mathbf{x} = \mathbf{w}_j \forall \mathbf{z}^* \in \mathbf{Z}^*(x)\} \\ \mathcal{A}^N &= \{j \in \mathcal{I}_c : \exists \mathbf{z}^* \in \mathbf{Z}^*(x) \text{ s.t.: } \mathbf{G}_j \mathbf{z}^*(x) - \mathbf{S}_j \mathbf{x} < \mathbf{w}_j\}.\end{aligned}\quad (5.3)$$

It can be noticed, that \mathcal{A} and \mathcal{A}^N are disjoint (the intersection of \mathcal{A} and \mathcal{A}^N is an empty set) and they union is \mathcal{I}_c . As such consider a set $\mathcal{A} \subseteq \mathcal{I}_c$, then the *critical region* associated with the set of active constraints \mathcal{A} is defined as:

$$\mathcal{C}_{\mathcal{A}} = \{\mathbf{x} \in \mathbf{K}^* : \mathcal{A}(x) = \mathcal{A}\}. \quad (5.4)$$

With the above the critical region $\mathcal{C}_{\mathcal{A}}$ is the set of all \mathbf{x} states such that constraints indexed by \mathcal{A} are active at the optimum of problem (5.1). Furthermore it can be proven, that the optimum is an affine function in the domain of \mathbf{K} and unique for every critical region. As such the problem can be separated into two parts:

1. Find the least dimension subset of \mathbf{K} which contains \mathbf{K}^* .
2. Partition \mathbf{K}^* into critical regions and find the optimum for every critical region.

The graphical representation of critical regions can be observed at Fig.(5.1). The algorithm starts from a starting point \mathbf{x}_0 and solves the linear programming problem and find $\mathbf{z}^*(\mathbf{x}_0)$. After this find the active constraints and define the corresponding critical region $\mathcal{C}_{\mathcal{A}}(\mathbf{x}_0)$. Its clear from the definition of one critical region that J^* is constant for any $\mathbf{x} \in \mathcal{C}_{\mathcal{A}}(\mathbf{x}_0)$. Next we find the optimum and the optimizer's value for $\mathbf{x} \in \mathcal{C}_{\mathcal{A}}(\mathbf{x}_0)$. and move on to the next critical region. If the optimum problem is not degenerate then finding the critical regions is straightforward, but in the contrary the outcome is defined by the algorithm's starting direction.

As it shall be described in section 4.4, the if the linear optimization could be described with quadratic programming the process yield more computational cost efficient results in a lot of cases. As such it is advised to apply above geometrical approach in a multi-parametric quadratic programming (mp-QP) environment, as it would be used in the explicit MPC. Consider a multi parametric quadratic program:

$$\begin{aligned}J^*(\mathbf{x}) &= \min_{\mathbf{z}} J(\mathbf{x}, \mathbf{z}) = \frac{1}{2} \mathbf{z}' \mathbf{H} \mathbf{z} \\ \text{subj. to } &\mathbf{G} \mathbf{z} \leq \mathbf{w} + \mathbf{S} \mathbf{x},\end{aligned}\quad (5.5)$$

and the variables are defined as by (5.1) additionally it is assumed that $\mathbf{H} \succ 0$. The goal is to find the value function $J^*(\mathbf{x})$ and the optimizer function $\mathbf{z}^*(\mathbf{x})$ in \mathbf{K}^* . The search of these functions proceeds by partitioning the set

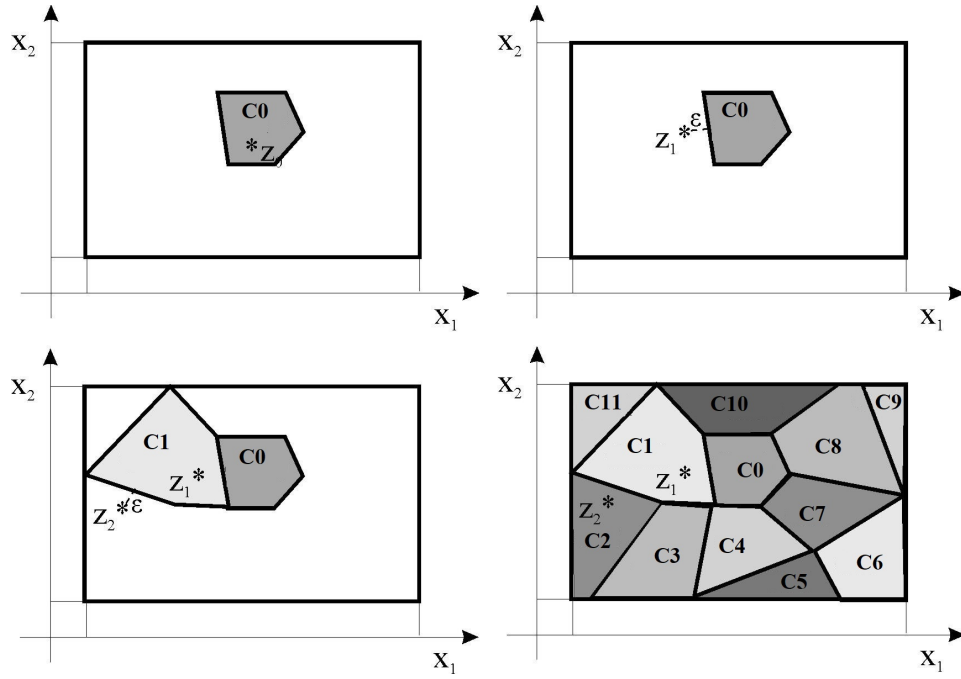


Figure 5.1: Partitioning incrementally the two dimensional parameter space to critical regions from $C0$ to $C11$.

of feasible states into critical regions as before. Note that the more general problem with $J(\mathbf{x}, \mathbf{z}) = \frac{1}{2}\mathbf{z}'\mathbf{H}\mathbf{z} + \mathbf{x}'\mathbf{F}\mathbf{x}$ can always be transformed into (5.5) using the variable substitution $\tilde{\mathbf{z}} = \mathbf{z} + \mathbf{H}^{-1}\mathbf{F}'\mathbf{x}$.

As previously let be j the j^{th} row of a matrix or the j^{th} element in a vector, also $\mathcal{J} = \{1, \dots, m\}$ be the set of constraint indices and for any $\mathcal{A} \subseteq \mathcal{I}_c$, also $\mathbf{G}_{\mathcal{A}}$, $\mathbf{w}_{\mathcal{A}}$, and $\mathbf{S}_{\mathcal{A}}$ be the submatrices of \mathbf{G} , \mathbf{w} and \mathbf{S} respectively, consisting rows, indexed by \mathcal{A} , and \mathbf{K}^* is full dimensional. with the definition displayed in (5.3), and (5.4) it can be showed that the critical regions of a multi parametric quadratic program are polyhedra. Let $(\mathcal{A}, \mathcal{A}^N) = (\mathcal{A}(\bar{\mathbf{x}}), \mathcal{A}^N(\bar{\mathbf{x}}))$ for some $\bar{\mathbf{x}} \in \mathbf{K}^*$, where for any given $\bar{\mathbf{x}} \in \mathbf{K}^*$, $J^*(\bar{\mathbf{x}})$ denotes the minimum value of the objective function for $\mathbf{x} = \bar{\mathbf{x}}$. Then:

1. the closure of $\mathcal{C}_{\mathcal{A}}$ is a polyhedron.
2. $\mathbf{z}^*(\mathbf{x})$ is an affine function of the state inside $\mathcal{C}_{\mathcal{A}}$, i.e.: $\mathbf{z}^*(\mathbf{x}) = \mathbf{F}_i\mathbf{x} + \mathbf{g}_i$ for all $\mathcal{C}_{\mathcal{A}}$.
3. $J^*(\mathbf{x})$ is a quadratic function of the state inside $\mathcal{C}_{\mathcal{A}}$, i.e.: $J^*(\mathbf{x}) = \mathbf{x}'\mathbf{M}_i\mathbf{x} + \mathbf{c}_i\mathbf{x} + \mathbf{d}_i$ for all $\mathbf{x} \in \mathcal{C}_{\mathcal{A}}$.

For proving the above, the first order Karush-Kuhn-Tucker (KKT) conditions (described in [99] in detail) for multi parameter quadratic programs are:

$$\mathbf{H}\mathbf{z}^* + \mathbf{G}'\mathbf{u}^* = 0, \mathbf{u} \in \mathbb{R}^m \quad (5.6a)$$

$$\mathbf{u}_i^*(\mathbf{G}_i\mathbf{z}^* - \mathbf{w}_i - \mathbf{S}_i\mathbf{x}) = 0, i = 1, \dots, m \quad (5.6b)$$

$$\mathbf{u}^* \geq 0 \quad (5.6c)$$

$$\mathbf{G}\mathbf{z}^* - \mathbf{w} - \mathbf{S}\mathbf{x} \leq 0. \quad (5.6d)$$

With the KKT conditions (5.6) the constraints of quadratic problem (5.5) can be written as:

$$\begin{array}{lll} \frac{dL}{d\mathbf{z}} \geq 0 & & \\ \frac{dL}{d\lambda} \geq 0 & \mathbf{z}'\mathbf{H} + \lambda\mathbf{G} \geq 0 & \\ \mathbf{z} \frac{dL}{d\mathbf{z}} = 0 & \iff & \mathbf{G}\mathbf{z} - \mathbf{w} - \mathbf{S}\mathbf{x} \leq 0 \\ \lambda g_l(\mathbf{x}) = 0 & & \mathbf{z}'(\mathbf{H}\mathbf{z} + \mathbf{G}'\lambda) = 0 \\ & & \mathbf{z} \geq 0, \lambda \geq 0, \\ \mathbf{z} \geq 0, \lambda \geq 0 & & \end{array} \quad (5.7)$$

where λ is the Lagrange multiplier, L is the Lagrange function and $g(\mathbf{x})$ is the equality constraint. Then can be applied to the active constraints of (5.5) applied on the critical region of $\mathcal{C}_{\mathcal{A}}$:

$$\begin{array}{lll} \mathbf{H}\mathbf{z} + \mathbf{G}'_{\mathcal{A}}\lambda_{\mathcal{A}} & = & 0 \\ \lambda_{\mathcal{A}}(\mathbf{G}_{\mathcal{A}}\mathbf{z} - \mathbf{w}_{\mathcal{A}} - \mathbf{S}_{\mathcal{A}}\mathbf{x}) & = & 0 \\ \mathbf{G}\mathbf{z} - \mathbf{w} - \mathbf{S}\mathbf{x} & \leq & 0 \\ \lambda_{\mathcal{A}} & \geq & 0. \end{array} \quad (5.8)$$

From (5.4) it follows:

$$\begin{array}{ll} \mathbf{z} & = -\mathbf{H}^{-1}\mathbf{G}'_{\mathcal{A}}\lambda_{\mathcal{A}} \\ 0 & = \lambda_{\mathcal{A}}(-\mathbf{G}_{\mathcal{A}}\mathbf{H}^{-1}\mathbf{G}'_{\mathcal{A}} - \mathbf{w}_{\mathcal{A}} - \mathbf{S}_{\mathcal{A}}\mathbf{x}), \end{array} \quad (5.9)$$

which then implies that:

$$\begin{array}{ll} \lambda_{\mathcal{A}} & = (-\mathbf{G}_{\mathcal{A}}\mathbf{H}^{-1}\mathbf{G}'_{\mathcal{A}})^{-1}(\mathbf{w}_{\mathcal{A}} + \mathbf{S}_{\mathcal{A}}\mathbf{x}) \\ \mathbf{z} & = -\mathbf{H}^{-1}\mathbf{G}'_{\mathcal{A}}(-\mathbf{G}_{\mathcal{A}}\mathbf{H}^{-1}\mathbf{G}'_{\mathcal{A}})(\mathbf{w}_{\mathcal{A}} + \mathbf{S}_{\mathcal{A}}\mathbf{x}). \end{array} \quad (5.10)$$

In this case \mathbf{z} serves as the optimum if the KKT conditions are fulfilled. Substituting into yields:

$$\begin{array}{ll} (-\mathbf{G}_{\mathcal{A}}\mathbf{H}^{-1}\mathbf{G}'_{\mathcal{A}})^{-1}(\mathbf{w}_{\mathcal{A}} + \mathbf{S}_{\mathcal{A}}\mathbf{x}) & \geq 0 \\ (\mathbf{G}_{\mathcal{A}} - \mathbf{H}^{-1}\mathbf{G}'_{\mathcal{A}})(-\mathbf{G}_{\mathcal{A}}\mathbf{H}^{-1}\mathbf{G}'_{\mathcal{A}})^{-1}(\mathbf{w}_{\mathcal{A}} + \mathbf{S}_{\mathcal{A}}\mathbf{x}) & \leq \mathbf{w} + \mathbf{S}\mathbf{x}. \end{array} \quad (5.11)$$

This inequality of (5.11) expresses the critical region of $\mathcal{C}_{\mathcal{A}}$, and for said region the optimizer can be expressed as:

$$\mathbf{z}^* = (-\mathbf{H}^{-1}\mathbf{G}'_{\mathcal{A}})(-\mathbf{G}_{\mathcal{A}}\mathbf{H}^{-1}\mathbf{G}'_{\mathcal{A}})^{-1}(\mathbf{w}_{\mathcal{A}} + \mathbf{S}_{\mathcal{A}}\mathbf{x}). \quad (5.12)$$

With this in hand the quadratic multi parametric program (5.5) can be solved the same way as the linear multi parametric program (5.1), and the optimum value can be calculated for every critical region explicitly, as the affine function of parameters.

5.4.1 Storage of critical regions

The issue of iterative model based controllers is that they require a lot of computational resource. The CPU load and required ROM consumption could increase exponentially the longer the more steps the control horizon is calculated. For this reason explicit model based predictive controllers (EMPC) were developed, where only the storage the critical regions and the signal coefficients for each critical region, so the matrices \mathbf{H} , \mathcal{K} , \mathbf{F} , \mathbf{G} are required. The on-line part of control consists of searching the critical region for the current states and calculating the necessary inputs for them. One method of storing entire critical regions in order to calculate them, and that is in the order in which the MP-LP or MP-QP problem is resolved. It has the disadvantage, that the search time can be high, as such starting from the top of the list, a linear search is not effective. The efficient method is to store critical regions already in a binary tree [0], [0], [0], [0]. The method of generating the binary tree is shown in (Fig.(5.2)).

The basic idea is to sort the critical regions depending on their adjacent sides. For example, in (Fig.(5.2).a.) side j_1 divides the state space into two, at the right of it are the regions $X_{2,3,4,5}$ and to the left are the regions $X_{1,2,6}$. They make up the nodes adjacent to the base node I_1 of the binary tree. Next the another side from the space is chosen defined by each node I_2 respectively I_3 , and the algorithm is continued until all the regions in the current node correspond to the same control signal, denoted by F on the shaft in fig. (Fig.(5.2).b.) Thus with this search pattern logarithmic search time can be achieved.

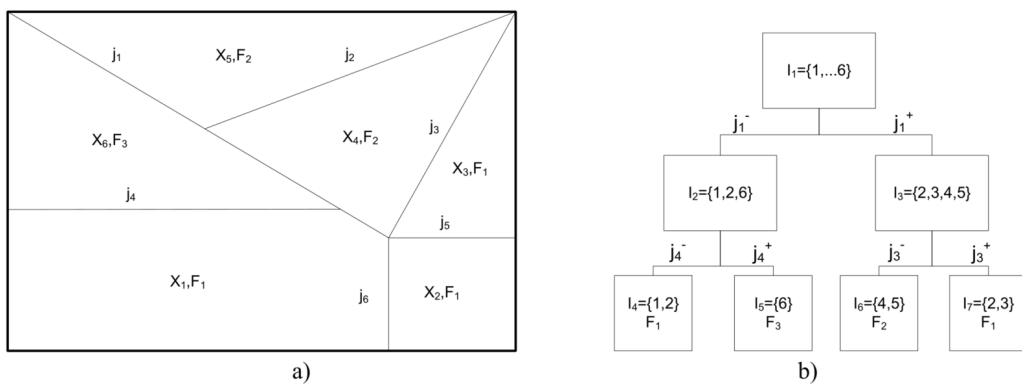


Figure 5.2: Basic search tree of an EMPC where, a) are the critical regions for a space of 2D parameters, b) the related binary tree.

The implementation of MPC in explicit form is very efficient up to a certain number of critical regions, because they do not require calculations but only

search in a table. For more complex problems or fast systems the method requires longer search time.

5.5 Notations used in the appendix

\mathcal{A}	Set if indices in states where the constraints are active
\mathcal{A}^N	Set if indices in states where the constraints are inactive
$\mathcal{C}_{\mathcal{A}}$	Critical region associated with the active constraints
\mathbf{F}	State coefficient matrix for calculating the optimal input
g	Autonomous function where there are no inputs
\mathbf{H}	Supplementary quadratic optimizer matrix
I_i	i^{th} node in critical region storage
\mathcal{I}_c	Set if indices of constraints
J	Cost (or value) function to optimize
J^*	Optimal cost value
\mathcal{J}	Set if indices of active constraints
\mathbf{K}	Controller gain
\mathcal{K}	Set of states respective to constraints
\mathcal{K}^*	Set of feasible states respective to constraints
L	Lagrange function
\mathbf{S}	General state constraint coefficient
\mathbf{u}^*	Optimal vector of input
\mathbf{w}	Unified constraint vector
X_i	i^{th} critical region in critical region search
\mathbf{x}	State vector of a linear time invariant model
$\bar{\mathbf{x}}$	Minimum state value of the objective function
\mathbf{Z}^*	Set of optimizers leading to feasible states
\mathbf{z}	Optimizer of linear multi parametric problem
\mathbf{z}^*	Optimizer, leading to a feasible state
λ	Lagrange multiplier

5.6 Abbreviations

AC:	Alternating current
ACSI:	Asymmetrical current source inverter
APPS:	Asynchronous Parallel Pattern Search
CPU:	Central processing unit
CSR:	Current source rectifier
CVUF:	Complex voltage unbalance factor
DC:	Direct current
EMPC:	Explicit model predictive control
HPF:	High pass filter
IGBT:	Insulated gate bipolar transistor
MAC:	Multiply and accumulate
MIMO	Multiple input, multiple output
MPC:	Model predictive control
MPT:	Model predictive control toolbox
MPPT:	Maximum power point tracking
MP-LP:	Multi parametric linear programming
MP-QP:	Milti parametric quadratic programming
ROM:	Read only memory
SFC:	State feedback control
SVM:	Space vector modulation
SVPWM	Space vector pulse width modulated
THD:	Total harmonic distortion
SHE:	Selective harmonic elimination
TPWM:	Trapezoidal pulse width modulation
VSR:	Voltage source rectifier
VU:	Voltage unbalance
VUF:	Voltage unbalance factor (i.e. TDV)

Bibliography

Publications

- [P1] **L. Neukirchner**, A. Göllei, P. Görbe, and A. Magyar, “Carbon footprint reduction via voltage asymmetry compensation of three-phase low voltage grid utilizing small domestic power plants,” *Chemical Engineering Transactions*, vol. 45, pp. 283–288, 2015.
- [P2] **L. Neukirchner**, P. Görbe, and A. Magyar, “Examination of different voltage asymmetry norms under transient behavior of three-phase low voltage power systems containing small domestic power plants,” in *PowerTech, 2015 IEEE Eindhoven*, IEEE, 2015, pp. 1–6.
- [P3] ——, “Voltage unbalance reduction in the domestic distribution area using asymmetric inverters,” *Journal of cleaner production*, vol. 142, pp. 1710–1720, 2017.
- [P0] **L. Neukirchner**, A. Göllei, P. Görbe, and A. Magyar, “Voltage unbalance reduction of a local transformer area with domestic asymmetrical inverter and optimal control design,” *Int. J. of Thermal & Environmental Engineering*, vol. 12, no. 2, pp. 129–134, 2016.
- [P0] **L. Neukirchner**, A. Magyar, A. Fodor, N. D. Kutasi, and A. Kelemen, “Constrained predictive control of three-phasebuck rectifiers,” *Acta Polytechnica Hungarica*, vol. 17, no. 1, 2020.
- [P0] **L. Neukirchner**, A. Fodor, and A. Magyar, “Modeling and parameter sensitivity analysis of a synchronous motor,” *Hungarian Journal of Industry and Chemistry*, vol. 39, no. 1, pp. 147–152, 2011.
- [P0] **L. Neukirchner** and A. Magyar, “Quasi-polynomial representation-based control of mechanical systems,” *Hungarian Journal of Industry and Chemistry*, vol. 42, no. 2, pp. 91–95, 2014.
- [P0] A. Göllei, P. Görbe, A. Magyar, and **L. Neukirchner**, “Measurement-based modelling and simulation of a hydrogenenerating dry cell for complex domestic renewable energy systems,” *Hungarian Journal of Industry and Chemistry*, vol. 42, no. 2, pp. 85–89, 2014.
- [P0] **L. Neukirchner** and A. Magyar, “Modelling a three-phase current source inverter,” *Hungarian Journal of Industry and Chemistry*, vol. 44, no. 2, pp. 105–111, 2016.

Literature

- [1] S. A. Shezan, S Julai, M. Kibria, K. Ullah, R Saidur, W. Chong, and R. Akikur, “Performance analysis of an off-grid wind-pv (photovoltaic)-diesel-battery hybrid energy system feasible for remote areas,” *Journal of Cleaner Production*, vol. 125, pp. 121–132, 2016.
- [2] F. Cucchiella, I. D’Adamo, and S. L. Koh, “Environmental and economic analysis of building integrated photovoltaic systems in italian regions,” *Journal of Cleaner Production*, vol. 98, pp. 241–252, 2015.
- [3] J. Kaldellis, M Simotas, D Zafirakis, and E Kondili, “Optimum autonomous photovoltaic solution for the greek islands on the basisof energy pay-back analysis,” *Journal of Cleaner Production*, vol. 17, no. 15, pp. 1311–1323, 2009.
- [4] M. Ortega, J. Hernández, and O. García, “Measurement and assessment of power quality characteristics for photovoltaic systems: Harmonics, flicker, unbalance, and slow voltage variations,” *Electric Power Systems Research*, vol. 96, pp. 23–35, 2013.
- [5] L. H. Saw, Y. Ye, and A. A. Tay, “Integration issues of lithium-ion battery into electric vehicles battery pack,” *Journal of Cleaner Production*, vol. 113, pp. 1032–1045, 2016.
- [6] P. D. Lund, J. Mikkola, and J Ypyä, “Smart energy system design for large clean power schemes in urban areas,” *Journal of Cleaner Production*, vol. 103, pp. 437–445, 2015.
- [7] P. Gnaciński, M. Pepliński, D. Hallmann, and P. Jankowski, “Induction cage machine thermal transients under lowered voltage quality,” *IET Electric Power Applications*, vol. 13, no. 4, pp. 479–486, 2019.
- [8] M. Savaghebi, A. Jalilian, J. C. Vasquez, and J. M. Guerrero, “Secondary control scheme for voltage unbalance compensation in an islanded droop-controlled microgrid,” *IEEE Transactions on Smart Grid*, vol. 3, no. 2, pp. 797–807, 2012.
- [9] A. Siddique, G. Yadava, and B. Singh, “Effects of voltage unbalance on induction motors,” in *Conference Record of the 2004 IEEE International Symposium on Electrical Insulation*, IEEE, 2004, pp. 26–29.
- [10] T. Brekken, N. Mohan, and T. Undeland, “Control of a doubly-fed induction wind generator under unbalanced grid voltage conditions,” in *2005 European Conference on Power Electronics and Applications*, IEEE, 2005, 10–pp.
- [11] C.-Y. Lee, B.-K. Chen, W.-J. Lee, and Y.-F. Hsu, “Effects of various unbalanced voltages on the operation performance of an induction motor under the same voltage unbalance factor condition,” *Electric Power Systems Research*, vol. 47, no. 3, pp. 153–163, 1998.

- [12] B. Meersman, B. Renders, L. Degroote, T. Vandoorn, and L. Vandevelde, “Three-phase inverter-connected dg-units and voltage unbalance,” *Electric Power Systems Research*, vol. 81, no. 4, pp. 899–906, 2011.
- [13] Y. Ates, M. Uzunoglu, A. Karakas, A. R. Boynuegri, A. Nadar, and B. Dag, “Implementation of adaptive relay coordination in distribution systems including distributed generation,” *Journal of cleaner production*, vol. 112, pp. 2697–2705, 2016.
- [14] M. T. Bina and A Kashefi, “Three-phase unbalance of distribution systems: Complementary analysis and experimental case study,” *International Journal of Electrical Power & Energy Systems*, vol. 33, no. 4, pp. 817–826, 2011.
- [15] P. Görbe, A. Magyar, and K. M. Hangos, “Reduction of power losses with smart grids fueled with renewable sources and applying ev batteries,” *Journal of cleaner production*, vol. 34, pp. 125–137, 2012.
- [16] P. Görbe, A. Fodor, A. Magyar, and K. M. Hangos, “Experimental study of the nonlinear distortion caused by domestic power plants,” *Applied Thermal Engineering*, vol. 70, no. 2, pp. 1288–1293, 2014.
- [17] N. Korovkin, Q. Vu, and R. Yazenin, “A method for minimization of unbalanced mode in three-phase power systems,” in *2016 IEEE NW Russia Young Researchers in Electrical and Electronic Engineering Conference (EIConRusNW)*, IEEE, 2016, pp. 611–614.
- [18] A. D. Martin, R. S. Herrera, J. R. Vazquez, P. Crolla, and G. M. Burt, “Unbalance and harmonic distortion assessment in an experimental distribution network,” *Electric Power Systems Research*, vol. 127, pp. 271–279, 2015.
- [19] P. G. Kini, R. C. Bansal, and R. S. Aithal, “A novel approach toward interpretation and application of voltage unbalance factor,” *IEEE transactions on industrial electronics*, vol. 54, no. 4, pp. 2315–2322, 2007.
- [20] H. Wen, D. Cheng, Z. Teng, S. Guo, and F. Li, “Approximate algorithm for fast calculating voltage unbalance factor of three-phase power system,” *IEEE Transactions on Industrial Informatics*, vol. 10, no. 3, pp. 1799–1805, 2014.
- [21] L. R. Araujo, D. Penido, S. Carneiro, and J. L. R. Pereira, “A three-phase optimal power-flow algorithm to mitigate voltage unbalance,” *IEEE Transactions on Power Delivery*, vol. 28, no. 4, pp. 2394–2402, 2013.
- [22] A. Von Meier, *Electric power systems: a conceptual introduction*. John Wiley & Sons, 2006.
- [23] C. Eugene, “A new simple and effective approximate formulation for determination of three-phase unbalance by the voltmeter method,” in *CIGRE 1986*, 1986, p. 11.

- [24] A Robert and J Marquet, “Assessing voltage quality with relation to harmonics, flicker and unbalance,” in *International Conference on Large High Voltage Electric Systems*, vol. 2, 1992, pp. 36–203.
- [25] C. L. Fortescue, “Method of symmetrical co-ordinates applied to the solution of polyphase networks,” *Transactions of the American Institute of Electrical Engineers*, vol. 37, no. 2, pp. 1027–1140, 1918.
- [26] A. H. Bonnett and G. Soukup, “Understanding the nema motor-generator standards of section mg-1-1993, revision 3, three-phase induction motors,” in *Record of Conference Papers. IEEE Industry Applications Society 44th Annual Petroleum and Chemical Industry Conference*, IEEE, 1997, pp. 225–238.
- [27] “IEEE recommended practice for electric power distribution for industrial plants (ieee red book),” 1986, pp. 1–609.
- [28] “IEEE standard for inverse-time characteristics equations for overcurrent relays,” 2019, pp. 1–25.
- [29] “IEEE guide for self-commutated converters,” 1987.
- [30] P Pillay and M Manyage, “Definitions of voltage unbalance,” *IEEE Power Engineering Review*, vol. 21, no. 5, pp. 50–51, 2001.
- [31] R. C. Dugan, M. F. McGranaghan, and H. W. Beaty, “Electrical power systems quality,” *New York, NY: McGraw-Hill*, c1996, 1996.
- [32] Y.-J. Wang, “An analytical study on steady-state performance of an induction motor connected to unbalanced three-phase voltage,” in *2000 IEEE Power Engineering Society Winter Meeting. Conference Proceedings (Cat. No. 00CH37077)*, IEEE, vol. 1, 2000, pp. 159–164.
- [33] L Pierrat and J. Meyer, “Unbalance factor it is as simple as abc,” *Revue Générale de l’Électricité*, vol. 1, no. 6, pp. 18–26, 1987.
- [34] Y.-J. Wang, “Analysis of effects of three-phase voltage unbalance on induction motors with emphasis on the angle of the complex voltage unbalance factor,” *IEEE Transactions on energy conversion*, vol. 16, no. 3, pp. 270–275, 2001.
- [35] A. K. Singh, G. Singh, and R Mitra, “Some observations on definitions of voltage unbalance,” in *2007 39th North American Power Symposium*, IEEE, 2007, pp. 473–479.
- [36] T.-H. Chen, C.-H. Yang, and N.-C. Yang, “Examination of the definitions of voltage unbalance,” *International Journal of Electrical Power & Energy Systems*, vol. 49, pp. 380–385, 2013.
- [37] R. Betz, T Summers, T Furney, *et al.*, “Symmetry compensation using a h-bridge multilevel statcom with zero sequence injection,” in *Industry Applications Conference, 2006. 41st IAS Annual Meeting. Conference Record of the 2006 IEEE*, vol. 4, 2006, pp. 1724–1731.

- [38] J. Hang, J. Zhang, M. Cheng, and J. Huang, “Online interturn fault diagnosis of permanent magnet synchronous machine using zero-sequence components,” *IEEE Transactions on Power Electronics*, vol. 30, no. 12, pp. 6731–6741, 2015.
- [39] S. Arnborg, G. Andersson, D. J. Hill, and I. A. Hiskens, “On undervoltage load shedding in power systems,” *International Journal of Electrical Power & Energy Systems*, vol. 19, no. 2, pp. 141–149, 1997.
- [40] K. Lee, T. M. Jahns, T. A. Lipo, and V. Blasko, “New control method including state observer of voltage unbalance for grid voltage-source converters,” *IEEE Transactions on Industrial Electronics*, vol. 57, no. 6, pp. 2054–2065, 2009.
- [41] Y. Xu, L. M. Tolbert, J. D. Kueck, and D. T. Rizy, “Voltage and current unbalance compensation using a static var compensator,” *IET Power Electronics*, vol. 3, no. 6, pp. 977–988, 2010.
- [42] Y. Li, D. M. Vilathgamuwa, and P. C. Loh, “Microgrid power quality enhancement using a three-phase four-wire grid-interfacing compensator,” *IEEE transactions on industry applications*, vol. 41, no. 6, pp. 1707–1719, 2005.
- [43] J. Hu, M. Marinelli, M. Coppo, A. Zecchino, and H. W. Bindner, “Coordinated voltage control of a decoupled three-phase on-load tap changer transformer and photovoltaic inverters for managing unbalanced networks,” *Electric Power Systems Research*, vol. 131, pp. 264–274, 2016.
- [44] Z. Wang, B. Wu, D. Xu, M. Cheng, and L. Xu, “Dc-link current ripple mitigation for current-source grid-connected converters under unbalanced grid conditions,” *IEEE Transactions on Industrial Electronics*, vol. 63, no. 8, pp. 4967–4977, 2016.
- [45] X. Wang, Y. W. Li, F. Blaabjerg, and P. C. Loh, “Virtual-impedance-based control for voltage-source and current-source converters,” *IEEE Transactions on Power Electronics*, vol. 30, no. 12, pp. 7019–7037, 2014.
- [46] X. Guo, Y. Yang, and X. Zhang, “Advanced control of grid-connected current source converter under unbalanced grid voltage conditions,” *IEEE Transactions on Industrial Electronics*, vol. 65, no. 12, pp. 9225–9233, 2018.
- [47] V. Vekhande, V. Kanakesh, and B. G. Fernandes, “Control of three-phase bidirectional current-source converter to inject balanced three-phase currents under unbalanced grid voltage condition,” *IEEE Transactions on power electronics*, vol. 31, no. 9, pp. 6719–6737, 2015.
- [48] M. Kheraluwala, R. W. Gascoigne, D. M. Divan, and E. D. Baumann, “Performance characterization of a high-power dual active bridge dc-to-dc converter,” *IEEE Transactions on industry applications*, vol. 28, no. 6, pp. 1294–1301, 1992.

- [49] S. Inoue and H. Akagi, “A bidirectional dc–dc converter for an energy storage system with galvanic isolation,” *IEEE Transactions on Power Electronics*, vol. 22, no. 6, pp. 2299–2306, 2007.
- [50] T. G. Kolda and V. J. Torczon, “Understanding asynchronous parallel pattern search,” in *High Performance Algorithms and Software for Nonlinear Optimization*, Springer, 2003, pp. 323–342.
- [51] S. S. Patnaik and A. K. Panda, “Three-level h-bridge and three h-bridges-based three-phase four-wire shunt active power filter topologies for high voltage applications,” *International Journal of Electrical Power & Energy Systems*, vol. 51, pp. 298–306, 2013.
- [52] N. A. Ninad and L. Lopes, “Per-phase vector control strategy for a four-leg voltage source inverter operating with highly unbalanced loads in stand-alone hybrid systems,” *International Journal of Electrical Power & Energy Systems*, vol. 55, pp. 449–459, 2014.
- [53] P. D. Hough, T. G. Kolda, and V. J. Torczon, “Asynchronous parallel pattern search for nonlinear optimization,” *SIAM Journal on Scientific Computing*, vol. 23, no. 1, pp. 134–156, 2001.
- [54] S Segui-Chilet, F. Gimeno-Sales, S Orts, G Garcera, E Figueres, M Alcaniz, and R Masot, “Approach to unbalance power active compensation under linear load unbalances and fundamental voltage asymmetries,” *International Journal of Electrical Power & Energy Systems*, vol. 29, no. 7, pp. 526–539, 2007.
- [55] M. H. A. Fábián, “Statistical data of the hungarian electricity system,” *Mavir Hungarian Independent Transmission Operator Company, Ltd.*, pp. 899–906, 2013.
- [56] A. Biczók, “Statistical data of the hungarian electricity system,” *Mavir Hungarian Independent Transmission Operator Company, Ltd.*, pp. 1–100, 2018.
- [57] I. Vajda, Y. N. Dementyev, K. N. Negodin, N. V. Kojain, L. S. Udu, I. A. Chesnokova, *et al.*, “Limiting static and dynamic characteristics of an induction motor under frequency vector control,” *Acta Polytechnica Hungarica*, vol. 14, no. 6, pp. 7–27, 2017.
- [58] B. Ghalem and B. Azeddine, “Six-phase matrix converter fed double star induction motor,” *Acta Polytechnica Hungarica*, vol. 7, no. 3, pp. 163–176, 2010.
- [59] S. Gupta and R. K. Tripathi, “Two-area power system stability improvement using a robust controller-based csc-statcom,” *Acta Polytechnica Hungarica*, vol. 11, no. 7, pp. 135–155, 2014.
- [60] D. Chen, J. Jiang, Y. Qiu, J. Zhang, and F. Huang, “Single-stage three-phase current-source photovoltaic grid-connected inverter high voltage transmission ratio,” *IEEE Transactions on Power Electronics*, vol. 32, no. 10, pp. 7591–7601, 2016.

- [61] B. Exposto, R. Rodrigues, J. Pinto, V. Monteiro, D. Pedrosa, and J. L. Afonso, “Predictive control of a current-source inverter for solar photovoltaic grid interface,” in *2015 9th International Conference on Compatibility and Power Electronics (CPE)*, IEEE, 2015, pp. 113–118.
- [62] M. Chebre, A. Meroufel, and Y. Bendaha, “Speed control of induction motor using genetic algorithm-based pi controller,” *Acta Polytechnica Hungarica*, vol. 8, no. 6, pp. 141–153, 2011.
- [63] R. Salloum, B. Moaveni, and M. R. Arvan, “Robust pid controller design for a real electromechanical actuator,” *Acta Polytechnica Hungarica*, vol. 11, no. 5, pp. 125–144, 2014.
- [64] F. Tahri, A. Tahri, A. Allali, and S. Flazi, “The digital self-tuning control of step a down dc-dc converter,” *Acta Polytechnica Hungarica*, vol. 9, no. 6, pp. 49–64, 2012.
- [65] H. Gao, D. Xu, B. Wu, and N. R. Zargari, “Model predictive control for five-level current source converter with dc current balancing capability,” in *IECON 2017-43rd Annual Conference of the IEEE Industrial Electronics Society*, IEEE, 2017, pp. 8230–8235.
- [66] Y. Han, L. Xu, M. M. Khan, and C. Chen, “Control strategies, robustness analysis, digital simulation and practical implementation for a hybrid apf with a resonant ac-link,” *Acta polytechnica hungarica*, vol. 7, no. 5, 2010.
- [67] H. Feroura, F. Krim, B. Tabli, and A. Laib, “Finite-set model predictive voltage control for islanded three phase current source inverter,” in *2017 5th International Conference on Electrical Engineering-Boumerdes (ICEEB)*, IEEE, 2017, pp. 1–5.
- [68] Z. Yan, X. Xu, Z. Yang, X. Wu, and Y. Wang, “Study of effective vector synthesis sequence for three-phase current rectifier,” in *2015 Fifth International Conference on Instrumentation and Measurement, Computer, Communication and Control (IMCCC)*, IEEE, 2015, pp. 1065–1070.
- [69] A. Ürmös, Z. Farkas, M. Farkas, T. Sándor, L. T. Kóczy, and Á. Nemcsics, “Application of self-organizing maps for technological support of droplet epitaxy,” *Acta Polytechnica Hungarica*, vol. 14, no. 4, pp. 207–224, 2017.
- [70] A. Chatterjee, R. Chatterjee, F. Matsuno, and T. Endo, “Augmented stable fuzzy control for flexible robotic arm using lmi approach and neuro-fuzzy state space modeling,” *IEEE transactions on industrial electronics*, vol. 55, no. 3, pp. 1256–1270, 2008.
- [71] T. Haidegger, L. Kovács, R.-E. Precup, B. Benyó, Z. Benyó, and S. Preitl, “Simulation and control for telerobots in space medicine,” *Acta Astronautica*, vol. 81, no. 1, pp. 390–402, 2012.
- [72] S. Vrkalovic, E.-C. Lunca, and I.-D. Borlea, “Model-free sliding mode and fuzzy controllers for reverse osmosis desalination plants,” *Int. J. Artif. Intell.*, vol. 16, no. 2, pp. 208–222, 2018.

- [73] C. B. Regaya, A. Zaafouri, and A. Chaari, “A new sliding mode speed observer of electric motor drive based on fuzzy-logic,” *Acta Polytechnica Hungarica*, vol. 11, no. 3, pp. 219–232, 2014.
- [74] K. Széll and P. Korondi, “Mathematical basis of sliding mode control of an uninterruptible power supply,” *Acta Polytechnica Hungarica*, vol. 11, no. 03, pp. 87–106, 2014.
- [75] S. F. Ahmed, C. F. Azim, H. Desa, and A.-S. T. Hussain, “Model predictive controller-based single phase pulse width modulation (pwm) inverter for ups systems,” *Acta Polytechnica Hungarica*, vol. 11, no. 6, pp. 23–38, 2014.
- [76] A. Kelemen, N. Kutasi, M. Imecs, and I. I. Incze, “Constrained optimal direct power control of voltage-source pwm rectifiers,” in *2010 IEEE 14th International Conference on Intelligent Engineering Systems*, IEEE, 2010, pp. 249–254.
- [77] M Rivera, S Kouro, J Rodriguez, B Wu, V Yaramasu, J Espinoza, and P Melila, “Predictive current control in a current source inverter operating with low switching frequency,” in *4th International Conference on Power Engineering, Energy and Electrical Drives*, IEEE, 2013, pp. 334–339.
- [78] A. Godlewska and A. Sikorski, “Predictive control of current source rectifier,” in *2015 Selected Problems of Electrical Engineering and Electronics (WZEE)*, IEEE, 2015, pp. 1–6.
- [79] N. Muthukumar, S. Srinivasan, K. Ramkumar, K. Kannan, and V. E. Balas, “Adaptive model predictive controller for web transport systems,” *Acta Polytechnica Hungarica*, vol. 13, no. 3, pp. 181–194, 2016.
- [80] N. Kutasi, A. Kelemen, and M. Imecs, “Constrained optimal control of three-phase ac-dc boost converters,” in *2010 IEEE International Conference on Automation, Quality and Testing, Robotics (AQTR)*, IEEE, vol. 1, 2010, pp. 1–6.
- [81] J. W. Kolar, H. Ertl, and F. C. Zach, “Design and experimental investigation of a three-phase high power density high efficiency unity power factor pwm (vienna) rectifier employing a novel integrated power semiconductor module,” in *Proceedings of Applied Power Electronics Conference. APEC'96*, IEEE, vol. 2, 1996, pp. 514–523.
- [82] N. Zargari and G Joos, “A current-controlled current source type unity power factor pwm rectifier,” in *Conference Record of the 1993 IEEE Industry Applications Conference Twenty-Eighth IAS Annual Meeting*, IEEE, 1993, pp. 793–799.
- [83] Y. Sato and T. Kataoka, “State feedback control of current-type pwm ac-to-dc converters,” *IEEE transactions on industry applications*, vol. 29, no. 6, pp. 1090–1097, 1993.

- [84] T. Nussbaumer, M. Baumann, and J. W. Kolar, “Comprehensive design of a three-phase three-switch buck-type pwm rectifier,” *IEEE Transactions on Power Electronics*, vol. 22, no. 2, pp. 551–562, 2007.
- [85] L. Malesani and P. Tenti, “Three-phase ac/dc pwm converter with sinusoidal ac currents and minimum filter requirements,” *IEEE Transactions on Industry Applications*, no. 1, pp. 71–77, 1987.
- [86] R Itoh, “Steady-state and transient characteristics of a single-way step-down pwm gto voltage-source convertor with sinusoidal supply currents,” in *IEE Proceedings B (Electric Power Applications)*, IET, vol. 136, 1989, pp. 168–175.
- [87] D. J. Tooth, S. J. Finney, and B. W. Williams, “Effects of using dc-side average current-mode control on a three-phase converter with an input filter and distorted supply,” *IEE Proceedings-Electric Power Applications*, vol. 147, no. 6, pp. 459–468, 2000.
- [88] M. Salo, “A three-switch current-source pwm rectifier with active filter function,” in *2005 IEEE 36th Power Electronics Specialists Conference*, IEEE, 2005, pp. 2230–2236.
- [89] M. Baumann, U. Drozenik, and J. W. Kolar, “New wide input voltage range three-phase unity power factor rectifier formed by integration of a three-switch buck-derived front-end and a dc/dc boost converter output stage,” in *INTELEC. Twenty-Second International Telecommunications Energy Conference (Cat. No. 00CH37131)*, IEEE, 2000, pp. 461–470.
- [90] M. Baumann and J. W. Kolar, “A novel control concept for reliable operation of a three-phase three-switch buck-type unity-power-factor rectifier with integrated boost output stage under heavily unbalanced mains condition,” *IEEE Transactions on Industrial Electronics*, vol. 52, no. 2, pp. 399–409, 2005.
- [91] L. Moussaoui and A. Moussi, “An open loop space vector pwm control for csi-fed field-oriented induction motor drive with improved performances and reduced pulsating torque,” *WSEAS Trans.-Circuits and Systems*, vol. 1, no. 2, pp. 71–77, 2005.
- [92] J. A. Rossiter, *Model-based predictive control: a practical approach*. CRC press, 2017.
- [93] W. H. Kwon and S. H. Han, *Receding horizon control: model predictive control for state models*. Springer Science & Business Media, 2006.
- [94] M. Baotic, “Optimal control of piecewise affine systems: A multi-parametric approach,” PhD thesis, ETH Zurich, 2005.
- [95] M. Herceg, “Real-time explicit model predictive control of processes,” PhD thesis, PhD thesis, 2009.
- [96] A. Grancharova and T. A. Johansen, “Survey of explicit approaches to constrained optimal control,” in *Switching and Learning in Feedback Systems*, Springer, 2005, pp. 47–97.

- [97] P. Antoniewicz, “Predictive control of three phase ac/dc converters,” PhD thesis, The Institute of Control and Industrial Electronics, 2009.
- [98] T. Geyer, *Low complexity model predictive control in power electronics and power systems*. Cuvillier Verlag, 2005.
- [99] F. Borrelli, A. Bemporad, and M. Morari, *Predictive control for linear and hybrid systems*. Cambridge University Press, 2017.
- [100] A. Bemporad, M. Morari, V. Dua, and E. N. Pistikopoulos, “The explicit linear quadratic regulator for constrained systems,” *Automatica*, vol. 38, no. 1, pp. 3–20, 2002.
- [101] G. Goodwin, M. M. Seron, and J. A. De Doná, *Constrained control and estimation: an optimisation approach*. Springer Science & Business Media, 2006.
- [102] D. Q. Mayne, J. B. Rawlings, C. V. Rao, and P. O. Scokaert, “Constrained model predictive control: Stability and optimality,” *Automatica*, vol. 36, no. 6, pp. 789–814, 2000.
- [103] P. Grieder, M. Kvasnica, M. Baotić, and M. Morari, “Stabilizing low complexity feedback control of constrained piecewise affine systems,” *Automatica*, vol. 41, no. 10, pp. 1683–1694, 2005.
- [104] S. a. Keerthi and E. G. Gilbert, “Optimal infinite-horizon feedback laws for a general class of constrained discrete-time systems: Stability and moving-horizon approximations,” *Journal of optimization theory and applications*, vol. 57, no. 2, pp. 265–293, 1988.
- [105] D. Q. Mayne and H. Michalska, “Receding horizon control of nonlinear systems,” *IEEE Transactions on automatic control*, vol. 35, no. 7, pp. 814–824, 1990.
- [106] M. Herceg, M. Kvasnica, C. Jones, and M. Morari, “Multi-Parametric Toolbox 3.0,” in *Proc. of the European Control Conference*, <http://control.ee.ethz.ch/~mpt>, Zürich, Switzerland, 2013, pp. 502–510.
- [107] Y. Zhang, Y. Yi, P. Dong, F. Liu, and Y. Kang, “Simplified model and control strategy of three-phase pwm current source rectifiers for dc voltage power supply applications,” *IEEE Journal of Emerging and Selected Topics in Power Electronics*, vol. 3, no. 4, pp. 1090–1099, 2015.
- [108] J. C. Wiseman, B. Wu, and G. Castle, “A pwm current-source rectifier with active damping for high power medium voltage applications,” in *2002 IEEE 33rd Annual IEEE Power Electronics Specialists Conference. Proceedings (Cat. No. 02CH37289)*, IEEE, vol. 4, 2002, pp. 1930–1934.
- [0] **L. Neukirchner.** (2019). Constrained predictive control of three-phase buck rectifiers simulation details, [Online]. Available: <http://virt.uni-pannon.hu/ver/index.php/en/projects/30-empc-csr>, 2019.
- [0] C. N. Jones, P. Grieder, and S. V. Raković, “A logarithmic-time solution to the point location problem for parametric linear programming,” *Automatica*, vol. 42, no. 12, pp. 2215–2218, 2006.

- [0] P. Tøndel, T. A. Johansen, and A. Bemporad, “Evaluation of piecewise affine control via binary search tree,” *Automatica*, vol. 39, no. 5, pp. 945–950, 2003.
- [0] P. Tøndel and N Trondheim, “Constrained optimal control via multi-parametric quadratic programming.,” PhD thesis, Citeseer, 2003.
- [0] N. Kutasi, A. Kelemen, and M. Imecs, “Vector control of induction motor drives with model based predictive current controller,” in *2008 IEEE International Conference on Computational Cybernetics*, IEEE, 2008, pp. 21–26.